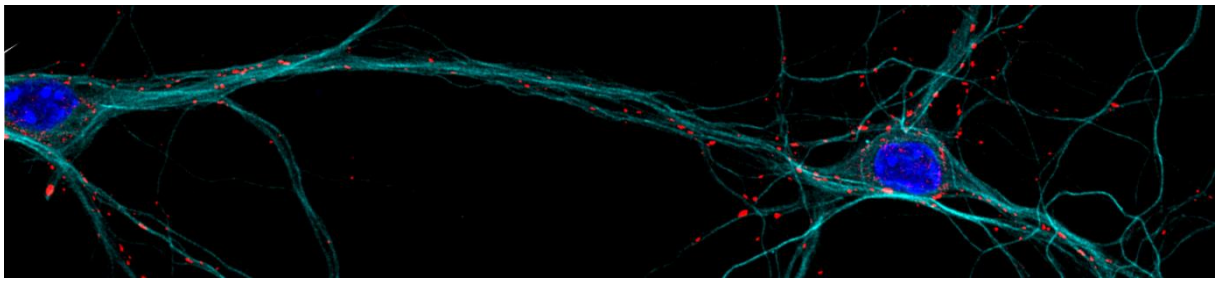

CORSO DI DOTTORATO IN NEUROSCIENZE

Curriculum: NEUROSCIENZE CLINICHE E SPERIMENTALI

CICLO XXXV

Dipartimento di Neuroscienze, riabilitazione, oftalmologia, genetica e scienze materno-infantili (DINOGMI) - Università degli Studi di Genova

"A role in pH homeostasis regulation by genes related to Neurodevelopmental Disorders: *TBC1D24* and *ATP6V1A*."

Candidate: Sara Pepe

Supervisor: Prof.ssa Anna Fassio

INDEX

INTRODUCTION

The role of synaptic genes in Neurodevelopmental Disorders

Brain functions mainly rely on the ability of neuronal cells to communicate with each other through neurotransmission. Neurotransmitter release is regulated by the fine-tuned recycling of synaptic vesicles (SVs), a process that involve several different proteins. Over the years, mutations in the most important genes for SV recycling uncovered a new category of brain disorders, belonging to the broad family of neurodevelopmental disorders (NDDs) (John et al. 2021). NDDs are a large and heterogeneous group of diseases characterized by the early onset of pathological manifestations such as developmental delay, cognitive and motor impairments and seizures. Based on clinical manifestations, NDDs can be categorized in different pathologies, comprising intellectual disability (ID), autism spectrum disorder (ASD) and developmental epilepsies (DE), including early onset epileptic encephalopathy (EEOE). Due to the very complex genetic background and etiology of these diseases, their precise pathophysiology and consequent therapeutic options are still far from being determined.

In 2021, Bonnycastle and colleagues categorized SV cycle-related genes based on the pathological phenotype of the main NDDs (**Figure 1**).

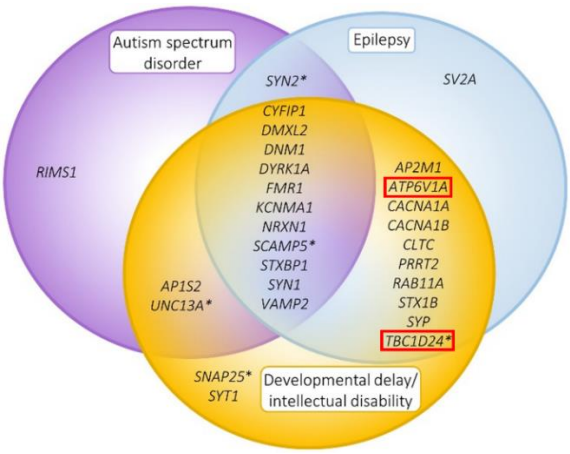

Figure 1. SVs life cycle genes categorized by NDD. The diagram shows genes mutated in the different subcategory of NDDs. The genes object of this project, namely TBC1D24 and ATP6V1A, are marked in red. Adapted from (Bonnycastle et al. 2021).

Interestingly, the genes identified encode for proteins involved in different steps of SV recycling, from priming and fusion events to endocytosis and recycling of SV cargoes (Bonnycastle et al. 2021).

This scenario highlights the point that there is no single specific event that, when dysregulated, causes NDDs, increasing the complexity and difficulty of finding a unique and reliable therapeutic strategy. However, depicting the precise mechanisms by which dysfunctional proteins impair SV homeostasis is a key starting point to uncover the related neuronal circuit defect and to provide the solutions needed for its recovery.

This thesis describes two related projects focused on the study of the genes *TBC1D24* and *ATP6V1A* (**Figure 1**, marked in red) in order to explore the physiological function of TBC1D24 and ATP6V1A proteins and the molecular mechanisms at the base of brain pathologies associated with mutations in *TBC1D24* or *ATP6V1A* genes.

TBC1D24

The gene *TBC1D24* was first identified in 1999, when Hirosawa and colleagues carried out a sequencing project about cDNAs expressed in the human brain and found its sequence among the identified cDNAs (Hirosawa et al. 1999). In the same period, Zara and colleagues identified the locus in chromosome 16p13.3 that is responsible for Familial Infantile Myoclonic Epilepsy (FIME), a severe early-onset brain disorder (Zara et al. 2000). Screening of possible candidate genes in patients led to the identification of two compound heterozygous missense mutations in *TBC1D24* gene (Falace et al. 2010). After this initial discovery, many other genetic variants have been described in patients affected by a broad spectrum of disorders, mainly represented by early-onset brain pathologies with epilepsy (Balestrini et al. 2016).

TBC1D24 expression

TBC1D24 mRNA is expressed in different human tissues including heart, liver, kidney, stomach and lungs, although the highest expression is observed in the brain and in particular in the cerebral cortex, hippocampus, dentate gyrus and olfactory bulb (Falace et al. 2010; Finelli et al. 2019; Tona et al. 2019).

TBC1D24 encodes for a multifunctional protein characterized by two functional domains. Interestingly, different alternatively spliced transcripts of the gene were described and only some of them encode for the full-length protein (Rehman et al. 2014). Of note, there is some evidence that some of the spliced variants could be enriched in a tissue- or cell-specific manner, leading to differential expression of complete or truncated form of the protein (Rehman et al. 2014; Tona et al. 2019). For example, micro-exon 4 of *Tbc1d24* is spliced in two variants in mouse brain and inner ear, being either included or excluded into mRNA and leading to full-length or truncated protein respectively. RNA quantification of the two splice variants in mouse brain at different developmental stages revealed a switch between the two during neurodevelopment, being the including one the most expressed in the adult mice. Mutations affecting micro-exon 4 have been related to a severe epileptic phenotype in mice while the function of spiral ganglion neurons of the inner ear seemed to be unaffected (Tona et al. 2019). All these findings suggest that modulation of the expression of *TBC1D24* is a critical point for understanding the functions of the protein in different tissues and to get insight on the molecular mechanisms of the pathologies associated with the many pathogenic mutations described in this gene.

TBC1D24 pathogenic mutations are very sparse all along the sequence of the gene, and they impact on different parts of the protein. However, almost all of them are related to disorders of neural connectivity (Mucha et al. 1993; Balestrini et al. 2016; Tona et al. 2019). In addition, *Tbc1d24* gradually increases its expression during embryonic brain maturation, and it stabilizes at postnatal stage (Falace et al. 2014; Aprile et al. 2019)., suggesting a predominant and fundamental role for TBC1D24 in brain development and function.

TBC1D24 structure

The full-length isoform of TBC1D24 is a protein of 559 amino acids characterized by the unique association of two different domains: the TBC domain (Tre2/Bub2/Cdc16), located at the N-terminus, and the TLDc domain, located at the C-terminus.

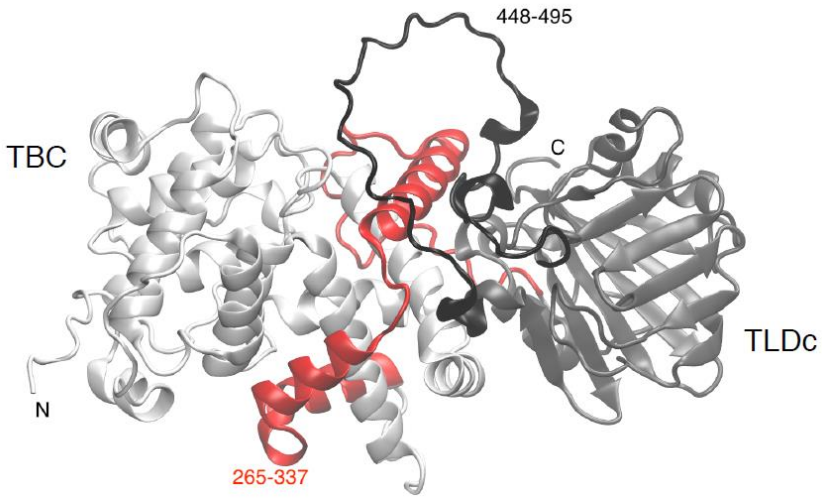

Figure 2. Predictive structure of the protein TBC1D24. Three-dimensional structural model of TBC1D24. The TBC domain is shown in light grey, the TLDc domain in dark grey. The aminoacidic loop between the domains is shown in red and the non-conserved loop within the TLDc domain in black. (Structural modelling was made by Luca Maragliano, Università Politecnica delle Marche, Ancona, Italy)

The TBC domain

The TBC (Tre-2/Bub2/Cdc16) domain is the characteristic domain of GTPase Activating Proteins (GAPs) for Rab GTPases (Frasa et al. 2012). The Rabs are small GTP-binding proteins which perform their function by cycling between an inactive (GDP-bound) and an active (GTP-bound) state. These proteins are specialized in regulation of intracellular membrane trafficking, and participate in the biogenesis, transport and fusion of membrane-bound organelles and vesicles (Stenmark 2009; Zhen and Stenmark 2015; Homma et al. 2021). The intrinsic hydrolysis capacity of Rabs is low. This is the reason why they are supported by GAPs, which accelerate the process and facilitate their inactivation (transition from GTP-bound to GDP-bound state). In addition, Rab proteins require the support of other accessories proteins, namely Guanine nucleotide Exchange Factors (GEFs), to be reloaded

with GTP and consequently be activated (Bos et al. 2007). The TBC domain is reported to act through a dual-finger mechanism: the crystallography of the domain shows that two distinct residues, an arginine and a glutamine, form the catalytic site which sustains GTP hydrolysis (Pan et al. 2006). This dual-finger mechanism is typical of most of the TBC-containing Rab GAPs, but some unconventional TBC-domain-containing proteins, which lack one or both the residues, have been described (Frasa et al. 2012). Importantly, TBC1D24 belongs to the unconventional Rab GAPs because its TBC domain lacks both the residues (R- and Q-) forming the typical dual-finger (Corbett et al. 2010; Frasa et al. 2012; Fischer et al. 2016).

The TLDc domain

The Tre2/Bub2/Cdc16 (TBC), lysin motif (LysM) domain catalytic (TLDc) domain is a highly conserved domain present in different mammalian proteins, hereby referred to as TLDc proteins, like NCOA7 and OXR1 (Finelli and Oliver 2017). The best-established function of this group of proteins is protection from oxidative stress, which has been demonstrated *in vitro* and for OXR1, NCOA7 and TBC1D24 also *in vivo* in the central nervous system (Finelli et al. 2016). Loss of OXR1 (oxidation resistance 1) leads to neurodegeneration both in mice and humans (Oliver et al. 2011; Wang et al. 2019) and its overexpression is responsible of ALS symptoms in animal models (Liu et al. 2015). On the contrary, overexpression of *Tbc1d24* increases viability of cells treated with arsenite, an oxidative stress inducer, but it has no effect in reducing reactive oxygen species (ROS) concentration (Finelli et al. 2016). Acute silencing of *Tbc1d24* is not enough to cause an increase in cell death, but pathological mutations into the TLDc domain abolish its protective effect and promote protein S-nitrosylation, suggesting a TLDc-mediated pathological mechanism in patients due to loss of resistance against oxidative stress in neurons.

Recently, a new role for TLDc proteins emerged: the TLDc motif has been proposed to constitute a novel protein–protein interaction domain that defines a new class of V-ATPase-associating proteins (Eaton et al. 2021). V-ATPase is a large, multisubunit protein complex

that acts as a proton pump and provide the correct acidification of intracellular comparments (Forgac 2007). In 2015, Merkulova and colleagues performed a proteomic analysis of V-ATPase interactions in the kidney. Among all the interactors, the TLDc proteins NCOA7 and OXR1 were identified (Merkulova et al. 2015). Deletion of NCOA7, which is highly expressed in kidney, resulted in downregulation of V-ATPase expression and less efficient urine acidification (Merkulova et al. 2015; Merkulova et al. 2018). In the brain, NCOA7 interacts with the cytosolic domain of V-ATPase and regulates its assembly and activity. Moreover, loss of *Ncoa7* in neurons leads to altered development, defective lysosomal formation and function (Castroflorio et al. 2021). OXR1 has also been reported to interact with the V1 cytosolic domain of V-ATPase in yeast. Its binding reduces the ATPase activity of the domain and prevents the formation of the holoenzyme *in vitro* (Khan et al. 2022). In addition, fibroblasts from patients affected by mutations in *OXR1* sequence display the accumulation of aberrant lysosomal structures, suggesting that it is required for normal lysosomal function (Wang et al. 2019).

Among the TLDc proteins that interact with V-ATPase, also Tldc1 (also known as mEAK7) and Tldc2 have been detected (Eaton et al. 2021). Tldc1 binds V-ATPase through its C-terminal and TLDc domain. Although it has been observed that Tldc1 binding induces a conformational change of V-ATPase's V1 domain, this interaction seems not to interfere with the ATPase activity and proton traslocation *in vitro*, resulting in unchanged intracellular organelles pH (Tan et al. 2022; Wang et al. 2022).

Interestingly, the V-ATPase itself also plays a role in protection from oxidative stress (Thorpe et al. 2004), and it is possible that protein complexes formed by TLDc proteins and the V-ATPase are involved in this process.

TBC1D24 function

The *TBC1D24* fly homologue *skywalker*

In 2011, Verstreken's group found out that the homologue of *TBC1D24* in *Drosophila*, the gene *Skywalker*, is expressed in the neuromuscular junction and it is essential for the regulation of

vesicular trafficking (Uytterhoeven et al. 2011). As TBC1D24, Skywalker lacks the arginine and glutamine residues in its TBC domain, but this does not seem to prevent its role as a GAP for the small GTPase Rab35 (Uytterhoeven et al. 2011). Rab35 is associated with the plasma membrane, and it is involved in many processes, but mostly in endocytic recycling (Klinkert and Echard 2016). The same role has been proposed in NMJ cells where its interaction with Skywalker controls the recycling of SVs, the neurotransmitter release and the degradation of synaptic proteins through the endo-lysosomal pathway (Uytterhoeven et al. 2011; Fernandes et al. 2014). In particular, the reduction of *Skywalker* expression facilitates the endosomal trafficking of SVs which results in the increase of both total and readily releasable pools of these structures (**Figure 3**). In addition, the excessive endosomal trafficking of SVs sustains an overly efficient rejuvenation of synaptic proteins (Fernandes et al. 2014) paired with augmented neurotransmission.(Uytterhoeven et al. 2011).

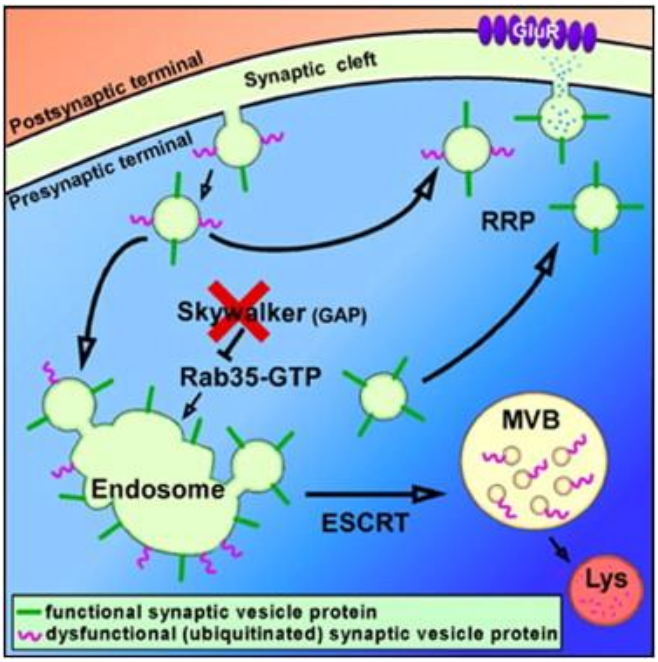

Figure 3.Skywalker at the synaptic terminal. At the pre-synaptic compartment of *Drosophila* NMJ, Skywalker is involved both in recycling vesicles processes and in rejuvenation of synaptic protein pools. From (Uytterhoeven et al. 2011)

Moreover, a lipid-binding pocket was discovered in the crystallized structure of the TBC domain of Skywalker (Fischer et al. 2016). This cationic pocket is conserved among *Skywalker*

homologues, including human *TBC1D24*, and allows the binding of different phosphoinositides, in particular phosphatidylinositol 4,5-bisphosphate (PI(4,5)P2). The kinase responsible of PI(4,5)P2 production is positively regulated by the small GTP-ase ARF6 (Honda et al. 1999) and PI(4,5)P2 acts as modulator of many different cellular pathways such as stress response, exocytosis, autophagy, endosomal acidification and fusion with lysosomes (Ho et al. 2012). Missense mutations in *Skywalker*, in the conserved residues mutated in human disease, cause the impairment of this binding and results in neurodegeneration and epileptic-like phenotype in flies.

The interaction between Tbc1d24 and Rab35 was described also in *Xenopus*, where it is involved in the migration of crestal neural cells (CNCs) during embryonic development. It has been shown that, upon translocation to cellular membranes, Tbc1d24 can control the Rab35-dependent endosome recycling of E-cadherin, a process fundamental for ensuring the correct migration of CNCs (Yoon et al. 2018). These findings further confirm the link between TBC1D24 and membrane trafficking/recycling through the modulation of effector proteins.

However, the mammalian TBC1D24 does not seem to specifically interact with Rab35 (Lin et al. 2020), suggesting that in neurons of higher organisms its function is predominantly mediated by other protein-protein interaction. As described in the following chapter, mammalian TBC1D24 has been shown to interact with ARF6. Interestingly, ARF6 and Rab35 can inhibit each other by recruitment of reciprocal GAPs (Chaineau et al. 2013; Dutta and Donaldson 2015). Therefore, it is possible that the ratio of active to inactive forms of Rab35 and ARF6 are critical to regulate TBC1D24-associated synaptic function.

TBC1D24 in mammals

In mammalian neurons, TBC1D24 was found to be enriched in the trans-Golgi network, especially in clathrin-coated vesicles, and expressed both at pre- and post-synaptic sites (Tona et al. 2019; Lin et al. 2020). Immunogold-labelling of TBC1D24 revealed its localization at pre-

synapses in vesiculate structures and at possible sites of endocytosis together with the membrane of the active zone (Tona et al. 2019).

TBC1D24 and ARF6

As described before, the TBC domain is involved in the regulation of small GTPases. It has been demonstrated that TBC1D24 binds the small GTPase ARF6 through its TBC domain, indeed pathogenic missense mutations in this specific domain decrease their interaction (Falace et al. 2010; Milh et al. 2013). ARF6 is a small GTPase involved in different cellular processes: regulation of endosomal-membrane trafficking and cytoskeletal organization (D'Souza-Schorey and Chavrier 2006), SV trafficking (Frittoli et al. 2008; Tagliatti et al. 2016), cell migration stimulation and cell guidance (Santy and Casanova 2001; Akiyama and Kanaho 2015), as well as neurite outgrowth and dendritic spine maturation (Albertinazzi et al. 2003; Miyazaki et al. 2005; Choi et al. 2006). However, the TBC domain present in human TBC1D24 lacks the typical residues (R- and Q-) required for GAP activity and inactivation of Rab GTPases (Corbett et al. 2010; Fischer et al. 2016). Interestingly, also TRE17 and TBC1D3, two proteins that lack the same critical arginine, bind the small GTPase ARF6 (Martinu et al. 2004; Frittoli et al. 2008). The TBC1D24/ARF6 interaction seems to inhibit the formation of active ARF6-GTP as lack of TBC1D24 causes the accumulation of ARF6 in the GTP-bound active form (Falace et al. 2014; Aprile et al. 2019; Lin et al. 2020). Together, these data support the hypothesis that TBC1D24 plays a key role in the regulation of ARF6 activation state.

One of the described roles for TBC1D24 is to sustain a correct neurodevelopment, as reported *in vitro* and *in vivo* at cortical and hippocampal level (Falace et al. 2010; Falace et al. 2014). Indeed, acute *Tbc1d24* knockdown *in vivo* at embryonic level leads to defects in migration and maturation of neurons, paired with curbed neurite outgrowth and functional abnormalities, including reduced frequency in excitatory currents (Falace et al. 2014). Moreover, acute silencing of the gene *in vitro* has been associated with defective axonal specification and reduced dendritic spines (Aprile et al. 2019; Lin et al. 2020). The direct correlation between these phenotypes and TBC1D24 is sustained by findings showing that overexpression of wild-type *Tbc1d24* in neurons leads to an increase in axonal outgrowth and branching, while

expressing mutated form of the gene in either the TLDc or TBC domain impairs this phenotype (Corbett et al. 2010; Falace et al. 2010; Milh et al. 2013; Balestrini et al. 2016). Interestingly, experimental evidence support the knowledge that TBC1D24 exerts its function on neuronal development through its interaction with ARF6, as the dominant negative form of the small GTPase rescue the neurodevelopmental phenotypes both in vitro and in vivo (Falace et al. 2010; Aprile et al. 2019; Lin et al. 2020).

TBC1D24 synaptic role

Acute silencing of *Tbc1d24 in vitro* decreases excitatory synaptic contacts, impairs axonal initial segment formation and results in decreased action potential firing (Aprile et al. 2019; Lin et al. 2020). This is also paired with a clear post-synaptic phenotype, with reduction of dendritic spines number both *in vitro* and *in vivo*. Lin and colleagues demonstrate that this phenotype is ARF6-dependent, indeed overexpression of negative-dominant form of ARF6 as well as its pharmacological inactivation rescue the post-synaptic defect (Lin et al. 2020).

Interestingly, a mouse model harbouring a *Tbc1d24* pathogenic mutation described in patients with focal epilepsy (Corbett et al. 2010; Afawi et al. 2016) showed a different phenotype. To note, the pathogenic mutation resulted in a significant loss of the protein due to instability and consequent degradation. At embryonic level, homozygous mutant neurons showed no alterations in excitatory synapses, firing frequency and dendritic spines number. However, post-synaptic specification showed enlarged heads together with increased mEPSC amplitude. Homozygous mice started to have spontaneous seizures at P21, right before their premature death as already shown for a different mouse model of TBC1D24-related disorder (Tona et al. 2019; Lin et al. 2020). Paired electrophysiological recordings of brain slices revealed an increased excitability of neurons. These findings suggest that genetic manipulation of *Tbc1d24* at different stage of brain development results in different phenotypes. How the decreased excitability of embryonic neurons that lack TBC1D24 switches during post-natal development is still unclear, although a possible origin is the enlarged nature of dendritic

spines. All together, these data suggest that TBC1D24 plays a crucial role in the maintenance of dendritic spine but not in their maturation.

At presynaptic sites, the involvement of TBC1D24 in vesicle trafficking and endocytosis was described by Finelli and colleagues in a mouse model of *Tbc1d24* haploinsufficiency. Briefly, reduction of the protein by half resulted in the slowdown of SV endocytosis (Finelli et al. 2019). This phenotype was paired with ultrastructural impairment of pre-synaptic morphology, which displayed aberrant accumulation of endosomal-like structures as shown also for neurons with defective activation of ARF6 (Tagliatti et al. 2016). Hence, it is possible that upon prolonged stimulation, the deficiency of TBC1D24 impairs SV recycling. Interestingly, a lack of the protein seems not to increase SV release, as described in *skywalker* mutants, further suggesting a differential role for TBC1D24 in higher organisms possibly mediated by ARF6 regulation.

Role of TBC1D24 in pathology

Over the years, many mutations in *TBC1D24* sequence have been reported in patients affected by a broad spectrum of disorders, including developmental and epileptic encephalopathies of different severity, hearing loss and composite syndromes such as DOORS (deafness, onychodystrophy, osteodystrophy, mental retardation, and seizures) (**Table 1**).

Clinical Phenotype	References	Inheritance	
Familial Infantile Myoclonic Epilepsy (FIME)	Falace et al., 2010	Autosomal recessive	Compound heterozygous missense mutations (p.Asp147His and p.Ala515Val)
	Poulat et al., 2015		Homozygous missense mutation (p.Glu153Lys)
	Shao et al., 2022		Homozygous in frame deletion (p.Ile81_Lys84del)
Focal epilepsy with cerebrocerebellar malformation	Corbett et al., 2010 Afawi et al., 2016	Autosomal recessive	Homozygous missense (p.Phe251Leu)
Severe and lethal epileptic encephalopathy with cerebral neurodegeneration	Guven and Tolun, 2013	Autosomal recessive	Homozygous truncating mutation (969_970delGT, Ser324Thrfs*3)

Malignant migrating partial seizures of infancy (MMPSI)	Milh et al., 2013	Autosomal recessive	Compound heterozygous nonsense mutations (p.Cys156* and p.Phe229Ser)
	Appavu et al., 2016		Compound heterozygous nonsense/missense mutations (p.Gln41Ter and p.Asn107Lys; p.Pro282Arg and p.Asn307Asp)
Autosomal dominant deafness-65 (DFNA65)	Zhang et al., 2014 Azaiez et al., 2014,	Autosomal dominant	Heterozygous (p.Ser178Leu)
	Parzefall et al., 2020		Heterozyogus (p.Asn307His)
	Oziębło et al., 2021		Heterozygous (p.Asp185Asn, p.His487Leu, p.His487Gln)
Autosomal recessive deafness-86 (DFNB86)	Rehman et al., 2014	Autosomal recessive	Homozygous missense mutations (p.Asp70Tyr, p.Arg293Pro)
	Bakhchane et al., 2015		Compound heterozygous frameshift (p.Arg241His and p.Val439Valfs*32; p.Arg214His and p.Glu153Lys)
	Xiang et al., 2020		Homozygous (p.Arg293Cys)
	Reis et al., 2022		Homozygous (p.Arg241His)
DOORS	Campeau et al., 2014 Santos et al., 2019	Autosomal recessive	Compound heterozygous (p.Arg242Cys and p.Arg40Cys, p.Arg242Cys and p.Gln20Glu, p.Gly110Ser and p.Leu333Phe, p.His336GlnfsTer12* and X) Homozygous (Arg242Cys, Arg40Leu)
	Atli et al., 2018		Homozygous (p.Gly428Arg)
Progressive Myoclonus Epilepsy (PME)	Muona et al., 2015	Autosomal recessive	Homozygous missense mutation (p.Arg360Leu)
Early Onset Epileptic Encephaloty and Hearing Loss	Stražišar et al. 2015	Autosomal recessive	Compound heterozygous missense and frameshift mutations (p.Asp11Gly and p.His336Glnfs*12)
Migrating Paroxysmal Myoclonus and Cerebellar Signs	Doummar et al. 2015	Autosomal recessive	Homozygous (p.Arg270His)
Lethal familial neonatal seizure disorder	Lozano et al.2016	Autosomal recessive	Compound heterozygous (p.Ala113Asp and p.Leu159Pro)
Sudden unexpected death in epilepsy (SUDEP)	Trivisano et al. 2017	Autosomal recessive	Compound heterozygous (c.679C>G and c.328G>A) Homozygoys (c.545C>T)
Dominant tonic-clonic and myoclonic epilepsy	Banuelos et al. 2017	Autosomal dominant	Heterozygous (p.Pro135Leu)

Severe disorder with epilepsy, Parkinsonian tremor, intellectual disability and psychosis	Banuelos et al. 2017	Autosomal recessive	Compound heterozygous missense mutations (p.Arg360Cys and p.Pro135Leu)
Alternating hemiplegia and epilepsia partialis	Ragona et al. 2017	Autosomal recessive	Compound heterozygous (p.Ala39Val and p.Glu153Lys)
Infantile-onset multifocal polymyoclonus and neurodevelopmental delay	Ngoh et al. 2017	Autosomal recessive	Compound heterozygous missense and frameshift mutations (p.Glu157Lys and p.Thr182Serfs*6)
Epilepsia partialis continua (EPC)	Zhou et al. 2018	Autosomal recessive	Homozygous (p.82_84del)
Nonconvulsive status epilepticus (NCSE), cerebellar ataxia and ophthalmoplegia	Li et al. 2018	Autosomal recessive	Compound heterozygous frameshift (p.Ser473Argfs*43 and p.Ala500Val)
Infantile-onset paroxysmal movement disorder and episodic ataxia	Zimmern et al. 2019	Autosomal recessive	Compound heterozygous (p.Pro102Ser and p.Val137Ala)
Rolandic epilepsy with paroxysmal exercise-induced dystonia	Luthy et al. 2019	Autosomal recessive	Compound heterozygous in frame deletion and missense mutations (p.Ile81_Lys84del and Ala500Val; Thr182Met and Gly511Arg)
	Steel et al. 2020		Compound heterozygous nonsense and frame-shift (pGln301* and p.Ser202Leu, p.Leu159Trpfs*10 and p.Arg227Leu)
Developmental and epileptic encephalopathy 16 (DEE16)	Nakashima et al., 2019	Autosomal recessive	Homozygous (p.Glu148Lys)
	Salemi et al., 2020		Compund heterozygous (p.Glu457Ala and c.1142 + 1 G>A)
	Uzunhan et al., 2020 Lee et al., 2022		Homozygous missense mutation (p.Ala500Val)
Epilepsy of infancy with migrating focal seizures (EIMFS)	Fang et al. 2021	Autosomal recessive	Compound heterozygous (p.Pro135Leu and p.Glu153*)
Auditory neuropathy spectrum disease (ANSD)	Sun et al. 2022	Autosomal recessive	Compound heterozygous (p.Arg65His + c.1638delT)
Alternating Hemiplegia of Childhood (AHC)	Cordani et al. 2022	Autosomal recessive	Homozygous missense mutation (p.Thr182Met)

Table 1. List of *TBC1D24*-related disorders.

To explain the spectrum of *TBC1D24*-associated disorders, it has been suggested that the pathogenic variants of *TBC1D24* may damage different binding motifs for its protein partners resulting in different phenotypes (Frasa et al. 2012). In addition, mutations may affect one or more alternative transcripts encoding different TBC1D24 protein isoforms (Rehman et al. 2014). Lastly, modifications in the genetic background of an affected individual may contribute to TBC1D24-associated disorder (Kammenga 2017).

Recently, Finelli and colleagues mapped some pathogenic mutations in TBC1D24 structure, finding that there is no clustering of a specific clinical sub-type or severity (Finelli et al. 2019).To date, a precise genotype/phenotype correlation is not available. Almost all the mutations found in *TBC1D24* are compound heterozygous or homozygous with a recessive inheritance and there is some evidence that the more severe clinical phenotypes with drug-resistant epilepsy or early death are associated with nonsense, frameshift or splice-site mutations (Balestrini et al. 2016). Moreover, analysis of protein levels in fibroblasts from patients affected by compound heterozygous mutations revealed a reduction in TBC1D24 abundance, suggesting a loss-of-function phenotype and proposing that variation in *TBC1D24* expression could be a marker of disease severity (Campeau et al. 2014; Lozano et al. 2016).

V-ATPases

The vacuolar (H+)-ATPases (V-ATPases) are membrane-bound protein complexes that function as proton pumps in all eukaryotic cells. V-ATPases hydrolyse ATP to move protons across membranes, thus they are the main source of intracellular organelles acidification (Forgac 2007; Cotter et al. 2015; Vasanthakumar and Rubinstein 2020). Luminal pH of intracellular compartments is a critical parameter for their function. Therefore, V-ATPases activity is fundamental for many cellular processes, including membrane trafficking (Forgac 2007), the targeting and post-translational modification of proteins in the Golgi apparatus (Khosrowabadi and Kellokumpu 2020) and the degradation of biological macromolecules in lysosomes (Mindell 2012). In neurons, the complex of V-ATPase is present also in the

membranes of SVs where it creates the electrochemical proton gradient essential for the uptake and release of neurotransmitters (Hnasko and Edwards 2012).

Structure

V-ATPases are composed of 16 different subunits organized in two domains: a cytosolic V1 domain that hydrolyses ATP and an integral V0 domain that translocates protons across membranes by a rotary mechanism (Nishi and Forgac 2002). Since V-ATPases are highly conserved across species, most of the structural analysis was conducted on the yeast form of the enzyme for the relative ease. The yeast V1 region is composed of subunits A_3, B_3, C, D, E_3, F, G_3 and H, while the V0 region contains subunits a, c_8, c', c'', d, e, f and Voa1p (Harrison and Muench 2018; Vasanthakumar and Rubinstein 2020; Oot et al. 2021). The V1 region is analogue between yeast and mammals, while the mammalian V0 region is composed of subunits a, c_x, c'', d, e and the accessory subunits ATP6AP1, also known as Ac45, and ATP6AP2, also known as (pro)renin receptor (PRR) (Burckle and Bader 2006; Abbas et al. 2020).

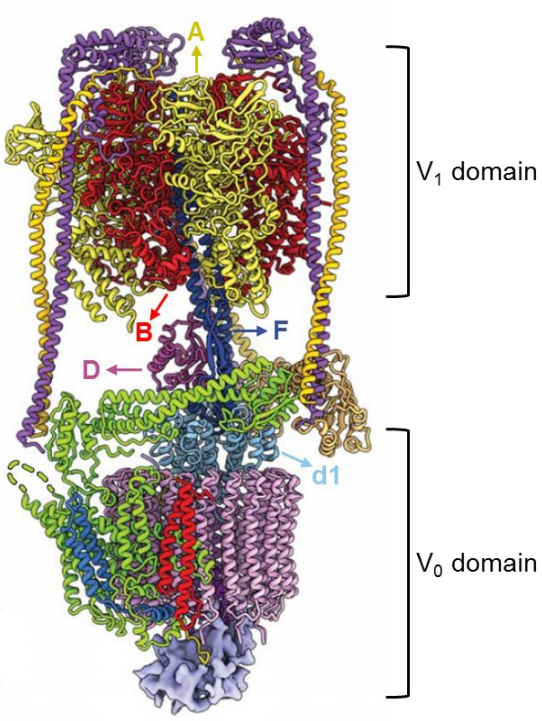

Figure 4. The atomic model of mammalian V-ATPase. The V-ATPase complex is composed of a cytosolic domain (V1), which is responsible for ATP hydrolysis at one type of AB interface, and an integral domain (V0), which is involved in proton translocation across the membrane. They are

connected by a central stalk, composed of subunits D and F of V1 and subunit d of V0, and multiple peripheral stalks. Adapted from (Abbas et al. 2020).

Rotatory functional mechanism

The proton pumping activity of V-ATPases is allowed by diverse conformational changes in the structure of the complex promoted by the free energy obtained through ATP hydrolysis. The hydrolysis of ATP occurs at the V1 domain: the A and B subunits form a hexamer (A_3B_3), and the chemical reaction happens at one type of AB interface. The energy obtained from the ATP hydrolysis drives the conformational change of a central rotor stalk embedded in the V1 domain formed by the subunits D and F. This rotation is translated to V0 region through subunit d, which form a structural link between the DF rotor/ V1 domain and the V0 domain (Nishi and Forgac 2002; Iwata et al. 2004).

In yeast, subunits c, c' and c'' form a channel (c-ring) inside the membrane which allows the proton transfer. In particular, the C-terminal domain of subunit a (a_{CT}), which is inserted in the membrane, forms two half-channels that create a pathway for protons (Kane 1995; Kane 2006). Protons enter from the cytosolic half-channel and encounter the negatively charged conserved glutamate residues of subunit c/c'/c''. During ATP hydrolysis, the c-ring rotates, the conserved glutamates present in each subunit become protonated and the protons are carried through the lipid bilayer before being released through the luminal half-channel (**Figure 5**). The three heterodimers of subunits E and G (peripheral stalks EG1-3) together with subunit H, subunit C, and the N-terminal domain of subunit a (a_{NT}) stabilize the catalytic hexamer (A_3B_3) and subunit a_{CT} during rotation of the central stalk for efficient energy coupling (Nishi et al. 2001; Nishi and Forgac 2002; Wilkens et al. 2004; Khan et al. 2022).

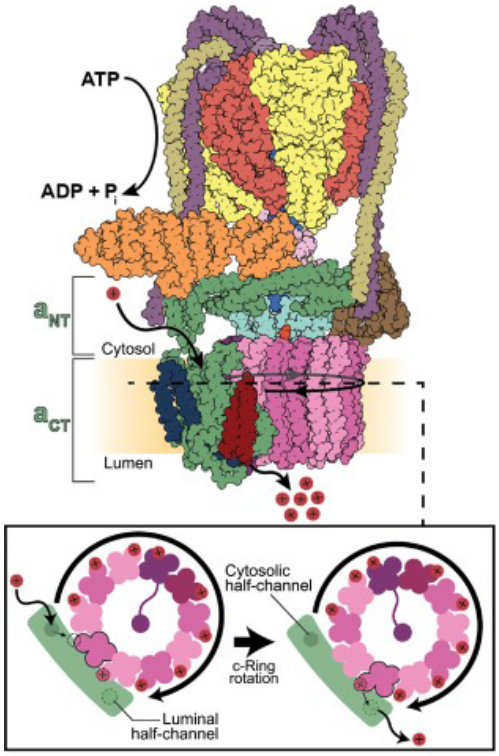

Figure 5.Scheme of the V-ATPase rotatory mechanism for proton translocation. Upon ATP hydrolysis at the AB interface (red and yellow) in the V1 domain, conformational changes in the central rotor stalk (blue, violet and cyan) and the c-ring (pink) drives proton passage through the membrane. Protons (red dots) enter through the cytosolic half-channel in subunit a (green), bind to glutamate residues and rotation of the ring allows their release at the other side of the membrane through the luminal half-channel of subunit a. Adapted from (Vasanthakumar and Rubinstein 2020).

Regulation of V-ATPase activity: reversible disassembly

V-ATPase activity is crucial for many cellular processes and consumes a large amount of cellular energy, thus it must be tightly regulated. The best-studied mechanism of V-ATPase regulation is called reversible disassembly, a process in which the V1 domain detaches from the membrane integral V0 domain with concurrent release of subunit C into the cytosol (**Figure 6**) (Parra et al. 2014; Oot et al. 2017). Upon the enzyme dissociation, both ATP hydrolysis at V1 site and proton translocation at V0 site are blocked (Graf et al. 1996; Parra et al. 2014; Couoh-Cardel et al. 2015; Oot et al. 2016).

Structural studies on the yeast enzyme showed that conformational changes of V1 and V0 subunits leads to the autoinhibition of the disassembled domains. In V0, autoinhibition is due to the association of the subunit a's N-terminal domain (a_{NT}) with the subunit d, an interaction

that is not present in the holoenzyme (Couoh-Cardel et al. 2015; Mazhab-Jafari et al. 2016; Roh et al. 2018) and prevents proton translocation across membranes. On the other side, in V1 domain autoinhibition is provided by the subunit H's C-terminal domain (H_{CT}), which rotates and moves from a binding site on a_{NT} to a binding site on A_3B_3. This change leads to the entrapment of ADP in a closed catalytic site and the consequent prevention of the hydrolysis process (Oot et al. 2016). However, the mammalian H_{CT} is different and lacks the loop found in yeast required for autoinhibition (Oot et al. 2016), suggesting a possible diverse mechanism in higher organisms.

Despite a recent progress with structure determination of holo V-ATPases from a variety of sources (Abbas et al. 2020; Wang et al. 2020a; Wang et al. 2020b), key aspects of the molecular mechanism of V-ATPase regulation by reversible disassembly remain largely elusive.

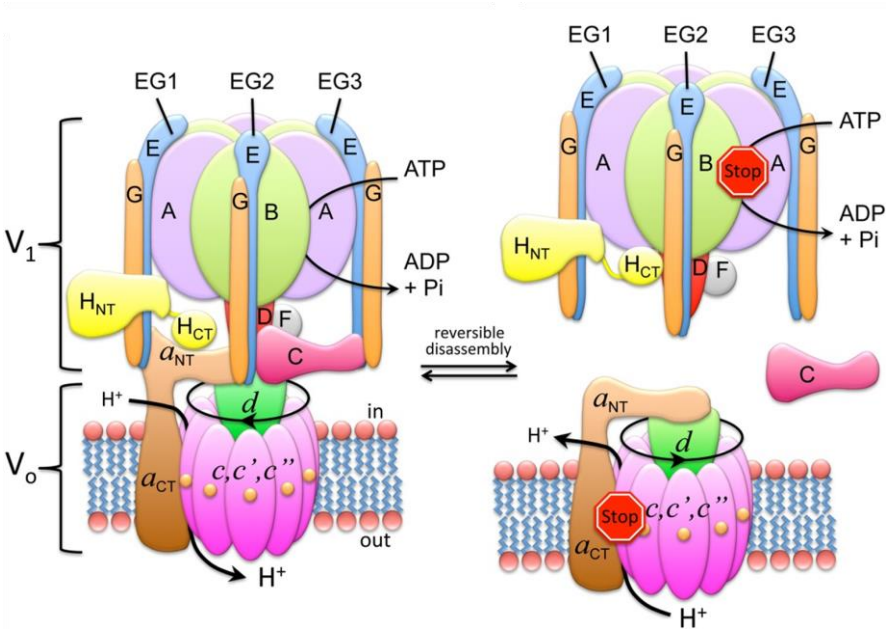

Figure 6. V-ATPase reversible dissociation mechanism. As shown in the picture, during reversible disassembly the V1 domain detaches from the V0 domain and both ATP hydrolysis and protons translocation are inhibited. In yeast, upon the separation of the two domains, subunit C severs from the V1 domain and conformational changes in subunit H and a lead to the autoinhibition of the respective domains. From (Oot et al. 2017)

This process is reversible and thus dissociated components can reassemble into a holoenzyme under favourable conditions. Much of the study on this V-ATPase regulatory

mechanism has been done in yeast and it has been shown that the process is conserved in higher organisms, although much less is known about the precise signalling pathways that intervene in these models. Dissociation of V-ATPase complex is triggered by different environmental stimuli, including nutrient availability, cellular maturation and grow factors (Kane 1995; Sumner et al. 1995; Trombetta et al. 2003; Sautin et al. 2005; Xu et al. 2012; Stransky and Forgac 2015). From studies in yeast, it is known that glucose starvation induces the disassembly of the complex (Kane 1995; Sumner et al. 1995). This process requires intact microtubule network (Xu and Forgac 2001) and V-ATPase to be catalytically active, suggesting that the complex needs to be in a particular conformation to undergo dissociation (Parra and Kane 1998). Interestingly, in mammalian cells both glucose starvation and elevated glucose concentration rapidly increase V-ATPase assembly (Nakamura 2004; Sautin et al. 2005) and lysosomal acidification in a phosphatidylinositol 4,5-bisphosphate 3-kinase (PI3K)- and 5′-AMP-activated protein kinase (AMPK)-dependent manner (McGuire and Forgac 2018). In addition, amino acid starvation increases assembly of the holoenzyme and lysosomal acidification in a PI3K-depedent way (Stransky and Forgac 2015). Finally, increased lysosomal assembly of V-ATPase was also found in dendritic cells in response to maturation stimulus and the process was mediated by PI3K and mTOR complex I (mTORC1) (Trombetta et al. 2003; Liberman et al. 2014).

In yeast, reassembly of the complex is sustained by different proteins, such as the enzymes aldolase and phosphofructokinase-I (Lu et al. 2007; Chan and Parra 2014), as well as the chaperone complex identified as “regulator of (H+)-ATPase of vacuoles and endosomes” (RAVE) (Seol et al. 2001; Smardon et al. 2002; Smardon et al. 2015). Upon glucose restoring, the RAVE complex interacts with V-ATPase and facilitate reintegration of free C subunits within the V1 subcomplex (Smardon and Kane 2007). Less is known about the mechanism in higher organisms, although evidence suggests that the yeast RAVE complex shares functional similarities with the Rabconnectin-3 complex of higher organisms (Jaskolka et al. 2021). Rabconnectin-3 complexes are important for V-ATPase-dependent organelle acidification (Yan et al. 2009; Merkulova et al. 2015) and promote V-ATPase assembly and activity on hair

cell SVs (Einhorn et al. 2012). Moreover, components of the Rabconnectin-3 complex are required for synaptic functionality, in particular for neurotransmitter loading into SVs, a process that relies on the acidic pH generated by synaptic V-ATPases (Bodzeta et al. 2017).

Role of V-ATPase in physiology

V-ATPases-mediated acidification is fundamental for the biological function of many intracellular compartments. This process intervenes in different pathways: 1) receptor-mediated endocytosis where it allows the uncoupling of ligand-receptor complexes; 2) proper sequential targeting of vesicles and proteins in the endocytic pathway; 3) acidification of lysosomes, required for degradative enzymatic function; 4) acidification of secretory granules and SVs, essential for the uptake of small molecules like hormone precursors and neurotransmitters; and 5) proper posttranslational modification of proteins in the trans-Golgi network (Maxfield and McGraw 2004; Mindell 2012; Vavassori and Mayer 2014; Kellokumpu 2019).

Moreover, emerging evidence supports the idea that the V-ATPase is not only involved in generating the acidic pH but also in sensing luminal pH of organelles and possibly transmitting this information to other proteins to support them in their targeting functions. For example, in renal cells, carrier vesicles-budding from endosomes for protein degradation is mediated by the small GTPases ARF6 and ARNO. The recruitment of the two proteins to the endosomal membrane is mediated by V-ATPase in a pH-dependent manner (Hurtado-Lorenzo et al. 2006). Other studies proposed the pH sensor role also in secretory granules of chromaffin cells, where V0 domain senses intragranular pH and controls exocytosis and synaptic transmission via the reversible dissociation of V1 at acidic pH (Poea-Guyon et al. 2013).

V-ATPase and autophagy

Maintenance of pH homeostasis by V-ATPase is fundamental in different cellular processes, including macroautophagy (hereby referred as to autophagy). Autophagy is a highly conserved self-degradative pathway that cells use to eliminate damaged proteins and organelles and to

recycle their components in response to nutrient fluctuations. The degradative capacity of autophagy relies on lysosomal catalytic enzymes, which function at the acidic lysosomal pH provided by V-ATPase (Yim and Mizushima 2020).

Autophagy starts with the formation of a U-shaped double-membrane structure, called phagophore, which expands and bends to sequester the cargo targeted for degradation either in non-selective ("bulk") or selective manner, the latter utilizing selective autophagy receptor proteins (Yang and Klionsky 2010; Rogov et al. 2014; Johansen and Lamark 2020). The closed autophagosome matures progressively by recruiting different proteins, which are necessary the fusion with mature lysosomes (Itakura et al. 2012; Hegedus et al. 2016). After fusion, the autophagic cargo is degraded into autolysosomes by the activity of lysosomal acidic hydrolases.

Additionally, it has been demonstrated that V-ATPase participates to the amino acid sensing along the mTORC1 complex (Colacurcio and Nixon 2016). The major cellular role of mTORC1 is to coordinate the balance between anabolism and catabolism in response to fluctuations in the levels of intra- and extracellular nutrients, primarily amino acids (Liu and Sabatini 2020). Under conditions of high amino acid availability, mTORC1 activates and promotes anabolic metabolism for the biosynthesis of necessary components for cell growth. At the same time, it represses catabolic programmes via unc-51-like autophagy activating kinase 1 (ULK1), thus leading to the inhibition of autophagy. On the other hand, upon stress conditions, including amino acid deprivation, mTORC1 inactivation stimulates the progression of autophagy to recycle cellular components (Sarkar 2013).

mTORC1 activation occurs at the lysosomal membrane, where the Ragulator complex interacts with the Rags and the complex of V-ATPase in an amino acid-dependent manner (Zoncu et al. 2011). The Ragulator promotes a structural rearrangement of the V-ATPase-Ragulator-Rags complex and activate Rags, which recruits mTORC1 to the lysosomal surface where it is activated by the Rheb GTPases already present on the lysosomal membrane (Zoncu et al. 2011). Although V-ATPase rotary motion is required for amino acid sensing and

mTORC1 recruitment to lysosomes, the proton gradient generated by the V-ATPase appears to be dispensable, indicating that the V-ATPase is functioning in a signalling fashion in this context (Zoncu et al. 2011). Moreover, the V-ATPase and mTORC1 signalling seems not only to respond to amino acid availability but also to control lysosomal amino acid concentration (Abu-Remaileh et al. 2017). Therefore, while generally thought as a downstream component of autophagy, V-ATPase can regulate upstream components of the process.

Autophagy is a housekeeping process, and it has a fundamental role in neuronal cells. Neurons are post-mitotic cells that cannot dilute damaged or toxic structures through cell division, and the complex and very specialized nature of these cells requires a constant and precise quality control of their proteins and organelles. Moreover, neurons are cells with great demand of energy and protein turnover, especially at synaptic regions. Hence, neuronal autophagy is highly regulated and compartmentalized (Sidibe et al. 2022). In neurons, differently from other cell types where autophagosomes biogenesis occurs in the cell body, the major sites of autophagosomes biogenesis are distal axons and presynaptic sites. Then, autophagosomes traffic retrogradly to the soma where they fuse with mature lysosomes to allow degradation (Sidibe et al. 2022). Emerging evidence suggests an interplay between autophagy and synaptic function. Indeed, neurons regulate the neuronal proteome in response to synaptic activity (Goo et al. 2017; Hafner et al. 2019) and, at the synapse, autophagy may be required for the turn-over of the local proteome and organelles.

At presynaptic sites, autophagy has been shown to regulate neurotransmission by controlling the axonal ER and synaptic vesicle pools (Hernandez et al. 2012; Gu et al. 2021; Kuijpers et al. 2021). In particular, loss of autophagy resulted in the accumulation of tubular ER in axons, leading to an elevated calcium release from ER stores and increased exocytosis of synaptic vesicles (Kuijpers et al. 2021). Moreover, impaired autophagosomal biogenesis has been demonstrated to increase the number of synaptic vesicles in the readily releasable pool and their rate of release (Gu et al. 2021). Conversely, modestly stimulating autophagy reduced the synaptic vesicle pool (Hernandez et al. 2012). Together with the finding that autophagosomes

contain synaptic vesicle proteins (Goldsmith et al. 2022), these results suggest that synaptic vesicles may be substrates for autophagic degradation in presynaptic terminals.

At post synaptic sites, autophagy participates to the degradation of different proteins including receptors and scaffolding proteins of dendritic spines (Shehata et al. 2012; Goldsmith et al. 2022; Kallergi et al. 2022). Furthermore, it has been suggested to play a role both in long-term potentiation (LTP) (Nikoletopoulou et al. 2017; Glatigny et al. 2019) and long-term depression (LTD) (Kallergi et al. 2022). For example, chemical induction of LTP stimulates autophagy which is required for the formation of new dendritic spines (Glatigny et al. 2019). At the same time, autophagy negatively regulates LTP potentially via degradation of postsynaptic scaffolding proteins (Nikoletopoulou et al. 2017). Moreover, induction of LTD by activation of NMDA receptors or metabotropic glutamate receptors triggers autophagosome formation in dendrites, and dendritic autophagy, in turn, promotes LTD (Kallergi et al. 2022). Thus, autophagy is emerging as a key modulator of synaptic plasticity with critical roles on both sides of the synapse.

V-ATPase at synapses

V-ATPase complex is expressed at high levels in neurons, where it plays additional and unique roles in neurotransmitter loading into SVs and into the regulation of synaptic transmission (Morel and Poea-Guyon 2015). In neurons, neurotransmitters are synthesized directly at the pre-synaptic terminal, where they are loaded into SVs by specific transporters and stored or released (Hnasko and Edwards 2012). V-ATPases are present in the membrane of every SV in one or two copies (Takamori et al. 2006) where they are responsible for the electrochemical proton gradient necessary for the activation of specific transporters for NTs (Michaelson and Angel 1980; Fuldner and Stadler 1982). Pharmacological inhibition of V-ATPase activity blocks neurotransmitter loading without affecting neurotransmitter release from already loaded vesicles (Poea-Guyon et al. 2013).

In addition to this central function, another role for V-ATPase has been proposed in SV fusion and neurotransmitter release (Morel et al. 2001). SV release involves SNARE proteins that associate in SNARE complexes. VAMP2, a v-SNARE protein present in the SV membrane, forms a trans-complex with two SNARE proteins of the presynaptic plasma membrane (t-SNAREs), namely syntaxin-1 and SNAP-25. This supercomplex provides the close proximity required for the fusion of vesicles with the presynaptic membrane (Sudhof 2013). Calcium influx triggers neurotransmitter release from docked and primed vesicles via the actions of additional proteins, namely synaptotagmins and complexins that bind to the SNARE complex and activate membrane fusion (Sudhof and Rothman 2009; Sudhof 2013).

First insights of the involvement of V-ATPase in this process were found in *Drosophila*. Loss of *Vha100-1*, the *Drosophila* orthologue of ATP6V0a1, led to vesicle accumulation in synaptic terminals together with a decrease in spontaneous release events. Remarkably, the levels of neurotransmitter loaded in SVs were not affected (Hiesinger et al. 2005). Interestingly, rapid and prominent decrease in neurotransmitter release was also observed in neurons upon photo-inactivation of the presynaptic ATP6V0a1 subunit (Poea-Guyon et al. 2013).

At nerve terminals, V-ATPase is present both on SV and pre-synaptic membrane. The V0 domain of the V-ATPase has been shown to interact with SNARE proteins, as VAMP2, and Ca2+/calmodulin (Di Giovanni et al. 2010; Wang et al. 2014). In particular, V-ATPase interaction with VAMP2 is selectively mediated by ATP6V0c-subunit and it persists when VAMP2 is engaged in a SNARE complex (Morel et al. 2003). The disruption of V0/VAMP2 interaction leads to inhibition of neurotransmitter release, supporting the hypothesis of a functional role of the V0 domain in synaptic fusion processes (Di Giovanni et al. 2010). The interaction of V0 domain with Ca2+/calmodulin occurs via a calmodulin-binding site in the ATP6V0a1-subunit (Zhang et al. 2008; Wang et al. 2014). By interacting with calmodulin, the subunit ATP6V0a1 can regulate the formation of SNARE complexes and so participate in the regulation of release events (Wang et al. 2014).

However, Bodzeta and colleagues provided direct evidence that V-ATPase is not part of the exocytic machinery, rather it modulates release upstream of docking to facilitate fusion of fully acidified, and hence neurotrasmitter-loaded, SVs (Bodzeta et al. 2017). Indeed, they propose that the V1 domain dissociates from the V0 before fusion starts and that this mechanism could represent the consensus for release, preventing the exocytosis of SVs that are empty or only partially filled with neurotransmitters (Bodzeta et al., 2017). These findings suggest that V-ATPase can sense luminal pH of SVs, as previously shown in non-neuronal cells (Hurtado-Lorenzo et al. 2006; Poea-Guyon et al. 2013). Interestingly, it is possible that this “pH-sensor” role takes part to the exo-endocytic cycle: when vesicles are fully acidified, it triggers the disassembly of the holoenzyme to stop proton pumping and allow for fusion, then the exposure to extracellular neutral pH recruits V1 domain to presynaptic membrane and SVs with fully assembled V-ATPase are endocytosed (Bodzeta et al. 2017).

In addition, it has been shown that V-ATPase activity on SVs can be modulated also by the clathrin coat that forms during endocytosis (Farsi et al. 2018). Indeed, newly endocytosed clathrin-coated vesicles contain the fully assembled complex of V-ATPase, which remains inactive until clathrin uncoating occurs (Farsi et al. 2018).

Altogether, these findings demonstrate that V-ATPase activity is tightly regulated in space and time at presynaptic terminals through its reversible disassembly and other possible accessory components of SV cycling machinery.

Role of V-ATPase in pathology

The central role of V-ATPase suggests that alterations in its functionality due to dysregulation or genetic mutations in V-ATPase subunit-encoding genes could lead to multiple diseases.

An important aspect is the existence of different isoforms of some V-ATPase subunits that determine a differential and cell/tissue-specific localization, and whose mutations are implicated in diverse human diseases:

- *ATP6V1B1*, *ATP6V0A4* and *ATP6V1C2* mutations: distal renal tubular acidosis (DRTA) and hearing loss (Stover et al. 2002, Jobst-Schwan et al. 2020);
- *ATP6V0A3* mutations: infantile malignant autosomal recessive osteopetrosis, characterized by abnormal bone remodelling, deficient haematopoiesis and neurological impairment (Frattini et al. 2000; Kornak et al. 2000);
- *ATP6V0A2*, *ATP6V1E1* and *ATP6V1A* mutations: autosomal recessive cutis laxa (CL), a systemic disorder with skin abnormalities and variable neurological and skeletal alterations (Fischer et al. 2012; Van Damme et al. 2017);
- *ATP6V1B2* mutations: Zimmermann-Laband syndrome (Kortum et al. 2015) and dominant deafness-onychodystrophy syndrome (DDOD) (Yuan et al. 2014).

Given the many roles of V-ATPase in neurons, alteration in V-ATPase function and genetic mutations have been associated to multiple neurological disorders. Many neurodegenerative diseases, including Alzheimer's disease (AD), Parkinson's disease (PD) and Huntington's disease (HD) share the specific phenotype of protein aggregates accumulation. Since the clearance of such biological products relies on the correct functioning of the endo-lysosomal degradative system and autophagy, it is not surprising that these diseases present an impaired V-ATPase function (Nah et al. 2015; Colacurcio and Nixon 2016; Bagh et al. 2017; Koh et al. 2019). For example, the AD-associated protein presenilin-1 (PS1) is required for proper glycosylation of the V-ATPase, which is necessary for its targeting to and acidification of the lysosome (Lee et al. 2010; Lee et al. 2015). Cells derived from AD patients with PS1 mutations showed impaired assembly of ATP6V0a1-containing V-ATPase holoenzymes on the lysosomal membrane and more alkaline lysosomes (Lee et al. 2010). Furthermore, V-ATPase disfunction was found associated with amyotrophic lateral sclerosis (ALS). ALS is mainly caused by mutations in genes encoding for ubiquilins (UBQLN2 and 4). In mice and human cells, UBQLN2 was shown to interact with ATP6V1G1 subunit and disruption of their interaction upon the loss of UBQLN2 leads to pH increase in autophagosomes paired with altered autophagy (Wu et al. 2020).

V-ATPase mutations have been linked also to neurodegeneration. Indeed, mutations in the accessory protein ATP6AP2, which is a fully-fledged part of the holoenzyme, result in impaired neuronal development and severe neurodegeneration (Dubos et al. 2015; Hirose et al. 2019). Both iPSC-derived neurons from a patient affected by *ATP6AP2* mutation and *Atp6ap2* knockdown in mice revealed altered lysosomal homeostasis with impaired protein degradation, possibly caused by decreased V-ATPase assembly (Hirose et al. 2019).

Emerging evidence correlates the altered function or expression of V-ATPase not only with neurodegeneration but also with impaired brain maturation. Indeed, mutations in V-ATPase subunits or regulatory proteins of the complex have been found in patients affected by neurodevelopmental disorders. In 2018, Fassio and colleagues described four *de novo* mutations in *ATP6V1A* gene in patients affected by developmental encephalopathy with epilepsy (Fassio et al. 2018). At neuronal level, *ATP6V1A* mutations alter lysosomal acidification leading to impaired neurite development and synaptic connectivity. Moreover, V-ATPase function was found altered also in patients affected by Ohthara Syndrome, a very severe early-onset epileptic encephalopathy (Esposito et al. 2019). Genetic screening revealed that patients carried mutation in *DMXL2* gene, which encodes for DMXL2 protein, also known as rabconnectin-3a, the homologue of yeast V-ATPase regulator RaV1p (Tata et al. 2014). In patients-derived cells, the loss of DMXL2 results in altered V-ATPase function with consequent impact onto lysosomal pH and autophagy process (Esposito et al. 2019). In neurons, silencing of *Dmxl2* generates the same phenotype, accompanied also by impaired neurite arborization and synaptic connectivity (Esposito et al. 2019). Interestingly, these findings propose a novel role for V-ATPase also in neuronal maturation, possibly through the regulation of lysosomal homeostasis and autophagy.

AIMS

The main aim of this project is to investigate on a novel role for TBC1D24 in neurons. TBC1D24 is a brain protein involved in neuronal maturation and synaptic function (Falace et al. 2014; Finelli et al. 2019; Lin et al. 2020), and it is mutated in a broad spectrum of neurodevelopmental diseases (Balestrini et al. 2016). The precise function of this protein and its correlation with pathology is still unclear. Recently findings proposed that TLDc domain-containing proteins, like TBC1D24, are interactors and regulators of the V-ATPase complex (Eaton et al. 2021). The goal of this project is to explore the interaction between TBC1D24 and the V-ATPase complex in brain cells and, employing a mouse model of chronic loss of *Tbc1d24*, to evaluate the impact of *Tbc1d24* loss on V-ATPase function, pH homeostasis and autophagy. Moreover, since both TBC1D24 and V-ATPase are present in synaptic terminals (Morel and Poea-Guyon 2015; Aprile et al. 2019; Finelli et al. 2019; Lin et al. 2020), the consequences of *Tbc1d24* loss in presynaptic pH regulation and autophagy were investigated.

Concurrently, another project involving V-ATPase was carried out in collaboration with Professor Guerrini's group (Azienda Ospedaliero Universitaria Meyer, Florence, Italy). The aim of this project is to evaluate the impact of *de novo* mutations in *ATP6V1A* gene described in patients affected by early onset epileptic encephalopathy and intellectual disability. Specifically, the effect of *ATP6V1A* mutations on protein stability and endo-lysosomal acidification was evaluated.

MATHERIALS and METHODS

Animal model and genotyping

Mouse model of chronic loss of *Tbc1d24* was generated by our collaborator Peter Oliver at the Medical Research Council Harwell Institute (Oxford, UK). Briefly, using CRISPR/Cas9 strategy, a 2-nucleotide mutation was inserted in exon 2 of *Tbc1d24* sequence that leads to a frameshift mutation generating a stop codon and a null allele. The homozygous mutation is lethal at embryonic level, so heterozygous (HET) mice were bred and mated to obtain Wild Type (WT), HET and Knock-Out (KO) embryos. The day of preparation (E15-16), genomic DNA was isolated from tails of embryos, and they were individually genotyped with the polymerase-chain reaction (PCR) technique as described in the section "**B. Genotyping PCR and purification**".

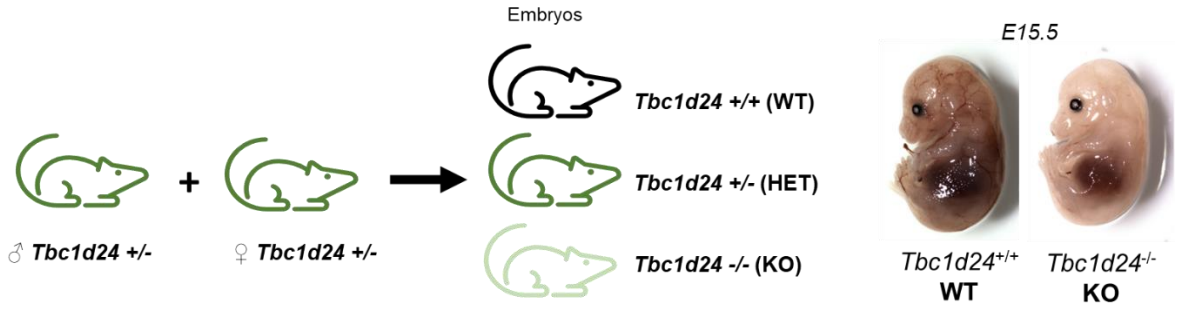

Figure 7. How to obtain WT and KO embryos. The cartoon illustrates the mating scheme and a representative picture of WT and KO embryos for *Tbc1d24*.

A. DNA extraction and quantification

Embryonic tails were collected and incubated in 100 µL of lysis buffer (Tris-HCl pH 7.5 0.1 M, EDTA 5 mM, SDS 0.2%, NaCl 0.2 M) supplemented with Proteinase K (1:50, Sigma, #P4850) overnight at 37°C. The day after, 60 µL of NaCl 5M were added, samples were vortexed and centrifuged at maximum speed for 10 minutes. The supernatant was collected and transferred into a new tube, mixed with equal volume of 100% ethanol and mixed by inversion for few times. Samples were centrifuged at maximum speed for 5 minutes and the supernatant was discharged. Pellets were resuspended with 70% ethanol and centrifuged at maximum speed

for 5 minutes. The supernatant was discharged, pellets were left dry for few minutes and resuspended in DNAse/RNAse free water (Invitrogen, #10977-035). DNA was quantified at NanoDrop Spectrophotometer (Marshall Scientific, #ND-1000) and used for PCR.

B. Genotyping PCR and purification

The PCR mix (20 µL) was obtained by mixing DNA (50 ng) and the specific primers (1 µM, F1 5'-3': GGAAAGTGTACCAGCGCCT; R1 5'-3': CATCGCTGCCAGTCAGAGTAG) with Master Mix (Phire™ Tissue Direct PCR Master Mix, Thermo-Fisher Scientific, #F-170S), which contains Taq DNA Polymerase, coloured dyes, $MgCl_2$ and dNTPs. The PCR amplifies a strand of about 300 bp. Genomic DNA amplified by the PCR was purified with the QIAquick PCR Purification Kit (Qiagen, #28106) according to manufacturer instruction. Purified PCR was resuspended in 40 µL of Elution Buffer and used for the enzymatic digestion.

C. Enzymatic digestion

Enzymatic digestion of purified PCR fragments was performed with BbvI/BseXI enzyme (Thermo-Fisher Scientific, #ER1452), which cuts in the middle of the amplified strand. The digestion mix (40 µL) was obtained by mixing purified PCR (20 µL) with 6 units of enzyme and the specific buffer (Thermo-Fisher Scientific #B31). Digestion was run overnight at 65°C and, at the end of digestion, enzyme was inactivated for 20 minutes at 80°C. Digestion production was run on a 2% agarose gel prepared by dissolving agarose (Invitrogen, #16500-500) in Tris Acetate-EDTA (TAE) Buffer (Tris 40 mM, EDTA pH 8 1 mM, acetic acid 20 mM, pH 8.5) and EuroSafe (EuroClone, #EMR440001,) at a final concentration of 0.1 µg/mL. The samples were prepared by adding Loading Buffer (Promega, #G190A) at a final concentration of 1X**,** loaded into the agarose gel and electrophoresed at 80 V in TAE Buffer. At the end of the run, the DNA fragments were visualized using Chemidoc transilluminator (BioRad). The embryos from which the isolated genomic DNA contain the bands corresponding to the molecular weight of 300 bp are wild type, instead to 300 and 150 bp are heterozygous, and to 150 bp are the homozygous mutants.

Cell culture, transfection and infection

A. Mouse cortical and hippocampal primary neurons

Cortical and hippocampal primary neurons from *Tbc1d24* chronic loss mouse model were derived from embryos at E15-16. Each embryo was treated independently. Cortices and hippocampi were dissected under a stereomicroscope in ice-cold HBSS. Cortices were incubated for 15 minutes while hippocampi for 10 minutes with 0,25% trypsin (Gibco) at 37°C. Then, trypsin was replaced with Neurobasal medium (Gibco, 1X) supplemented with 10% Fetal Bovine Serum (FBS, Gibco), 1% GlutaMAX (Gibco) and 1% Penicillin-Streptomycin (Gibco). The digested tissues were mechanically dissociated, cells were counted and plated on 25 mm coverslips or Petri dishes coated with Poly-L-Lysine (0.1 mg/mL for Petri dishes and 1 mg/mL for coverslips). After at least 2 hours from plating, the medium was replaced with new Neurobasal medium supplemented with B27 (Gibco, 1X), 1% GlutaMAX (Gibco) and 1% penicillin-streptomycin (Gibco) (hereby, complete Neurobasal medium). Cultures were maintained in a 5% CO_2 humidified incubator at 37°C.

B. Fibroblasts

Fibroblasts were derived from skin biopsies for Patients 1, 2, 16, 18 and controls matched for sex and age at biopsy. Fibroblasts were cultured in RPMI 1640 medium (Life Technologies) supplemented with 20% FBS, 1% GlutaMAX and 1% Penicillin/Streptomycin in a 5% CO_2 humidified incubator at 37°C.

C. COS7

COS7 cells for pulldown and co-immunoprecipitation experiments were grown in Advanced DMEM (Life Technologies) supplemented with 10% FBS, 1% GlutaMAX and 1% Penicillin/Streptomycin (hereby, complete A-DMEM medium) in a 5% CO_2 humidified incubator at 37°C.

D. Cell transfection

For pulldown experiments, COS7 cells were transfected with the following vectors: p3xFLAG-TBC1D24 (FLAG-TBC1D24), p3xFLAG-BAP (FLAG-BAP) and p3xFLAG (FLAG). For co-immunoprecipitation experiments, transfection was performed with the following pairs of vectors: FLAG-TBC1D24 + HA-ATP6V1B2, FLAG-TBC1D24 + untagged ATP6V1A, FLAG-ATP6V1B2 + pCAGG-hTBC1D24-GFP, FLAG-ATP6V1A + pCAGG-hTBC1D24-GFP. FLAG-BAP was used as negative control in each pair.

The day before transfection, $3x10^6$ cells were plated on 60mm Petri dishes in complete A-DMEM medium. The day of transfection the complete medium was replaced with culture medium without supplements 1 hour before the transfection. For each Petri dish, the transfection buffer was prepared as follows: 4 µL of polyethyleneimine (PEI) were diluted in 36 µL of water and mixed with a solution containing 6 µg of cDNA in 200 µL of culture medium without supplements for 10 minutes. The transfection reaction was added to the cells for 1 hour and 30 minutes in a 5% CO_2 humidified incubator at 37°C. Then, the transfection solution was removed and replaced with complete fresh A-DMEM medium.

For colocalization experiments, hippocampal neurons at 12 days *in vitro* (DIV) were cotransfected with TBC1D24-mCherry and ATP6V1B2-eGFP vectors. For Lysotracker experiments, hippocampal neurons were transfected at 10 DIV with pCAGG-GFP and pCAGG-hTBC1D24-GFP vectors. The transfection was performed using Lipofectamine 2000 (Invitrogen). For each well, the transfection buffer was prepared as follows: 1 µL of Lipofectamine was diluted in 45 µL of Neurobasal medium without supplement and incubated for 5 minutes at room temperature. Then, 0.1 µg of cDNA was diluted in 45 µL of Neurobasal medium without supplement and mixed with the Lipofectamine solution for 20 minutes. Immediately before transfection, the conditioned Neurobasal medium of cells was removed, stored and replaced with 210 µL/well of fresh Neurobasal medium without supplement. The transfection solution was added to the cells and left for 30 minutes in a 5% CO_2 humidified

incubator at 37°C. Then, the transfection solution was removed and replaced with 2 mL of conditioned Neurobasal medium. Experiments were performed after 2 days.

E. Cell infection

a. Virus production: HEK293T cells at low passage were plated onto 15 cm plates ($4*10^6$ cells/plate) and maintained in Iscove's Modified Dulbecco's Medium supplemented with 10% FBS and 1% GlutaMAX (hereby complete medium) in a 5% CO_2 humidified incubator at 37°C. Cells were transfected using the calcium phosphate method with the following lentiviral plasmids: pREV and pMDL packaging plasmids, VSVG envelope plasmid, pADV enhancer of protein expression plasmid and lentiviral plasmids encoding for transgenes of interest, in particular pLenti-PGK-sypHyGFP for synaptophysin-pHluorin and FU-Syp-mCherry-P2A-eGFP-LC3 (Hoffmann et al. 2019) for synaptic autophagy. The transfection medium was replaced with fresh medium after 16 hours. After 48 hours of transfection, supernatant of cells was collected and centrifuged at 1000 rpm for 3 minutes at 4°C to remove cell debris, passed through a 0.45 µm filter and ultracentrifuged for 2 hours at 20000 xg at 4°C. After ultragentrifugation, the supernatant was discharged and viral pellets resuspended in PBS, aliquoted and stored at -80°C until use.

b. Virus titration: to determine viral particles concentration, HEK293T were plated in a 6-well plate (10^5 cells/well) in complete medium. The day after, the following serial dilutions were prepared:

- 10^{-3} (dilute 2 µL of viral preparation in 2 mL of medium)
- 10^{-4} (dilute 200 µL of 10^{-3} in 1.8 mL of medium)
- 10^{-5} (dilute 200 µL of 10^{-4} in 1.8 mL of medium)
- 10^{-6} (dilute 200 µL of 10^{-5} in 1.8 mL of medium)
- 10^{-7} (dilute 200 µL of 10^{-6} in 1.8 mL of medium)

The medium was removed from the wells and substituted with serial dilutions. One well was kept non-infected to be used as a control.

After 72 hours of infection, samples were prepared for titre measurement with FACS sorting as follows. The medium was removed, cells were rinsed with 1 mL of warm PBS and incubated with Tryple (Thermo-Fisher Scientific, #12604013) for 3 minutes in a 5% CO_2 humidified incubator at 37°C. Then, cells from each well were collected in 2 mL of complete medium in falcon tubes and centrifuged at 1000 xg for 5 minutes. Supernatants were discharged, pellets were resuspended in 2 mL of warm PBS flickering the tube and washed for 5 minutes protected from light. Cells were pelleted by centrifugation for 5 minutes at 1000 xg and fixed by adding 1 mL for each tube of 4% paraformaldehyde (PFA) in PBS for 15 minutes protected from light. After fixation, cells were rinsed with PBS and centrifuged at 1000 xg for 5 minutes (three times). Finally, cells were resuspended in 100 µL of PBS, transferred to FACS compatible tubes and kept at 4°C protected from light until FACS analysis (performed within the same day).

c. Infection: Both for pHluorin and synaptic autophagy experiments, hippocampal neurons were infected at 14 DIV and analysed at 17-19 DIV. The day of infection, 800 µL of the conditioned medium was collected from each well, mixed with equal volume of fresh complete Neurobasal medium and stored at 4°C (conditioned medium). Viral particles were diluted in 400µL/well of complete Neurobasal medium and added to the cells maintained in a 5% CO_2 humidified incubator at 37°C for the next 18-20 hours. At the end of the incubation, the infection medium was removed and replaced with the conditioned one.

Biochemical experiments

A. Protein extraction and quantification

For quantitative analysis of protein expression, both fibroblasts and neurons at 12 DIV were placed on ice and washed 3 times with cold PBS. Protein lysates were extracted using the following lysis buffer: 50 mM Tris (pH 7.4), 150 mM NaCl, 1 mM EDTA, 1% Triton X-100,

protease inhibitor cocktail (Cell Signalling, #5871). Lysates were centrifuged at 12000 rpm for 15 minutes at 4°C. The supernatant was collected in a clean tube, quantified and stored at -20°C. Protein concentration was calculated by performing BCA Protein Assay with a commercial kit (ThermoFisher, #23228) following the manufacturer instruction.

B. Western blot

a. Sample Preparation: protein lysates were mixed with Laemmli Sample buffer [according to (Laemmli 1970)]. Samples were boiled at 99°C for 5 min to allow protein denaturation and reduction of disulphide bonds.

b. SDS-PAGE: Samples were loaded in a polyacrylamide gel made by a separating (25% 1.5 M Tris HCl pH 8.8, 8-12% Acrylamide, 0.1% SDS, 0.1% ammonium persulfate, 0.01% TEMED) and a stacking gel (25% 0.5 M Tris HCl pH 6.8, 3% Acrylamide, 0.1% SDS, 0.1% ammonium persulfate, 0.01% TEMED). The electrophoretic runs were performed at 80-110 V in Tris/Glycine/SDS buffer (BioRad, #1610732) using an electrophoresis chamber (BioRad). To follow the separation of proteins at different molecular weights, a pre-stained molecular weight marker was loaded in parallel to the samples (Thermo-Fischer Scientific, #26619).

c. Western blot: At the end of the run, proteins were transferred from the acrylamide gel to a 0.2 µm nitrocellulose membrane (Amersham, #10600001) in Transfer Buffer (25 mM Tris HCl, 190 mM glycine pH 8.3, 20% methanol) for 2.5 hours at 350 mA or overnight at 40 mA at 4°C. The occurring of the transfer reaction and an approximate equal loading of protein in each lane were determined by a brief staining of the membrane with 0.1% Ponceau (0.1% Poinceau, 7% trichloroacetic acid). Membranes were washed in Tris-Buffered Saline (TBS) (200 mM NaCl, 50 mM Tris HCl, pH 7.4) supplemented with 0.1% Triton X-100 (TBS-T) and blocked for 1 hour in 5% non-fat dry milk diluted in TBS-T. Then, membranes were incubated with primary antibodies diluted in blocking buffer for 3 hours at room temperature or overnight at 4°C. After the incubation with primary antibodies, membranes were washed three times (5 minutes each) with TBS-T and incubated with corresponding peroxidase-conjugated secondary antibodies for

1 hour at room temperature. Then, membranes were rinsed three times with TBS-T (10 minutes each) and incubated with the ECL substrate (BioRad, #170-5061) for 30 seconds/1 minute. Proteins' signals were acquired using Chemidoc (BioRad) and the densitometric analysis of immunoreactive bands was performed with the ImageLab software. Primary and secondary antibodies for Western blot were used at the indicated concentration: ARF6 1:1000 (Sigma, #A5230), ATP6V0a1 1:2000 (Novus, NBP1-89342), ATP6V1A 1:1000 (Abcam, #ab137574), ATP6V1B2 1:2000 (Abcam, #ab73404), FLAG 1:1000 (Sigma, #F7425), GAPDH 1:5000 (Cell Signalling, #2113), NaK3/ATP1A3 1:2000 (Invitrogen, #MA3-915), LAMP1 1:1000 (Abcam, #ab24170), TBC1D24 1:1000 (Novus, #NBP1-82925), Vinculin 1:200 (Sigma, #V4505), goat anti-rabbit HRP conjugate 1:3000 (BioRad, #170-6515), goat anti-mouse HRP conjugate 1:5000 (BioRad, #170-6516).

C. Pulldown and co-immunoprecipitation

a. COS7 cells: COS-7 cells were transfected as previously described (see **D. Cell transfection** section). After 24 hours, cells were harvested in lysis buffer and centrifuged at 10000 x g for 10 minutes at 4°C. Kept an aliquot for input, the supernatant was incubated with anti-FLAG® M2 Affinity Gel (Sigma-Aldrich, #A2220) following the manufacturer guidelines. FLAG-tagged protein pulldown and co-immunoprecipitated proteins were evaluated by Western blot with anti-FLAG, anti-ATP6V1B2, anti-ATP6V1A and anti-TBC1D24 antibodies.

b. Brain: For pulldown of endogenous TBC1D24 from brain lysates, the Pierce Crosslink Immunoprecipitation Kit (Thermo Fisher Scientific) was used as specified by the manufacturer. Antibody against TBC1D24 was coupled to the Pierce Protein A/G Plus Agarose for 1 hour, and then crosslinked to the resin using the DSS crosslinker (2.5 mM in DMSO) for 1 hour. Subsequently, 500–1000 µg of brain lysates were incubated on the column overnight at 4 °C. Immunoprecipitated TBC1D24 and co-immunoprecipitated proteins were evaluated by Western blot with anti-ATP6V1B2, anti-ATP6V1A and anti-TBC1D24 antibodies.

D. Subcellular fractionation

For cytosol/membrane fractionation experiments, neurons at 12 DIV were placed on ice and washed three times (5 minutes each) with cold PBS. Neurons were then scraped into homogenization buffer (250 mM sucrose, 1 mM EDTA) supplemented with protease inhibitor cocktail (Cell Signalling, #5871) and phosphatase inhibitor cocktail (Cell Signalling, #5870). Homogenate was collected, homogenized 8-10 times through a 29 g syringe needle and centrifuged at 500 xg for 10 minutes at 4°C to remove intact cells and nuclei. The supernatant was collected and ultracentrifuged at 45000 rpm for 30 minutes at 4°C to pellet the membrane fraction. After ultracentrifugation, the supernatant was collected in a clear tube (cytosolic fraction), quantified and stored at -20°C. The pellet was rinsed 3 times, resuspended with the homogenization buffer (membrane fraction), quantified and stored at -20°C. The cytosolic and membrane fractions were then separated by SDS-PAGE. The quality of subcellular fractionation and the distribution of V-ATPase subunits were evaluated by Western blot using anti-Vinculin (cytosolic marker), anti-NaK3 (membrane marker), anti-ATP6V1A, anti-ATP6V1B2 and anti-ATP6V0A1 antibodies (see **B. Western blot)**.

E. ARF6 Activation Assay

ARF6 activation state was determined using a commercial kit for specific pulldown of ARF6-GTP (Cytoskeleton, #BK033-S), according to manufacturer's instructions. Total lysates and pulled-down fractions were then separated by SDS -PAGE and the levels of ARF6-GTP and total ARF6 were evaluated by Western blot using an anti-ARF6 antibody (see **B. Western blot**).

Immunocytochemistry and Live Imaging experiments

A. Immunofluorescence and immunocytochemistry

For colocalization experiments in neurons, cells were transfected as described previously. After 48 hours from transfection, neurons were washed with PBS at 37°C to remove culture medium and fixed in 4% PFA + 4% sucrose in PBS for 15 minutes at room temperature. Excess of PFA was removed by washing three times (5 minutes each) with PBS and coverslips were immediately mounted with ProLong Gold Antifade Mountant with DAPI (Thermo-Fisher Scientific, #P36935). Z-stack images of neurons positive for both overexpressed proteins were taken with a confocal microscope (SP8, Leica) using 63x oil-immersion objective. Pearson's coefficient was calculated in each focal plane in total cell area using the plugin JACoP of ImageJ software.

For immunocytochemistry experiments, both fibroblasts and neurons (12-18 DIV) plated on glass coverslips were fixed as described before. After fixation, cells were permeabilized with 0.1% Triton X-100 in PBS for 10 minutes at room temperature. Then, coverslips were incubated with blocking solution (5% FBS in PBS) for 30 minutes. Primary antibodies were diluted in blocking solution and incubated for 1 hour at room temperature or overnight at 4°C. Coverslips were washed three times (5 minutes each) with PBS and incubated for 1 hour at room temperature with fluorescent secondary antibodies diluted in blocking solution. For fibroblasts, Alexa Fluor 546 Phalloidin (1:40, Thermo-Fisher Scientific, #A22283) was incubated together with secondary antibodies. Finally, coverslips were washed three times (5 minutes each) with PBS and mounted with ProLong Gold Antifade Mountant with DAPI. Primary and secondary antibodies for immunocytochemistry were used at the following concentrations: LAMP1 1:200 (Sigma, #L1418), MAP2 1:200 (Sigma, #M9942), LC3B 1:100 (Sigma, #L7543), p62 1:200 (Sigma, #P0067), Alexa Fluor 488 1:500 (Thermo-Fisher Scientific, #A11029), Alexa Fluor 647 1:500 (Thermo-Fisher Scientific, #A21450).

B. Lysotracker Deep Red Experiments

The LysoTracker and LysoSensor probes are molecules that enter the cells and once they are in the acidic organelles, they become protonated at their weak base side chain. This protonation leads to the retaining of the probe into the organelles and de-quenches the fluorescence of the dye. Given the acidic nature of organelles belonging to the endo-lysosomal pathway, LysoTracker and LysoSensor probes can be used to analyse the acidification and pH of such structures.

Fibroblasts plated on glass coverslips were incubated with 200 nM Lysotracker Deep Red (LTR, Life Technologies, #L12492) for 1 hour in culture medium at 37°C in a humidified atmosphere with 5% CO_2. Cells were immediately fixed as described before, stained with Phalloidin and coverslips were mounted with ProLong Gold Antifade Mountant with DAPI.

Neurons at 10 DIV were transfected as described before. The day of the experiment, neurons were incubated with 100 nM LTR for 30 minutes in culture medium at 37°C in a humidified atmosphere with 5% CO_2, immediately fixed as described before and coverslips were mounted with ProLong Gold Antifade Mountant with DAPI.

Both fibroblasts' and neurons' coverslips were analysed within 12 hours to prevent LTR signal decay. Images were taken with a confocal microscope (SP8, Leica) using 63x oil-immersion objective.

C. LysoSensor Experiments

Two different types of LysoSensor were used: LysoSensor yellow/blue dextran (Thermo-Fisher Scientific, #L22460) that enters the cells through endocytosis and LysoSensor yellow/blue DND-160 (Thermo-Fisher Scientific, #L7545) that passively permeates cellular membranes. The ratiometric nature of these dyes is due to a double excitation and emission spectra depending on the pH of the environment: in acidic organelles they have predominantly yellow fluorescence (exc: 381nm, emi: 521nm), and in less acidic organelles the have blue

fluorescence (exc: 335nm, emi: 452nm) (**Figure 8**). The ratio of fluorescence at the two excitation wavelengths (340/380 nm) is directly proportional to pH.

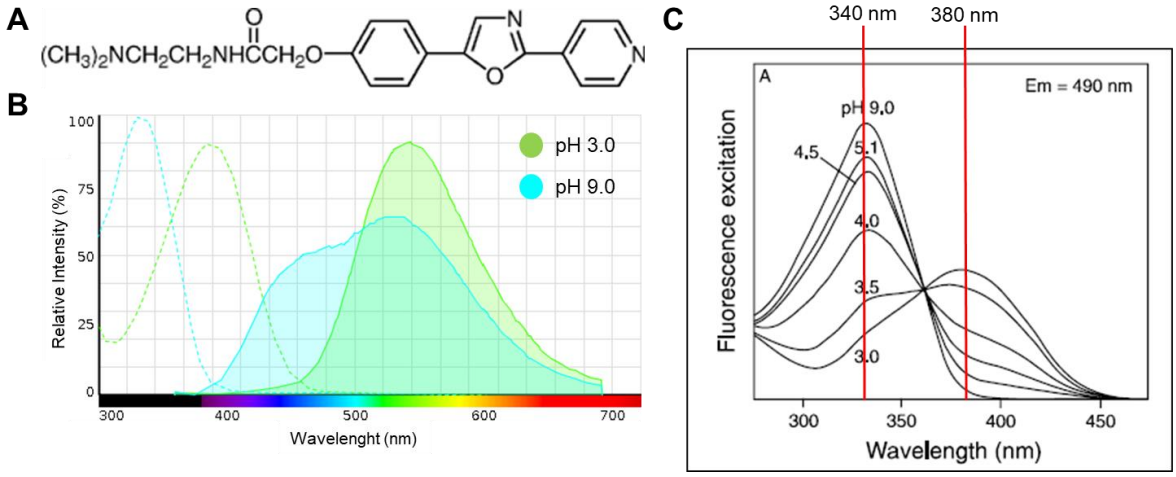

Figure 8. The ratiometric nature of LysoSensor Yellow/Blue. A) representation of LysoSensor molecule; B) excitation and emission spectra of the dye; C) the pH-dependent spectral response of LysoSensor Yellow/Blue with double-excitation and single emission.

To measure the pH of endo/lysosomal compartments, fibroblasts plated on glass coverslips were incubated overnight with 0.1 mg/mL LysoSensor Yellow/Blue dextran in complete medium at 37 °C in a humidified atmosphere with 5% CO_2. Cells were then washed in complete fresh medium for 1 hour and live imaged in acquisition buffer (125mM KCl, 25mM NaCl, 25mM HEPES, pH 7.4) with double excitation at 340 ± 10 nm or 380 ± 10 nm and single emission using a 400 nm long-pass filter at epifluorescence microscope (Olympus 1X81, 60x oil-immersion objective). A pH calibration curve was then performed for each experimental group on the day using MES buffers supplemented with 10 µM Monensin and 10 µM Nigericin at defined pH values (125 mM KCl, 25 mM NaCl, 25 mM MES – pH 6.5, 6.0, 5.5, 5.0, 4.5, 4.0, 3.5). Images of samples were acquired with double excitation at 340 ± 10 nm or 380 ± 10 nm and single emission using a 400 nm long-pass filter at epifluorescence microscope (Olympus 1X81, 60x oil-immersion objective). LysoSensor ratios (340/380 nm) were calculated from background subtracted images. To generate the pH calibration curve, ratios at the different pH values were fitted to a linear regression with the GraphPad Prism6 software. For pH

calculations, experimentally measured sample ratios were converted into absolute pH values by interpolation in the respective calibration curve (**Figure 9**).

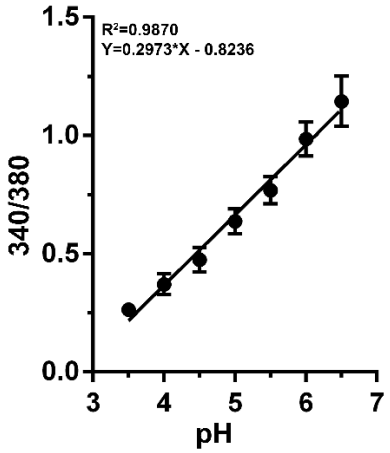

Figure 9. Representative calibration curve of LysoSensor Yellow/Blue dextran.

Neurons at 12 DIV plated on glass coverslips were incubated for 3 minutes with 10 µM LysoSensor Yellow/Blue DND-160 in complete medium at 37 °C in a humidified atmosphere with 5% CO_2. Cells were then washed in Tyrode's solution (140 mM NaCl, 2.5 mM KCl, 10 mM HEPES, 10 mM glucose, 2 mM $CaCl_2$, 1 mM $MgCl_2$, pH 7.4) and live imaged with double excitation at 340 ± 10 nm or 380 ± 10 nm and single emission using a 400 nm long-pass filter on an epifluorescence microscope (Olympus 1X81, 60x oil-immersion objective). LysoSensor ratios (340/380 nm) were calculated from background subtracted images.

D. Synaptic autophagy evaluation

For the synaptic autophagy evaluation, the FU-Syp-mCherry-P2A-eGFP-LC3 lentivirus was used. The lentiviral construct allows the co-expression of mCherry-tagged Synaptophysin (syp-mCherry) and eGFP-tagged LC3 (eGFP-LC3). The presence of the self-cleaving small peptide P2A between the coding sequences for the two proteins leads to the cleavage of the initially fully-transcribed fusion protein at post-translational level. Thus, the final localization of syp-mCherry and eGFP-LC3 is completely independent. Neurons were infected at 14 DIV with FU-Syp-mCherry-P2A-eGFP-LC3 lentivirus and analyzed at 17-19 DIV after fixation. Images of

neurons consisted of a stack of images taken through the z-plane of the cells. Z-stacks of neurons were taken with a confocal microscope (SP8, Leica) using 63x oil-immersion objective. Settings were kept constants for all acquisitions within each experiment. The counting of synapses positive for LC3 was performed by colocalization analysis between syp-mCherry and eGFP-LC3 signals. Colocalization puncta with areas of 0.1-2 μm^2 were considered *bona fide* synapses. To evaluate the abundance of LC3 within synaptic terminals, ROIs of 2 μm^2 were drawn on random syp-mCherry positive puncta and the average fluorescence intensity of eGFP-LC3 was measured.

E. Synaptophysin-pHluorin experiments

Neurons at 17-19 DIV were maintained in Tyrode's solution supplemented with 10 µM 6-cyano-7-nitroquinoxaline-2,3-dione (CNQX) and 50 µM d-2-amino-5-phosphonovaleric acid (D-AP5) into an imaging chamber (~200 µL volume; Quick Exchange Platform; Warner Instruments) through a laminar flow perfusion system. To evaluate SV pH, the protocol was adapted from the one described by Egashira and colleagues (Egashira et al. 2016). Prior to performing the SV pH protocol, neurons were stimulated with a KCl-rich solution (50 mM KCl, 92.5 mM NaCl, 10 mM HEPES, 10 mM glucose, 2 mM $CaCl_2$, 1 mM $MgCl_2$, 10 µM CNQX and 50µM d-APV, pH 7.4) in order to identify active synapses. Briefly, neurons were recorded in Tyrode's solution for 10 seconds (baseline), KCl solution was perfused for 20 seconds and then washed out with Tyrode. After 1 minute of recovery, the SV pH protocol was performed as follow:

- 10 second of basal recording in Tyrode's;
- 15 seconds of acidic quench in MES solution pH 5.5 (140 mM NaCl, 2.5 mM KCl, 10 mM MES, 10 mM glucose, 2 mM $CaCl_2$, 1 mM $MgCl_2$, 10 µM CNQX and 50 µM d-APV);
- 15 seconds of recovery in Tyrode's;
- 15 seconds of total fluorescence recording in ammonium-rich solution (50 mM NH_4Cl, 90 mM NaCl, 2.5 mM KCl, 10 mM MES, 10 mM glucose, 2 mM $CaCl_2$, 1 mM $MgCl_2$, 10 µM CNQX and 50µM d-APV, pH 7.4);
- 30 seconds of final recovery in Tyrode's.

For F_0 and F_{max} evaluation, fluorescence from basal recording and ammonium-rich solution application were used, respectively.

The observed fluorescence of sypHy in a specific terminal derives both from the surface fraction of the probe (S) that is exposed to the extracellular pH and from its vesicular fraction (1-S) that experiences SV pH. S can be calculated as described in the following formula:

$S = \frac{\frac{F0}{Fmax} - \frac{Fmes}{Fmax}}{1 - \frac{FpH5.5}{FpH7.4}}$, where F_0 is basal fluorescence, F_{mes} is fluorescence during acidic quenching and F_{max} is fluorescence during application of ammonium-rich solution. $\frac{FpH5.5}{FpH7.4} = \frac{\frac{1}{1+10^{nHx(pKa-5.5)}}}{\frac{1}{1+10^{nHx(pKa-7.4)}}}$ is a theoretical value derived from the Henderson–Hasselbalch equation and was calculated as in the formula, where the pKa value of sypHy was 7.1 and the nH value (Hill coefficient) was 1.35 (Egashira et al. 2015). Then, S was used to calculate the fluorescence intensity relying on SV luminal pH (F_{pHv}), as shown in the following formula: $\frac{FpHv}{Fmax} = \frac{\frac{F0}{Fmax} - S}{1 - S}$. Finally, F_{pHv} was used to calculate SV pH (pHv) using the following formula:

$$pHv = pKa - \frac{\log\left(\frac{1+10^{nHx(pKa-7.4)}}{\frac{FpHv}{Fmax}} - 1\right)}{nH}.$$

Statistical Analysis

The statistical analysis was performed with GraphPad Prism 6 software and it is described in the figure legends. All data were tested for normality (D'Agostino & Pearson test for n≥8) and outliers (ROUT test) before performing statistical tests.

RESULTS

Part 1

TBC1D24 interacts with ATP6V1B2 and ATP6V1A subunits of V-ATPase.

Recently, Merkulova and colleagues mapped the interactome of the V1B1 subunit of V-ATPase in kidney tissue using proteomic analysis. Among the interactors, they found some TLDc-domain containing proteins such as NCOA7, OXR1 and TBC1D24 (Merkulova et al. 2015; Eaton et al. 2021). ATP6V1B1 is the specific isoform of the kidney, while B2 isoform is ubiquitous and the only one present in the brain. Since *TBC1D24* is highly expressed in the brain and mutations in its sequence are mainly related to brain diseases (Balestrini et al. 2016), we investigated if TBC1D24 could interact with V1B2 and other subunits of V-ATPase complex in brain tissue. We performed preliminary pulldown experiments in COS-7 transfected with FLAG-tagged form of human TBC1D24 (**Figure 10,** A, FLAG panel, 70 kDa); BAP-FLAG (**Figure 10**, A, FLAG panel, 55 kDa) and FLAG only resins were used as negative controls. By immunoblotting we revealed the specific immunoprecipitation of endogenous Atp6v1b2 and its molecular partner Atp6v1a (**Figure 10**, A). To confirm the interaction, we also performed co-immunoprecipitation experiments in COS-7 cells overexpressing FLAG-tagged form of TBC1D24 together with HA-tagged ATP6V1B2 or untagged ATP6V1A. In the reverse experiments we employed FLAG-tagged ATP6V1A or ATP6V1B2 with untagged TBC1D24. With all the different combinations of overexpressed proteins, we confirmed the interaction of TBC1D24 with the two main subunits of the V1 domain of V-ATPase (**Figure 10**, B). Given the predominant expression and function of TBCD14 in the brain, we were interested in investigating the TBC1D24/V-ATPase interaction also in this tissue. Thus, we immunoprecipitated endogenous Tbc1d24 from total mouse brain lysates and we found the co-immunoprecipitation of both endogenous Atp6v1b2 and Atp6v1a proteins confirming the interaction of endogenous proteins in brain tissue (**Figure 10**, C). Moreover, we performed colocalization experiments in neurons. Since the lack of reliable antibodies for Tbc1d24 for

immunostaining in neurons, we co-expressed mCherry-tagged TBC1D24 and eGFP-tagged ATP6V1B2. The analysis of fluorescent signals revealed a high degree of colocalization of the two proteins as quantified by Pearson's coefficient (**Figure 10**, D).

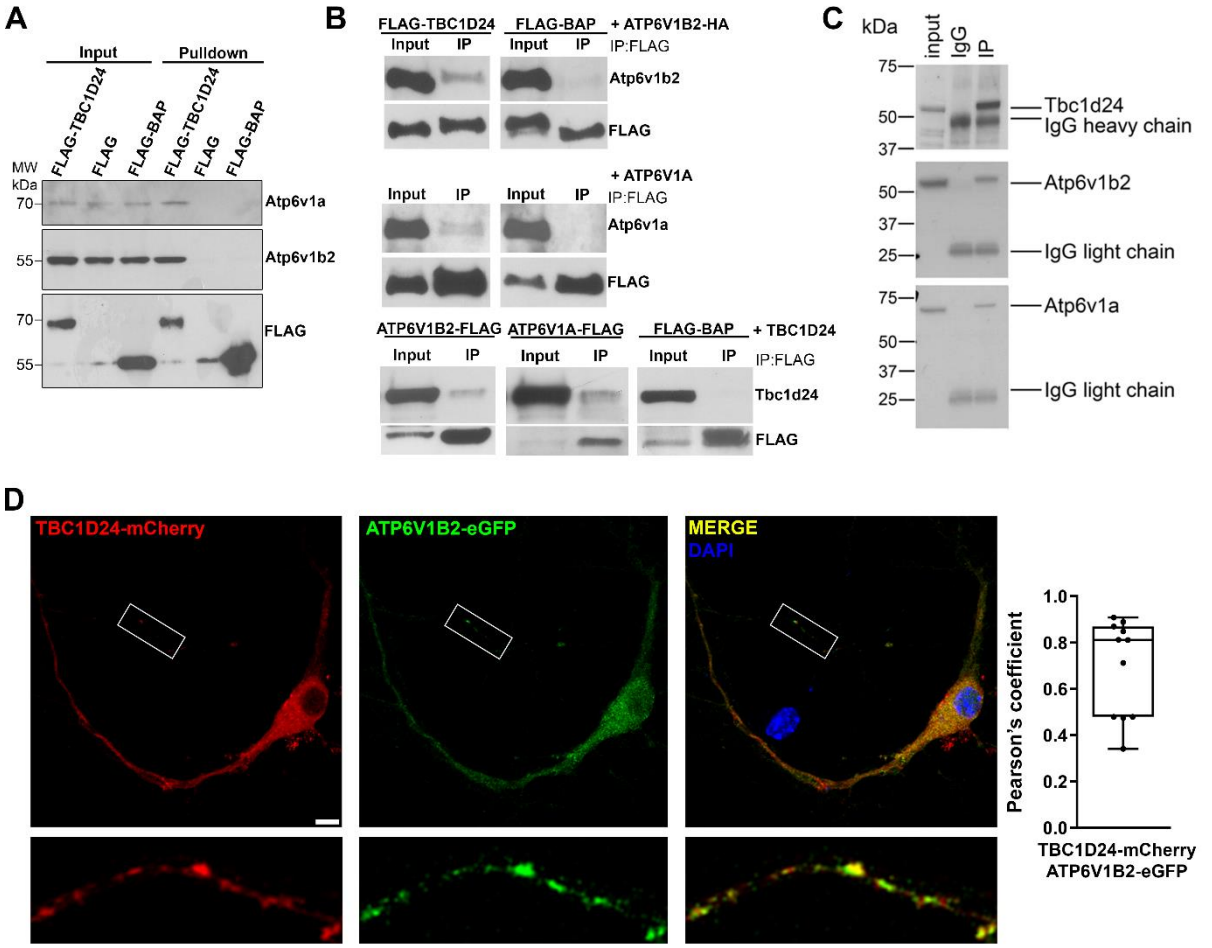

Figure 10. TBC1D24 interacts with the A and B2 subunits of the V1 domain of V-ATPase. A) Western blot showing pulldown of endogenous Atp6v1a and Atp6v1b2 by TBC1D24-FLAG in COS-7 cells; B) Western blot showing co-immunoprecipitation experiments performed in COS-7 cells transfected with FLAG-TBC1D24 + ATP6V1B2-HA/ATP6V1A vectors and ATP6V1B2/ATP6V1A-FLAG + TBC1D24. For A) and B) FLAG-BAP was used as negative control and anti-FLAG antibody was used to verify the correct immunoprecipitation of overexpressed proteins; C) Western blot showing pulldown of endogenous Atp6v1a and Atp6v1b2 by endogenous Tbc1d24 from total brain lysates of mouse embryos. Specific IgG against Tbc1d24 were used as negative controls; D) *left*, representative images of neurons at 14 DIV transfected with mCherry-tagged TBC1D24 and eGPF-tagged ATP6V1B2. White rectangles indicate regions shown at high magnification (bottom). Scale bar: 10µm; *right*, graph shows the colocalization rate between TBC1D24-mCherry and ATP6V1B2-eGFP signals expressed by Pearson's coefficient. Data are mean ±SEM from n=11 neurons.

Chronic loss of *Tbc1d24* results in the impairment of intracellular organelles' acidification and abundance.

To determine the relevance of the interaction between TBC1D24 and V-ATPase and the role of TBC1D24 in V-ATPase function in brain cells, we employed a mouse model of *Tbc1d24* chronic loss, generated in the group of Peter Oliver (MRC Harwell Institute, Oxford, UK) using CRISPR/Cas9 strategy. Two nucleotides were introduced in *Tbc1d24* exon 2 that resulted in a frameshift mutation generating a premature stop codon and a null allele. The homozygous mutation is lethal at late embryonic/perinatal level, so we prepared cortical and hippocampal primary cultures from E15.5 embryos. Heterozygous animals (HET) were mated to obtain Wild Type (WT), HET or Knock Out (KO) embryos. We confirmed the genotype of the embryos by PCR followed by enzymatic digestion (**Figure 11**, A and B), and the complete loss of the protein by Western blot (**Figure 11**, C).

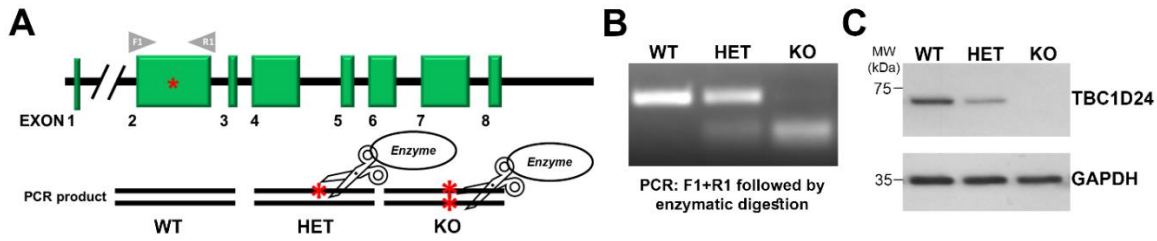

Figure 11. Genotyping strategy and *Tbc1d24* expression level in cortical neurons from WT, HET and KO embryos. A) schematic representation of *Tbc1d24* sequence and genotyping strategy. Red asterisks represent the 2-nucleotides insertion; B) representative genotyping analysis from genomic DNA of WT, HET and KO embryos; C) representative Western blot of Tbc1d24 and GAPDH obtained from mouse cortical neurons (5 DIV).

First, we investigated whether the loss of Tbc1d24 could impact on V-ATPase activity and consequent intracellular organelles acidification. To verify this hypothesis, we treated hippocampal neurons from WT and KO embryos with Lysotracker and Lysosensor probes. KO neurons displayed a significant decrease in Lysotracker intensity and in the number of positive puncta with respect to WT neurons. This phenotype was completely reverted when human-TBC1D24 was reintroduced by overexpression in KO neurons (KO OE TBC1D24), with no impact on WT cells (WT OE TBC1D24) (**Figure 12**, A). To evaluate if the decrease in

Lysotracker staining was due to an increased pH or a lower number of intracellular organelles, we performed Lysosensor yellow/blue DND-160 and LAMP1 (lysosomal marker) evaluation. We found that KO neurons displayed a significantly higher ratio of Lysosensor yellow/blue DND-160 compared to WT, which correlates with a rise in endo-lysosomal pH (**Figure 12**, B).

We also revealed an increase in LAMP1 signal by both immunocytochemistry and Western blot experiments (**Figure 12**, C) in KO cells. Maintenance of the correct pH within the lumen of acidic organelles is a crucial parameter for their maturation and function. Thus, the acidification impairment found in KO cells could lead to a defective endo-lysosomal maturation with accumulation of non-functional and aberrant lysosomes, albeit further experiments are needed to clarify this point. Taken all together, these data support the hypothesis that loss of Tbc1d24 leads to the impairment of intracellular organelles acidification, interfering with V-ATPase activity.

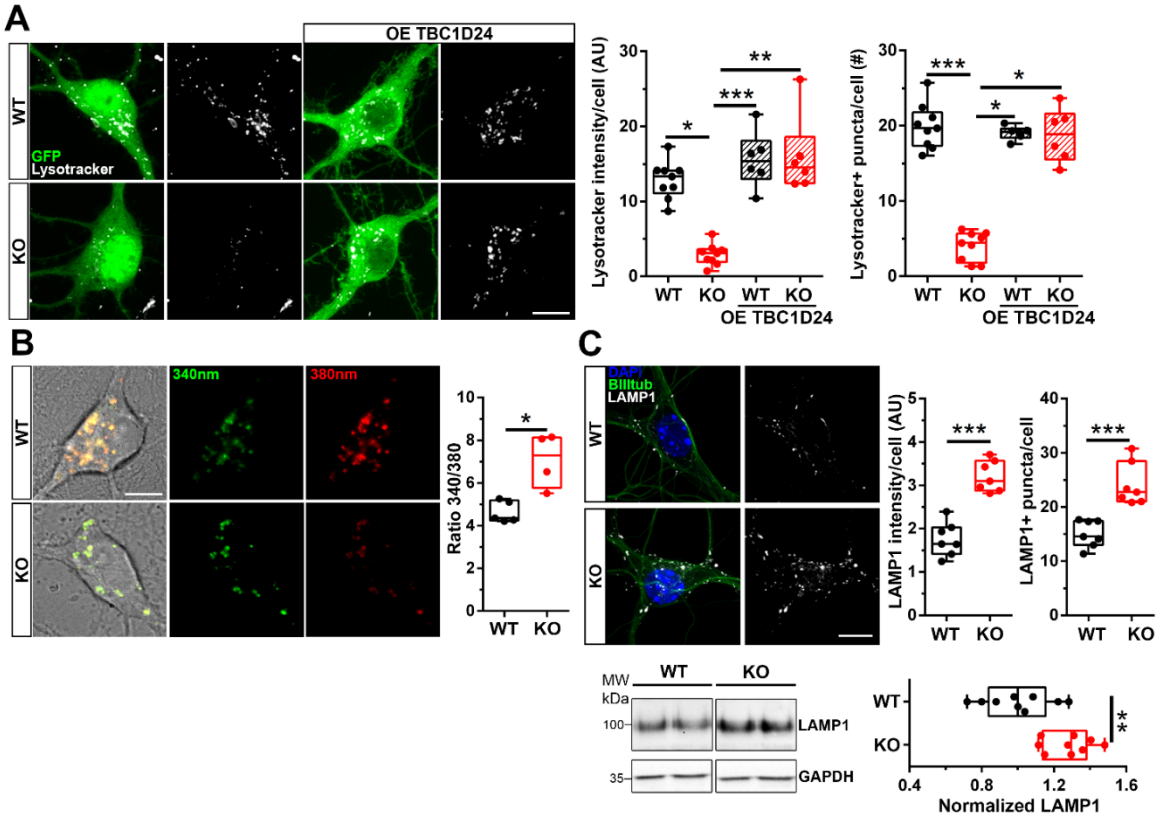

Figure 12. TBC1D24 KO neurons present acidification impairment of intracellular organelles. A) *Left*, representative images of Lysotracker (white; 100 nM, 30 min) signal in mouse hippocampal neurons from WT and KO embryos (12 DIV). Lysotracker intensity and positive puncta were evaluated at soma level identified by GFP signal (green); *right*, graphs show Lysotracker mean fluorescent intensity and positive puncta quantifications. Each dot in both graphs represents the mean fluorescent intensity

of at least 20 neurons derived from one embryo. Box plots show min to max values from n=6-9 embryos. *P≤0.05, **P≤0.01, ***P≤0.001, Kruskal-Wallis/Dunn's test; B) representative images of Lysosensor yellow/blue DND-160 live staining at 340 (green) and 380 nm (red) excitation in mouse hippocampal neurons from WT and KO embryos (12 DIV). Lysosensor yellow/blue DND-160 signal was measured at soma level identified by bright field. Graph shows quantification of Lysosensor yellow/blue DND-160 ratio (340/380nm) in WT and KO neurons. Each dot represents the mean ratio of at least 15 neurons from one embryo. Box plots show min to max values from n=4-5 embryos. *P≤0.05, Mann-Whitney test; C) *upper panel*, representative images of LAMP1 staining (white) in mouse hippocampal neurons from WT and KO embryos (12 DIV). LAMP1 signal was evaluated at soma level identified by the neuron specific microtubules marker β-III tubulin (BIIItub) signal (green). Graphs show LAMP1 fluorescent intensity and positive puncta quantifications. Each dot in the graphs represents the mean of at least 15 neurons derived from one embryo. Box plots show min to max values from n=7 embryos. *** P≤0.001, Mann-Whitney test; *lower panel*, representative Western blot of LAMP1 from mouse cortical neurons lysates of WT and KO embryos (12 DIV). Graph shows the densitometric analysis of LAMP1 signal normalized on GAPDH and expressed as percentage of WT. Each dot in the graphs represents neuronal lysate from one different embryo (n=9 embryos). **P≤0.01, unpaired t-test. For A), B) and C), scale bar: 10µm.

TBC1D24 impacts on the assembly state of V-ATPase

V-ATPase complex functions with a rotatory mechanism promoted by the hydrolysis of ATP at the V1 cytosolic domain and the translocation of protons through the V0 transmembrane domain. The regulation of V-ATPase activity mainly occurs by controlling the reversible association of the two domains [(**Figure 13**, A) and (Forgac 2007; Lafourcade et al. 2008; McGuire et al. 2016)]. Thus, we investigated if the impairment in intracellular acidification due to the lack of TBC1D24 could be related to an altered assembly state of V-ATPase complex. First, we analyzed total protein amount of different V-ATPase subunits either belonging to the cytosolic V1 domain (Atp6v1a and Atp6v1b2) or to the transmembrane V0 domain (Atp6v0a1). We did not find any difference in the subunits' expression between WT and KO samples (**Figure 13**, B). Next, we performed subcellular fractionation experiments to evaluate the cytosolic versus membrane fractionation of the same subunits. Densitometric analysis revealed a significant increase in the amount of cytosolic Atp6v1a and Atp6v1b2 in KO neurons with respect to WT, paired with a significant reduction in their membrane localization (**Figure 13**, C). No significant variations were detected for Atp6v0a1, which was found to be only enriched in membrane fraction both in WT and KO samples (**Figure 13**, C).

The results suggest that, without altering their expression, loss of TBC1D24 leads to a cytosolic shift of V1 subunits resulting in a decreased number of complete and possibly active V-ATPase complexes.

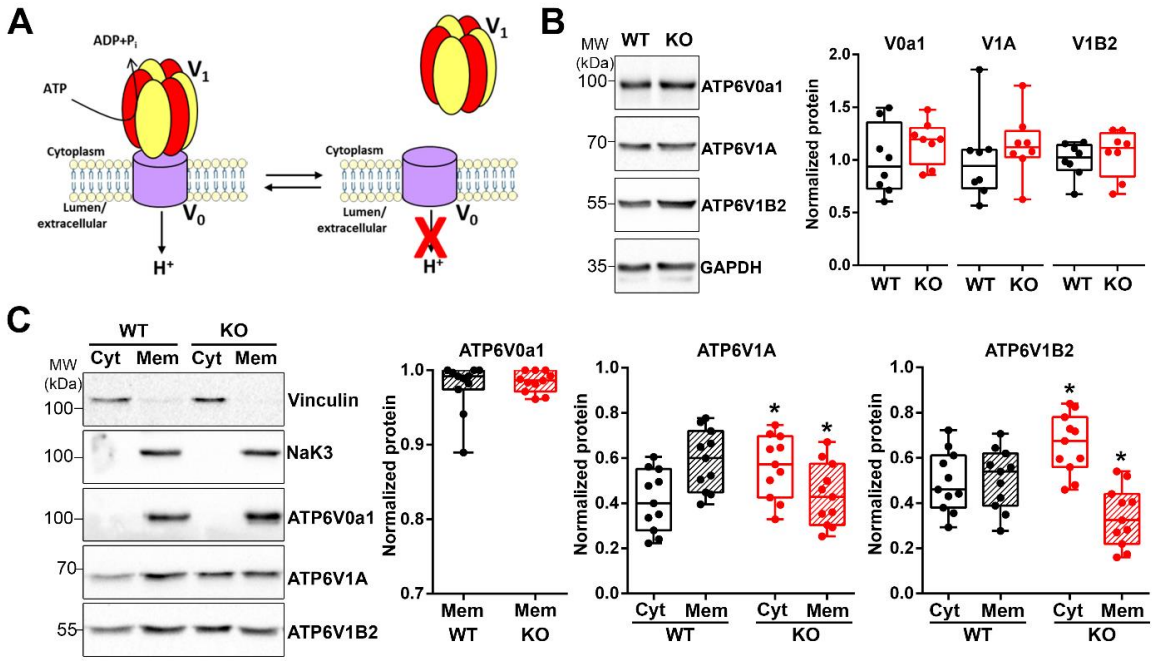

Figure 13. Lack of TBC1D24 affects V0/V1 assembly. A) cartoon showing the reversible association mechanism of V-ATPase complex; B) *left*, representative Western blot of Atp6v0a1, Atp6v1a and Atp6v1b2 subunits from mouse cortical neurons lysates of WT and KO embryos (12 DIV); *right*, graphs show the densitometric analysis of Atp6v0a1, Atp6v1a and Atp6v1b2 signals. Protein signal was normalized on GAPDH and expressed as percentage of WT. Each dot in the graphs represents neuronal lysate from a single embryo. Box plots show min to max values from n=8 embryos for WT and KO. Unpaired t-test, Mann-Whitney test; C) *left*, representative Western blot of cytosol (C)/membrane (M) separation from lysates as in B. Signal from three different subunits (Atp6v0a1, Atp6v1a and Atp6v1b2) from V1 or V0 domain was analysed. Vinculin and Nak3 were used as cytosolic and membrane markers, respectively; *right*, graphs show densitometric analysis of Atp6v0a1, Atp6v1a and Atp6v1b2 signals. Cytosolic fractions were normalized on Vinculin and membrane fractions on Nak3. Atp6v0a1 was not determined in the cytosolic fraction of both WT and KO lysates. Data are expressed as percentage of total protein. Each dot in graphs represents neuronal lysate from a single embryo. Box plots show min to max values from n=11 embryos for WT and KO. *P≤0.05, One-Way ANOVA, Sidak's multiple comparisons test.

Tbc1d24 loss of expression leads to a defective autophagy process.

Autophagy is a major intracellular degradation system that plays a housekeeping role in removing misfolded or aggregated proteins, as well as damaged organelles. The most studied form of autophagy is macroautophagy, which delivers unwanted cytoplasmic material to degradation via double-membraned structures called autophagosomes. At the end of the

process, autophagosomes fuse with lysosomes, which contain a range of catalytic enzymes able to digest all types of biological molecules. Many of the lysosomal enzymes require a specific range of pH to be functional, and the maintenance of lysosomal pH depends on the activity of V-ATPase complex.

Since Tbc1d24 loss affects intracellular organelles' acidification and influences the assembly state of V-ATPase, we examined weather KO neurons display a defective autophagy process.

An experimental method to monitor autophagy is the detection of LC3 and p62 protein levels. LC3 protein undergoes different post-traductional modification. First, LC3 is cleaved to become LC3-I, which is soluble and cytosolic. Then, LC3-I conjugates to phosphatidylethanolamine (PE) to form LC3-II, which is recruited to autophagosomal membranes (**Figure 14**, A). Based on the observation that LC3-II is degraded upon fusion of autophagosomes with lysosomes, the levels of LC3-II can be used as a marker for the autophagic flux (Klionsky et al. 2012). Moreover, other types of autophagic cargo are degraded during autophagy, like the autophagic receptor p62. p62 is a multifunctional protein that can recognize ubiquitin or polyubiquitin chains, and then delivers polyubiquitinated cargoes to autophagic degradation (**Figure 14**, A) via the specific LC3-interacting domain. p62 is degraded in autolysosome and pharmacological or genetic disruption of autophagy results in its accumulation.

We found that KO neurons at 12 DIV displayed an increase in both LC3-II and p62 signals evaluated by Western blot analysis (**Figure 14**, B). This finding was confirmed by immunocytochemistry experiments in which we evaluated LC3 and p62 expression at somatic level, where the autophagosome-lysosome fusion mainly occurs (**Figure 14**, C and D). LC3 and p62 staining revealed a condensate localization of the two proteins in KO cells which suggest their accumulation in autophagic organelles. Together with biochemical experiments, these data are suggestive of a possible impairment in the degradation step of the autophagic flux.

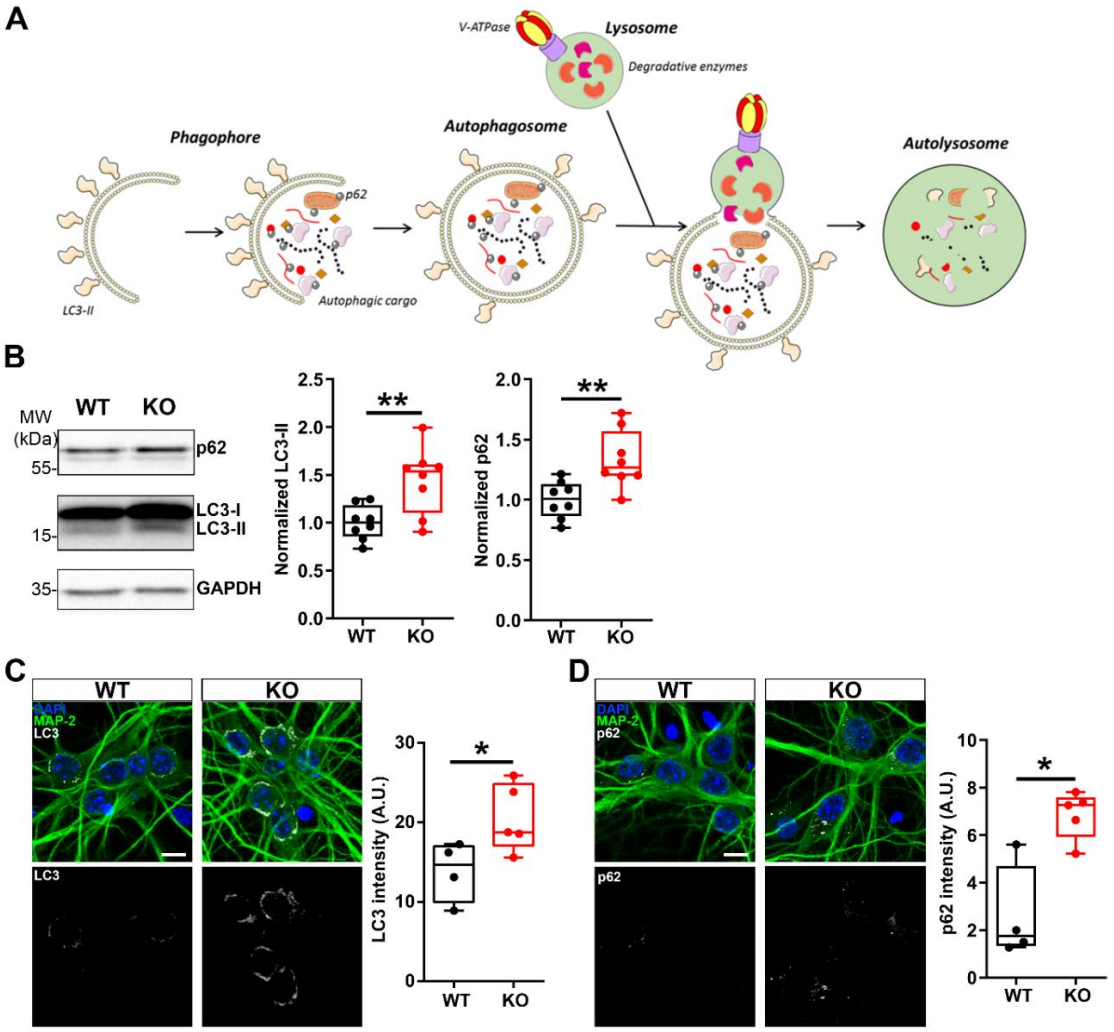

Figure 14. *Tbc1d24* KO neurons show impaired autophagy. A) cartoon illustrating the autophagy pathway. V-ATPase contributes to proper autophagy progression by providing the acidic pH required by lysosomal degradative enzymes; B) *left*, representative Western blot of LC3 I/II and p62 from mouse cortical neuronal lysates (12 DIV) of WT and KO embryos; *right*, graphs show LC3-II and p62 densitometric analysis normalized on GAPDH signal. KO values are expressed as percentage of WT. Box plots show min to max values from n=8 embryos for both WT and KO. **P≤0.01, unpaired t-test; C and D) *left*, representative images of LC3 (C) and p62 (D) staining (white) in WT and KO hippocampal neurons (12 DIV). Fluorescence intensity was evaluated at soma level identified by MAP-2 signal (green). Scale bar: 10µm; *right*, graphs show LC3 (C) and p62 (D) fluorescence intensity quantification. Each dot in the graphs represents the mean fluorescent intensity of at least 20 cells derived from one embryo. Box plots show min to max values from n=4/5 embryos for WT/KO. *P≤0.05, Mann-Whitney test.

Tbc1d24 loss interferes with synaptic morphology and function.

To better understand the role of TBC1D24 in neurons, it is important to note that it is enriched in synaptic terminals where it plays a role in neurotransmission and SV cycling (Finelli et al. 2019; Lin et al. 2020; Taoufiq et al. 2020). The impairment of synaptic function could be related

to defect in morphology and abundance of SVs and organelles. To depict the synaptic ultrastructure of KO mice neurons, we studied the synaptic 3-D reconstructions from transmission electron microscopy (TEM) (**Figure 15**). The morphological analysis of KO synapses revealed a decrease in SV number with respect to WT synapses, paired with a preserved density of docked SVs (**Figure 15**, B and C). Moreover, a significant increase in the number, area and volume of endosomal-like structures was observed in KO synapses (**Figure 15**, D, E and F). These data suggest that chronic loss of *Tbc1d24* leads to the accumulation of aberrant endosomal-like structures, that engulf the synapse at the expense of SVs, and possibily alter synaptic function.

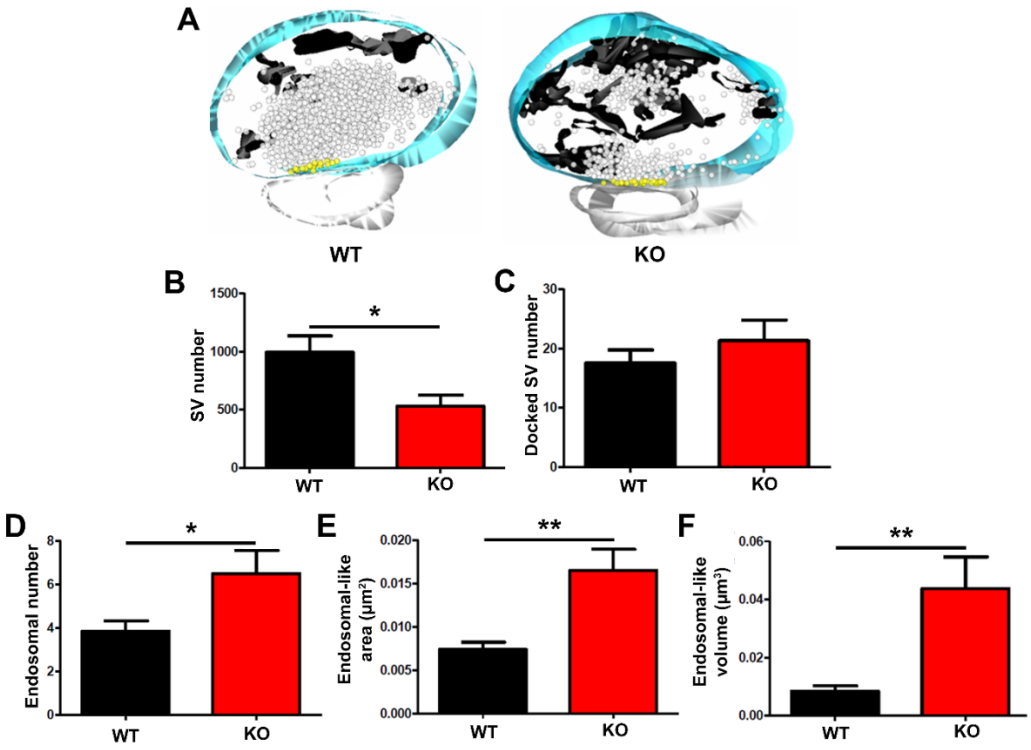

Figure 15. *Tbc1d24* loss results in the accumulation of aberrant endosomal-like structure and decreased SV number. A) 3D reconstructions of synaptic terminals from serial ultrathin sections obtained from WT and KO synapses. Total SVs and SVs physically docked at the AZ are depicted as light grey and yellow spheres, respectively. Endosomal-like structures are shown in black. B-F) Graphs show the morphometric analysis of total SV number (B), docked SV number (C) and endosomal-like number (D), area (E) and volume (F) of 3D reconstructed synapses. Data are expressed as the mean ± SEM (n=14 synapses for WT and KO, from 3 different preparations). *P≤0.05, **P≤0.01; Mann–Whitney test. (EM was performed by Enrico Castroflorio, MRC Harwell Institute, Oxford)

Neurons are very specialized cells that possess a precise polarization and synaptic connections are the key elements for their functional properties. In particular, presynaptic

compartments need to have an efficient quality control of proteins and organelles to sustain the neurotransmitter release machinery, which rapidly and efficiently recycles neurotransmitter-filled SVs. Hence, presynaptic proteins must be continuously replaced in a specific and highly coordinated manner. Different pathways are involved in this task and presynaptic autophagy is one of them. Since Tbc1d24 loss interferes with the autophagy pathway at soma level, we analysed if its loss could impact also on presynaptic autophagy. We employed a lentiviral construct which allows the co-expression with independent localization of mCherry-tagged synaptophysin (Syp), as a presynaptic marker, and eGFP-tagged LC3, as marker for autophagosomes (**Figure 16**, A and (Hoffmann et al. 2019)).

To identify wheter KO neurons displayed variations in the localization and number of autophagosomal structures at the their presynaptic terminals, we evaluated the number of eGFP-LC3-positive presynaptic sites by measuring the colocalization rate beween eGFP-LC3 and Syp-mCherry signals. Then, we measured the fluorescence intensity of eGFP-LC3 into Syp-mCherry positive puncta. The results showed an increased number of presynatic terminals positive for LC3 structures (**Figure 16**, C *left*) and also a higher eGFP-LC3 fluorescence intensity in Syp-mCherry positive puncta (**Figure 16**, C *right*) in KO neurons with respect to WT. These data suggest that loss of Tbc1d24 alters presynaptic autophagy leading to the accumulation of autophagosomal structures at synaptic sites.

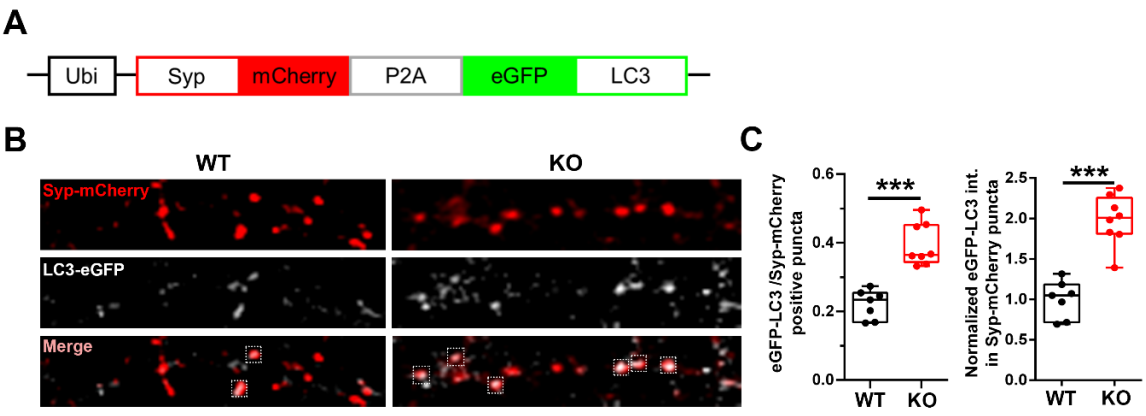

Figure 16. Tbc1d24 KO neurons accumulate autophagosomes at presynaptic terminals. A) schematic representation of the lentiviral construct encoding for Syp-mCherry and eGFP-LC3. Ubi: ubiquitin promoter; P2A: post-translational cleavage site; B) representative images of Syp-mCherry (red) and eGFP-LC3 (white) in WT and KO hippocampal neurons (18 DIV) infected with the construct in A.

Dotted squares show colocalization puncta; C) *left*, graph shows percentage of presynaptic terminals positive for eGFP-LC3 structures. At least 25 branches from 5 different fields have been analysed for every coverslip. Each dot in the graph represents the mean of one coverslip; *right*, graph shows the mean fluorescence intensity of eGFP-LC3 in Syp-mCherry positive puncta. At least 50 dots from 5 different fields have been analysed for every coverslip. Each dot in the graph represents the mean of one coverslip. Box plots show min to max values from n=4/5 embryos WT/KO. ***P≤0.001, unpaired t-test/Mann-Whitney test.

SV homeostasis and recycling are crucial for neurotransmission, which is based on the accumulation of neurotransmitters into SVs and their release in the synaptic cleft upon fusion of SVs with the presynaptic membrane. Two proteins present on the SV membrane ensure neurotransmitters loading into SVs: the complex of V-ATPase, which acidifies and charges positively the vesicles lumen, and the neurotransmitter transporter, which translocates cytosolic neurotransmitters into the vesicle lumen in exchange for protons.

Given the impairment in acidification and V-ATPase assembly caused by *Tbc1d24* loss, we wondered if the absence of the gene could also interfere with SV acidification.

To answer this question, we took advantage of the fluorescent probe synaptophysin-pHluorin (sypHy). SypHy is a fusion protein between a pH-sensitive GFP (pHluorin) and the presynaptic protein synaptophysin, which targets the fluorophore to the interior of SVs. The principle at the base of sypHy function is that the low pH of SV lumen (~ 5.5) quenches the fluorescence of the probe, which is restored by exposure to higher pH.

The basal fluorescence of sypHy (F_0) depends on the localization of the probe at both SV lumen and the surface of presynaptic membrane, where it is transported during SV recycling. For this reason, sypHy basal fluorescence is influenced by both SV and extracellular pH. KO neurons displayed a higher F_0 value compared to WT, with no variations in F_{max} which represents the total fluorescence of the probe present at the synaptic terminal (**Figure 17**, B *upper*). This phenotype could be due to a higher surface-exposed fraction of sypHy or to an increased pH into SVs.

In order to answer this question, we started to evaluate SV pH and surface fraction of sypHy as described by Egashira and colleagues (Egashira et al. 2016). Briefly, surface probes were

quenched with an acidic buffer (pH 5.5) and the total fluorescence at pH 7.4 was measured after the application of ammonium solution (50mM, pH 7.4) (**Figure 17**, A). Then, surface fraction and SV pH were calculated as described in **MATHERIALS and METHODS, section E. Synaptophysin-pHluorin experiments**. Preliminary experiments revealed that loss of *Tbc1d24* affects sypHy localization within the synaptic terminal as indicated by the higher surface fraction of sypHy in KO neurons (**Figure 17**, B *lower*). Moreover, KO neurons displayed an increase in SV pH (**Figure 17**, B *lower*) which suggests that *Tbc1d24* loss could interfere in V-ATPase proton-pumping activity also at synaptic level. Further experiments are planned to better clarify this phenotype.

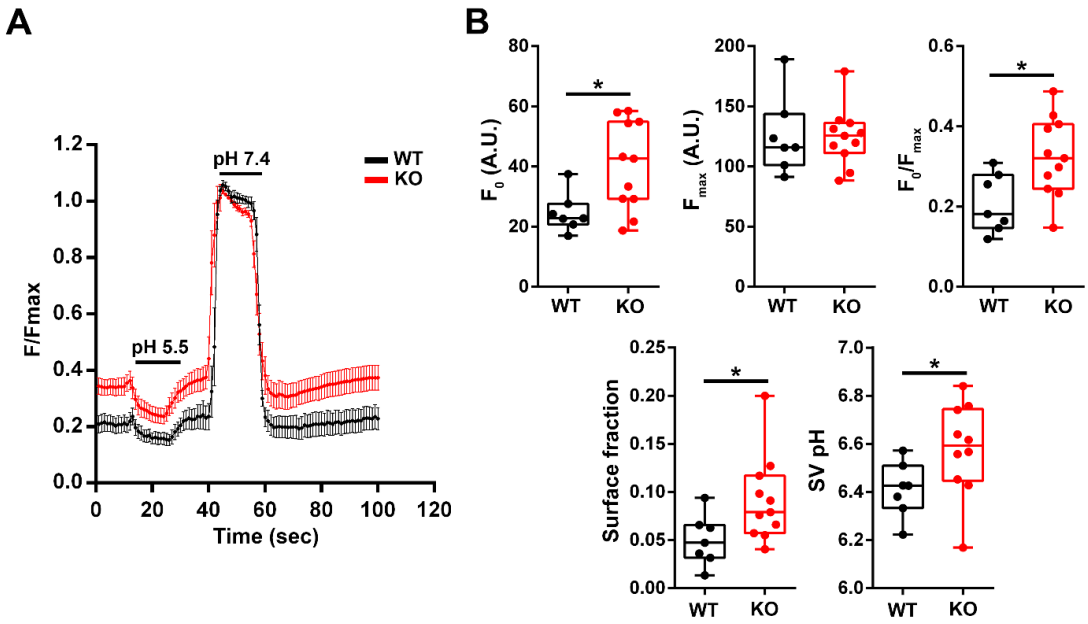

Figure 17. Measuring SV pH. A) representative trace of the protocol showing normalized sypHy fluorescence changes in response to acidic quenching (pH 5.5) and ammonium solution (NH4Cl 50 mM, pH 7.4); B) *upper*, graphs show quantification of basal (F_0) and total (F_{max}) fluorescence intensity of sypHy and their ratio (F_0/F_{max}); *lower*, graphs show measurements of surface fraction of sypHy and synaptic vesicles pH (SV pH). Each dot in the graphs represent the mean of 15-30 ROIs from one coverslip. Box plots show min to max values from n=3-4 embryos WT/KO. *p≤0.05, unpaired t-test;/Mann-Whitney test.

TBC1D24 KO neurons exhibit a dysregulated ARF6 activation.

TBC1D24 is known to interact with the ADP ribosylation factor 6 (ARF6), a small GTPase implicated in neuronal maturation, endosomal-membrane trafficking and SV cycling (D'Souza-Schorey and Chavrier 2006; Falace et al. 2014; Tagliatti et al. 2016).

The small GTPases requires additional proteins, namely GAPs and GEFs, to cycle between their GTP-bound (active) and GDP-bound (inactive) state. The TBC domain is characteristic of GAP proteins, which sustain the GTP to GDP transition of small GTPases. TBC1D24 contains an unconventional form of such a domain which lacks the residues involved in catalytic activity. It has been shown that TBC1D24 interacts with ARF6-GDP, it inhibits the formation of active ARF6-GTP (Falace et al. 2014) and that acute silencing of the protein increases ARF6-GTP levels (Aprile et al. 2019; Lin et al. 2020).

We wandered if chronic loss of *Tbc1d24* could interfere with the activation state of ARF6. Total neural lysate from WT and KO neurons were incubated with GGA3-PBD beads to pulldown the GTP-bound form of ARF6. The results showed that KO neurons exhibit higher levels of active ARF6 with respect to WT (**Figure 18**). These data suggest that chronic loss of *Tbc1d24* blocks ARF6 in the active form.

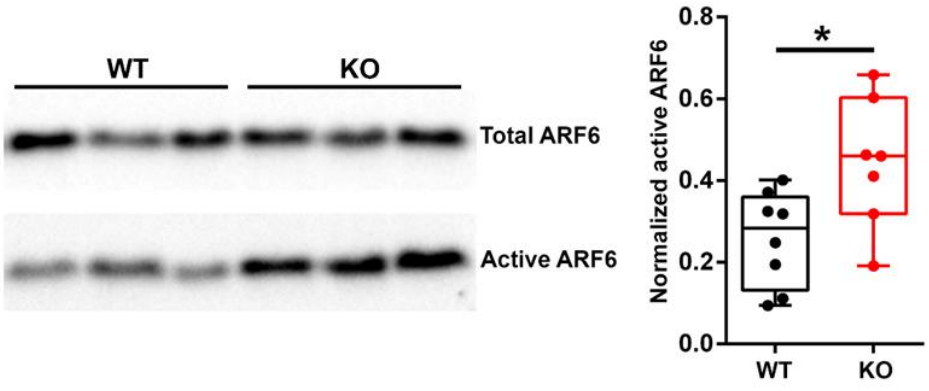

Figure 18. Chronic loss of TBC1D24 leads to the accumulation of active GTP-bound ARF6. *Left*, representative Western blot of total and immunoprecipitated active (GTP-bound) ARF6 in WT and KO lysates at 12 DIV; *right*, graph shows densitometric analysis of active ARF6 normalized on total. Box plots show min to max values from n=8/7 embryos for WT/KO; Mann Whitney test. *p≤0.05

Part 2

Structure/function study of de novo ATP6V1A mutations.

In collaboration with the group of Professor Guerrini (Azienda Ospedaliero Universitaria Meyer, Florence, Italy), we described *de novo* mutations in *ATP6V1A* gene in a cohort of 26 patients affected by epileptic encephalopathy with different severity (Guerrini et al. 2022).

In silico analysis of *ATP6V1A* mutations revealed that all substitutions but one (Pro27Arg) affect amino acids mapping in central domain of the subunit, surrounding the catalytic site and near the phosphate-binding loop (blue spheres, **Figure 19**).

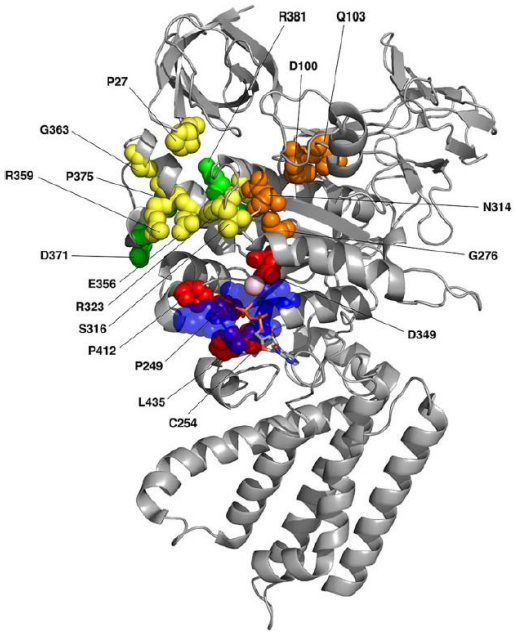

Figure 19. The Cryo-EM structure of ATP6V1A from the mammalian V-ATPase. Mutation sites are drawn as red, yellow, green and orange spheres if they are near the phosphate-binding loop (p-loop, blue spheres), A/B interface, A/D or non-catalytic A/B interface, and uncharacterized locations, respectively. The pink sphere represents the magnesium ion and the bound ADP molecule is drawn as sticks.

When mapped in the structure of its homologue in rat, some of the pathogenic mutations cluster in regions of the protein linked to V-ATPase activity, such as near the ATP-binding site (red spheres, **Figure 19**) or at the ATP6V1A/B catalytic interface (yellow spheres, **Figure 19**), suggesting that such mutations could perturb protein functions. The remaining mutations are

located either in the ATP6V1A/B non-catalytic interface (green, **Figure 19**), where they are predicted to perturb ATP6V1A/B interaction, or in a less structurally characterized part of the subunit (orange spheres, **Figure 19**), where the specific amino acidic substitutions could perturb amino acidic interactions and affect protein stability.

Starting from the availability of patients' fibroblasts, we characterized four different mutations: p.Asp100Tyr (orange – Pat.1) and p.Glu356Asp (yellow – Pat.18) related to a severe neurological phenotype and p.Asp349Asn (red – Pat.2) and p.Gly363Val (yellow – Pat.16) related to a milder neurological phenotype (see **Table 2** for clinical description).

Patient/Sex	1/f	2/M	16/M	18/F
Age at Follow-up	14y	8y	22y	6y
ATP6V1A mutation	c.298G>T (p.Asp100Tyr) *de novo*	c.1045G>A (p.Asp349Asn) *de novo*	c.1088G>T (p.Gly363Val) *de novo*	c.1068G>T (p.Glu356Asp) *de novo*
Clinical diagnosis	Infantile onset developmental and epileptic encephalopathy	Intellectual disability/epilepsy	Intellectual disability/epilepsy	Infantile onset developmental and epileptic encephalopathy
Head circumference	At birth: 32cm (3rd%; -1.9 SD) 12y: 44.5 (<1st%; -7 SD)	At birth: 33cm (10th%; +1.2 SD)	At birth: 36.5 (65th%; +0.4 SD)	2y6m: 46cm (8th%; -1.3 SD)
Age and symptoms at first clinical presentation	11m, hypotonia, dev. delay, seizures	1m, dev. delay, jerky movement	1y3m, generalized seizures	6m, diffuse hypotonia, dev. delay, infantile spasms
Epilepsy/Severity	+/severe	+/mild	+/severe in infancy/childhood, then remission	+/severe in infancy, then controlled on GVG and sporadic focal seizures upon attemped AED withdrawals
Age at seizure onset	11m	2y10m	1y3m	6m
Seizures types	Convulsive s. during fever onset, then infantile spasms, tonic, focal clonic, focal occipital	Convulsive s. during fever at onset, then focal occipital	Generalized tonic-clonic seizures, then absence and myoclonic; seizure free since 4y6m on TPM and VPA	Infantile spasms, focal seizures, focal status epilepticus

Interictal EEG	Slow background, diffuse and multifocal epileptiform discharges	Posteriorly dominant, multifocal epileptiform discharges	4y: normal background; bilateral, right predominant frontotemporal spike/polyspike/sharp waves at 3-5 Hz	2y6m: bilateral FT spikes 5y: left CT spikes
Brain MRI	11y: hypomielination, mild brain and cerebellar atrophy. MRS: normal	7y: normal	2y6m: normal	5y: hypomielination, left cerebello-pontine angle arachnoid cyst with compression of the middle cerebellar peduncleand displacement of the adjacent vestibulocochlear nerve
Clinical phenotype	Profound delay, nonverbal, no visual fixation, hypotonic/dyskinetic quadriparesis, nonambulatory, early puberty (9y), microcephaly	Moderate intellectual disability (FSDQ: 53), poor language, headache, amelogenesis imperfecta/enamel dysplasia diagnosed at 3y, optic atrophy	Mild-moderate intellectual disability, behavioural abnomalities with mild autistic traits, poor language, OCD and ADHD	Intellectual disability, nonverbal, walks with support, motor stereotypies

Table 2. Table describing the clinical phenotypes of patients carrying ATP6V1A mutations chosen for our in vitro experiments.

ATP6V1A mutations affects protein stability and intracellular organelles' pH.

To investigate the impact of the mutations on ATP6V1A stability and function, we compared patients' fibroblasts with control cells that were matched for passage in culture, sex and age of biopsy from healthy donors.

By Western blot analysis, we found that the *ATP6V1A* expression level was significantly lower for Patient 1, as previously reported in different cellular systems (Fassio et al. 2018). None of Patient 2, 16 and 18 reported a significant decrease in ATP6V1A levels (**Figure 20**, A). These results indicate that p.Asp100Tyr results in impaired stability of the ATP6V1A subunit, whereas p.Asp349Asn, p.Gly363Val and p.Glu356Asp are compatible with its physiological expression.

Since V-ATPase is a proton pump, we next evaluated intracellular organelle acidification using Lysotracker dye. In fibroblasts of Patients 1 and 18, we identified a decrease in Lysotracker staining with respect to controls. Differently, fibroblasts of Patients 2 and 16 exhibited the opposite phenotype (**Figure 20**, B).

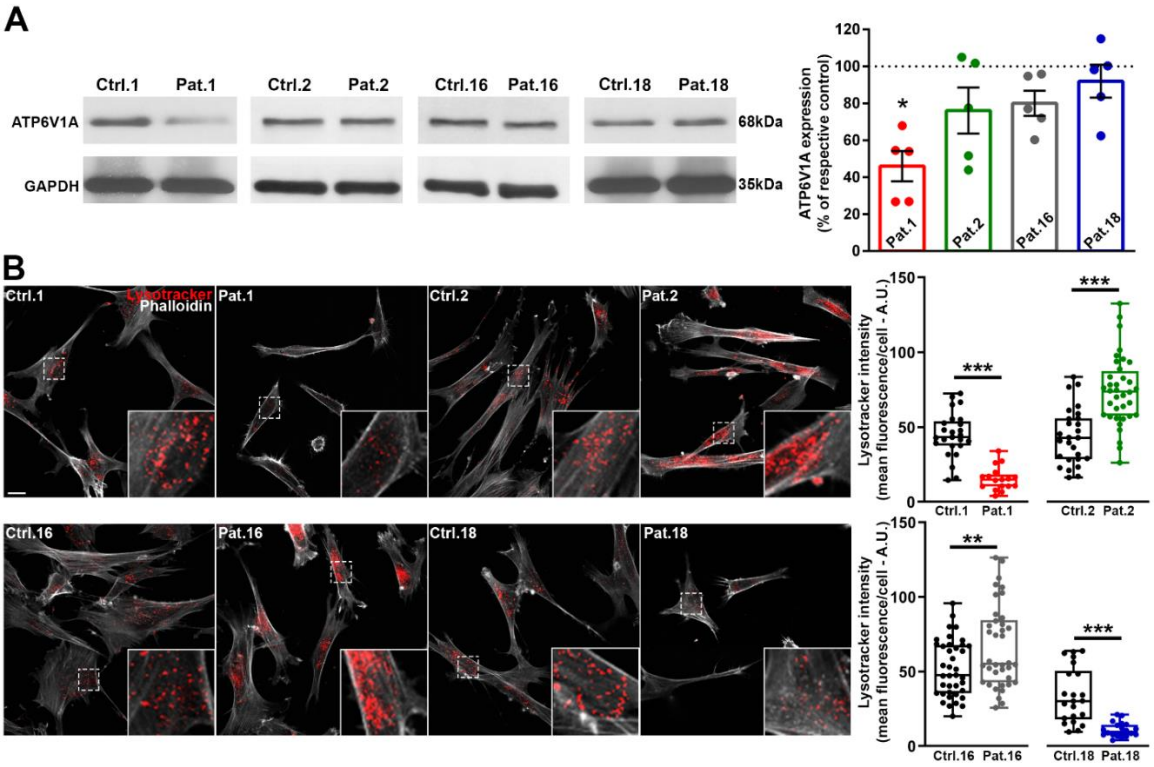

Figure 20. Effect of ATP6V1A mutations on protein expression and intracellular organelles acidification. A) *Left*, representative Western blots from fibroblasts lysates of indicated patients and relative controls, *right*, graph shows the densitometric analysis of ATP6V1A. ATP6V1A signal was normalized on GAPDH and expressed as percentage of the respective control for each patient. Data are means ± SEM (n=5). Kruskal-Wallis/Dunn's tests. *P≤0.05; B) *left*, representative images of fibroblasts incubated with Lysotracker (red; 200nM, 1h) and stained with Phalloidin (white). Scale bar: 20µm; *right*, graphs show the quantification of Lysotracker intensity. Lysotracker signal was measured in whole cell body identified by Phalloidin staining. Each dot represents the mean fluorescence intensity of a cell. Box plots show data from 26/19 cells for Ctrl.1/Pat.1, 13/20 cells for Ctrl.2/Pat.2, 19/15 cells for Ctrl.16/Pat.16, 22/18 cells for Ctrl.18/Pat.18. **P≤0.01, ***P≤0.001; unpaired t-test.

A change in the non-ratiometric Lysotracker probe can reflect either a decrease in the cell density of acidic organelles or a change in their lumenal pH. To clarify this point, we performed LAMP1 staining, as marker for late endosomes and lysosomes, the most acidic intracellular organelles. LAMP1 evaluation revealed a decrease in the signal in fibroblasts from Patients 1 and 18, while no variations were detected in fibroblasts from Patients 2 and 16 (**Figure 21**, A). To obtain an absolute measure of the endo-lysosomal pH, we next employed the ratiometric probe Lysosensor Yellow/blue dextran. These experiments revealed a pH increase in fibroblasts of Patients 1 and 18 and an opposite pH decrease in those of Patients 2 and 16 (**Figure 21**, D). These findings suggest that the p.Asp100Tyr and p.Glu356Asp substitutions

cause impaired proton pumping, which results in the basification of lysosomal pH. This phenotype could derive from either a loss of expression of the ATP6V1A subunit (p.Asp100Tyr) or loss of the catalytic function, hypothesized for p.Glu356Asp which affects the ATP6V1A/B catalytic interface. Conversely, the p.Asp349Asn and p.Gly363Val substitutions resulted in a different cellular phenotype, characterized by no change in the endo-lysosomal marker abundance and decreased pH, compatible with increased proton pumping activity and consequent hyper-acidification of intracellular organelles.

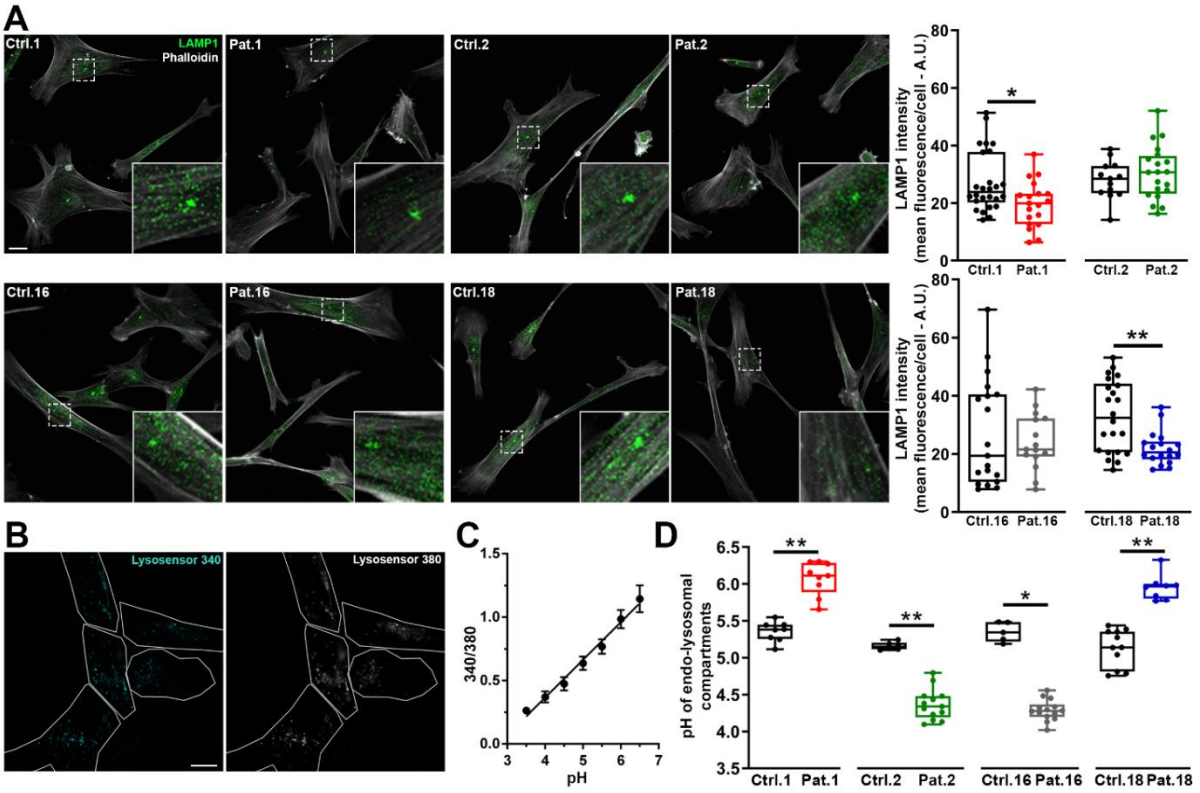

Figure 21. LAMP1 evaluation and pH measurements of endo-lysosomal organelles. A) *left*, representative images of fibroblasts stained with LAMP1 (green) and Phalloidin (white). Scale bar: 20µm; *right*, graphs show the quantification of LAMP1 intensity. LAMP1 signal was measured in whole cell body identified by Phalloidin staining. Each dot represents the mean fluorescence intensity of a cell. Box plots show data from 26/19 cells for Ctrl.1/Pat.1, 13/20 cells for Ctrl.2/Pat.2, 19/15 cells for Ctrl.16/Pat.16, 22/18 cells for Ctrl.18/Pat.18; B) representative images of fibroblasts incubated with LysoSensor yellow/blue dextran and visualized in live at 340 nm and 380 nm excitation. White lines represent cells detected in bright field and used as ROIs for intensity measurement; C) the calibration curve, obtained by plotting the fluorescence intensity 380/340 ratios as a function of pH, was fitted with linear regression. Data are means ± SEM from the 5 cells shown in B; D) pH values derived from 340/380 ratios and relative calibration curves. Each dot represents the mean pH from a single coverslip. 5-14 coverslips have been analysed for each experimental group with an average of 14 cells analysed for each coverslip. Scale bar: 10µm. *P < 0.05, **P < 0.01; unpaired t-test/Mann-Whitney test.

Ultrastructural analysis of patients-derived fibroblasts.

The degradative capacity of the endo-lysosomal system relies on V-ATPase proton-pumping capacity, which is required to reach the optimal pH for enzymatic activity. Thus, the incorrect acidification of these organelles could lead to the accumulation of non-degraded materials inside the cells with consequent aberrant modifications of organelles morphology.

In collaboration with Laura Masuelli at Department of Experimental Medicine of the University of Rome 'Sapienza' (Rome, Italy), we performed electron microscopy analysis and found that control fibroblasts appeared thin and elongated with centrally located nuclei and well-organized nucleoli. Moreover, they showed condensed mitochondria, slightly dilated endoplasmic reticulum and small lysosomes (**Figure 22**, A–C). Conversely, fibroblasts from patients showed several cytoplasmic single membrane-bounded vacuoles filled with heterogeneous substances, resembling lysosomal structures (**Figure 22**, D–Q). Most vacuoles in fibroblasts from Patient 1 were filled with osmiophilic material and lamellated membrane structures resembling phospholipids (**Figure 22**, D and E). In Patient 2 fibroblasts, the vacuolar structures contained small electron-dense granular materials, lamellated membrane structures and osmiophilic material. Furthermore, few lipid droplets were found in the cytoplasm (**Figure 22**, G and H). In Patient 16 fibroblasts vacuoles were packed with lamellated membrane structures and abundant lipid droplets were present (**Figure 22**, L–N). In Patient 18 fibroblasts, vacuolar structures were very heterogeneous and filled with osmiophilic material and substances with different electron densities. Lipid droplets were also present in the cells from Patient 18 (**Figure 22**, O-Q).

These findings further support the hypothesis that V-ATPase impairment upon *ATP6V1A* mutations leads to alteration in lysosomal function and accumulation of undegraded material.

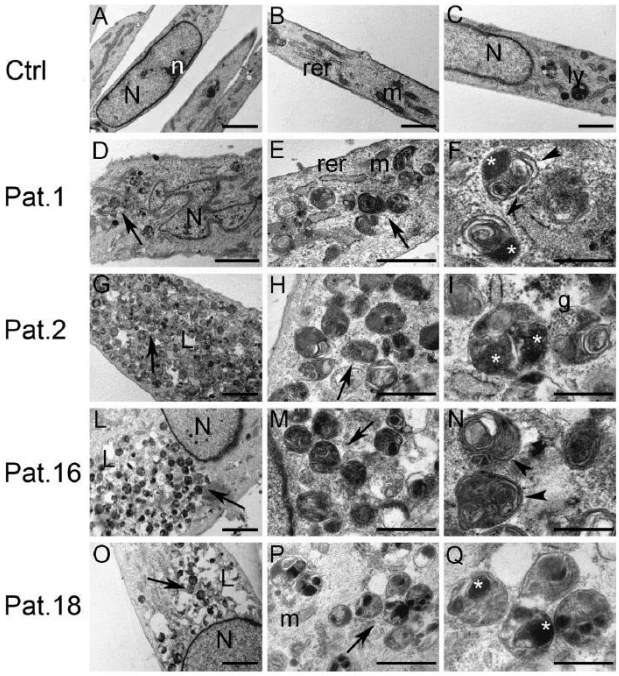

Figure 22. Ultrastructural analysis of patient-derived fibroblasts. (A–C) Control fibroblasts. (D–Q) Fibroblasts from Patient 1 (D and E), Patient 2 (G–I), Patient 16 (L–N) and Patient 18 (O–Q). Fibroblasts from patients bearing ATP6V1A pathogenic variants showed several cytoplasmic single membrane bounded vacuoles filled with heterogeneous substances, resembling autolysosomes (arrows in D, E, G, H, L, M, O and P). Vacuoles from patients' fibroblasts were filled with various substances, such as lamellated membrane structures (arrowheads in F and N), osmiophilic material (asterisks in F, I and Q), electron-dense granular material (g in I) and substances with different electron-density (Q). N = nucleus; n = nucleolus; rer = rough endoplasmic reticulum; m: mitochondria; ly = lysosome; L = lipid droplets; arrows = cytoplasmic single membrane-bounded vacuoles; arrowheads = lamellated membrane structures; asterisks = osmiophilic material; g = electron-dense granular material. Scale bars = 2 μm (A, D, G, L and O), 1 μm (B and C), 500 nm (E, H, M and P), 200 nm (F, I, N and Q).

DISCUSSION

The regulation of intracellular pH is a fundamental process for cellular viability and function. Indeed, the specific tasks of the different intracellular organelles mainly rely on pH establishment and maintenance (Casey et al. 2010). This is especially true for the endo-lysosomal system, where the progressive acidification of membrane-bound structures makes them appropriate for distinct functions, from the efficient sorting and trafficking of different cargoes to their proper degradation or recycling.

Compared to other cell types, neurons display a highly elaborated and polarized morphology, which creates additional complexity in the segregation and regulation of protein trafficking between their soma, dendrites, and axons. The functional properties of neurons rely on synaptic contacts, where the neurotransmission occurs. Noteworthy, these neuronal compartments display a heavy sorting and recycling of their proteins both at pre- and post-synaptic sites, which sustain the fine-tuned SV cycling and trafficking of postsynaptic receptors that allows and regulates neurotransmitters release. At the presynaptic site, providing the correct pH within the lumen of SVs is one of the limiting steps for neurotransmitter loading (Morel and Poea-Guyon 2015). Recently, Ivanova and Cousin proposed that the recycling and sorting machinery that controls SV fate shares some similarities with the endo-lysosomal system, from protein composition to functional mechanisms. One great example of interconnection between the endo-lysosomal system and the SV recycling machinery is the V-ATPase complex. Indeed, V-ATPase is expressed in the membrane of both endo-lysosomal organelles and SVs, where it is the main protein complex that pumps protons and provides the correct pH required by the different compartments. However, very little is known about how V-ATPase function is regulated in the different compartments and at the synapse to obtain different levels of acidification.

Our experimental work proposes a novel and yet undescribed role for TBC1D24 as an interactor and regulator of the V-ATPase complex in the brain. Indeed, we provide evidence that Tbc1d24 interacts with Atp6v1b2 and Atp6v1a subunits of V-ATPase in brain cells (**Figure**

10). The disruption of this interaction upon *Tbc1d24* loss results in the cytosolic shift of V-ATPase's V1 domain (**Figure 13**) with consequent impairment of intracellular organelles acidification and increased pH (**Figure 12**). This phenotype is suggestive of a defective association of the complex, and it has been already shown for other V-ATPase modulators, such as the accessory protein ATP6AP2 (Hirose et al. 2019). Moreover, other TLDc proteins have been shown to interact with V-ATPase and to modulate its activity (Castroflorio et al. 2021; Khan et al. 2022; Tan et al. 2022). However, they impact on the functionality of V-ATPase in different manners, possibly because of their diverse expression and subcellular localizations. Together with these findings, our results contribute to sustain the hypothesis that TLDc proteins act as V-ATPase regulators (Eaton et al. 2021) and that TBC1D24 is a positive regulator of V-ATPase activity, although further investigation is needed to depict the precise molecular mechanism of this interaction.

Maintenance of pH homeostasis is fundamental in different cellular processes, including autophagy. Autophagy is the self-degradative pathway that cells use to eliminate damaged proteins and organelles and to recycle their components in response to nutrient fluctuations. The degradative capacity of autophagy relies onto lysosomal catalytic enzymes, which are active at the low pH provided by V-ATPase (Yim and Mizushima 2020). In neurons, autophagy has a fundamental role due to the post-mitotic and long living nature of these cells. Indeed, dysfunctional autophagy has been associated with several brain pathologies, mostly neurodegenerative diseases, in which the accumulation of misfolded proteins and damaged organelles triggers neurotoxicity (Colacurcio and Nixon 2016). Interestingly, increasing evidence highlights a role for lysosomal and autophagy homeostasis also in neurodevelopmental diseases with epilepsy (Ebrahimi-Fakhari et al. 2016; Fassio et al. 2020). Many autophagy-related genes have been described mutated in paediatric patients with diverse neurodevelopmental syndromes. In addition, some V-ATPase-related genes, such as *ATP6AP2* and *DMXL2*, resulted to be mutated in patients with severe neurodevelopmental disorders characterized by the early-onset of seizures, brain shrinkage and defective autophagy (Esposito et al. 2019; Hirose et al. 2019). Our results reveal the accumulation of

the autophagic markers LC3-II and p62 upon *Tbc1d24* loss (**Figure 14**), a phenotype that suggest the impairment of autophagic degradation. Moreover, a parallel increase in LC3 signal was found in presynaptic terminals (**Figure 16**). Additional experiments are needed to clarify if and how the acidification impairment observed in *Tbc1d24* KO neurons is correlated with the presynaptic accumulation of LC3-positive structures. Together with the phenotype of impaired lysosomes filled with undegraded materials found in *ATP6V1A* patients' fibroblasts (**Figure 22**), these findings further confirm the involvement of lysosomal functionality and autophagy in neurodevelopmental diseases, identifying the disruption of pH regulation and defective autophagy as a possible pathogenic mechanism of the disorders associated with *TBC1D24* and *ATP6V1A* mutations.

Together with V-ATPase, TBC1D24 is one of the many proteins present at the synapse, where it is involved in synaptic transmission and vesicle cycling (Uytterhoeven et al. 2011; Finelli et al. 2019; Lin et al. 2020; Taoufiq et al. 2020). Indeed, partial loss of *Tbc1d24* is sufficient to provoke impaired excitatory transmission and recycling of SVs (Finelli et al. 2019). These functional phenotypes are accompanied by an altered synaptic morphology, with the accumulation of endosomal-like structures that engulf the synapse (Finelli et al. 2019). Our data from 3-D reconstructions of synapses show a more severe phenotype upon complete loss of *Tbc1d24*, characterized by analogous accumulation of endosomal-like structures accompanied by a net decrease in the total number of SVs at the synaptic terminal (**Figure 15**). An important step in the SV cycling is the acidification of the SV lumen upon endocytic retrieval which allows for neurotransmitter loading. Once these steps occur, SVs are directly released or stored in clusters ready to undergo exocytosis. Although not accurately explored, it is possible that without proper acidification through V-ATPase, SV clustering and recycling are impaired, and their sub-cellular localization altered with the accumulation of endosomal-like structures known to represent sorting stations at the synaptic terminal for SV quality control. Our pHluorin experiments suggest defective SV acidification upon *Tbc1d24* loss, sustaining a role for TBC1D24 in the regulation of V-ATPase also at the synapse (**Figure 17**). Interestingly, haploinsufficiency of *Tbc1d24* results in defective SV cycling (Finelli et al. 2019),

which is possibly related to their improper acidification. Although further investigation is needed to describe the exact function of TBC1D24 on SV cycle, the impaired acidification phenotype may explain the synaptic and neurotransmission defects observed upon the loss of *Tbc1d24* (Finelli et al. 2019; Lin et al. 2020).

V-ATPase assembly and activity regulation at the synapse is still poorly understood. It has been shown that the V1/V0 association mechanism could intervene also in SV cycling (Bodzeta et al. 2017), being V1 dissociation necessary for SV exocytosis. Additional work revealed that V-ATPase is fully assembled in newly endocytosed vesicles, with its activity blocked by the clathrin coat (Farsi et al. 2018). Moreover, V-ATPase may be able to recruit selected regulators of vesicular trafficking, as demonstrated for the small GTPase ADP-ribosylation factor 6 (ARF6) in non-neuronal cells (Hurtado-Lorenzo et al. 2006). ARF6 can regulate the size of the releasable pool of SVs and directly signal the retrieved SVs toward the next round of fusion (Tagliatti et al. 2016). Interestingly, TBC1D24 interacts and regulates ARF6 activity in neurons (Falace et al. 2014; Aprile et al. 2019; Lin et al. 2020). We confirm that loss of Tbc1d24 leads to the accumulation of ARF6 stuck in the GTP-bound form (**Figure 18**), suggesting the aberrant activation of the small GTPase and a possible impairment in its function. TBC1D24 is the unique protein in humans that contains both a TBC and a TLDc domain and it is possible to speculate that V-ATPase/ARF6/TBC1D24 form a supercomplex in synaptic compartments that participates to the quality control of SV acidification and recycling. Additional investigation on the cooperative regulation between these proteins will be helpful to fully elucidate the precise mechanism that controls proper SV acidification and sorting upon endocytosis.

Altogether, our data on TBC1D24 and ATP6V1A demonstrates that alterations of V-ATPase function, either by interfering with its assembly state or by genetic mutations in genes encoding for single V-ATPase subunits, lead to alteration in pH homeostasis, with consequent lysosomal disfunction, autophagy deficit and concomitant synaptic impairment. We propose these processes to be the common pathological traits at the base of neurodevelopmental diseases associated with *TBC1D24* and *ATP6V1A* mutations.

BIBLIOGRAPHY

Abbas YM, Wu D, Bueler SA, Robinson CV and Rubinstein JL. (2020). "Structure of V-ATPase from the mammalian brain". *Science*. 367;6483,1240-1246. doi:10.1126/science.aaz2924.

Abu-Remaileh M, Wyant GA, Kim C, Laqtom NN, Abbasi M, et al. (2017). "Lysosomal metabolomics reveals V-ATPase- and mTOR-dependent regulation of amino acid efflux from lysosomes". *Science*. 358;6364,807-813. doi:10.1126/science.aan6298.

Afawi Z, Oliver KL, Kivity S, Mazarib A, Blatt I, et al. (2016). "Multiplex families with epilepsy: Success of clinical and molecular genetic characterization". *Neurology*. 86;8,713-722. doi:10.1212/WNL.0000000000002404.

Akiyama M and Kanaho Y. (2015). "Physiological functions of the small GTPase Arf6 in the nervous system". *Small GTPases*. 6;3,160-164. doi:10.1080/21541248.2015.1043041.

Albertinazzi C, Za L, Paris S and de Curtis I. (2003). "ADP-ribosylation factor 6 and a functional PIX/p95-APP1 complex are required for Rac1B-mediated neurite outgrowth". *Mol Biol Cell*. 14;4,1295-1307. doi:10.1091/mbc.e02-07-0406.

Aprile D, Fruscione F, Baldassari S, Fadda M, Ferrante D, et al. (2019). "TBC1D24 regulates axonal outgrowth and membrane trafficking at the growth cone in rodent and human neurons". *Cell Death Differ*. 26;11,2464-2478. doi:10.1038/s41418-019-0313-x.

Bagh MB, Peng S, Chandra G, Zhang Z, Singh SP, et al. (2017). "Misrouting of v-ATPase subunit V0a1 dysregulates lysosomal acidification in a neurodegenerative lysosomal storage disease model". *Nat Commun*. 8;14612. doi:10.1038/ncomms14612.

Balestrini S, Milh M, Castiglioni C, Luthy K, Finelli MJ, et al. (2016). "TBC1D24 genotype-phenotype correlation: Epilepsies and other neurologic features". *Neurology*. 87;1,77-85. doi:10.1212/WNL.0000000000002807.

Bodzeta A, Kahms M and Klingauf J. (2017). "The Presynaptic v-ATPase Reversibly Disassembles and Thereby Modulates Exocytosis but Is Not Part of the Fusion Machinery". *Cell Rep*. 20;6,1348-1359. doi:10.1016/j.celrep.2017.07.040.

Bonnycastle K, Davenport EC and Cousin MA. (2021). "Presynaptic dysfunction in neurodevelopmental disorders: Insights from the synaptic vesicle life cycle". *J Neurochem*. 157;2,179-207. doi:10.1111/jnc.15035.

Bos JL, Rehmann H and Wittinghofer A. (2007). "GEFs and GAPs: critical elements in the control of small G proteins". *Cell*. 129;5,865-877. doi:10.1016/j.cell.2007.05.018.

Burckle C and Bader M. (2006). "Prorenin and its ancient receptor". *Hypertension*. 48;4,549-551. doi:10.1161/01.HYP.0000241132.48495.df.

Campeau PM, Kasperaviciute D, Lu JT, Burrage LC, Kim C, et al. (2014). "The genetic basis of DOORS syndrome: an exome-sequencing study". *Lancet Neurol*. 13;1,44-58. doi:10.1016/S1474-4422(13)70265-5.

Casey JR, Grinstein S and Orlowski J. (2010). "Sensors and regulators of intracellular pH". *Nat Rev Mol Cell Biol*. 11;1,50-61. doi:10.1038/nrm2820.

Castroflorio E, den Hoed J, Svistunova D, Finelli MJ, Cebrian-Serrano A, et al. (2021). "The Ncoa7 locus regulates V-ATPase formation and function, neurodevelopment and behaviour". *Cell Mol Life Sci*. 78;7,3503-3524. doi:10.1007/s00018-020-03721-6.

Chan CY and Parra KJ. (2014). "Yeast phosphofructokinase-1 subunit Pfk2p is necessary for pH homeostasis and glucose-dependent vacuolar ATPase reassembly". *J Biol Chem*. 289;28,19448-19457. doi:10.1074/jbc.M114.569855.

Choi S, Ko J, Lee JR, Lee HW, Kim K, et al. (2006). "ARF6 and EFA6A regulate the development and maintenance of dendritic spines". *J Neurosci*. 26;18,4811-4819. doi:10.1523/JNEUROSCI.4182-05.2006.

Colacurcio DJ and Nixon RA. (2016). "Disorders of lysosomal acidification-The emerging role of v-ATPase in aging and neurodegenerative disease". *Ageing Res Rev*. 32;75-88. doi:10.1016/j.arr.2016.05.004.

Corbett MA, Bahlo M, Jolly L, Afawi Z, Gardner AE, et al. (2010). "A focal epilepsy and intellectual disability syndrome is due to a mutation in TBC1D24". *Am J Hum Genet*. 87;3,371-375. doi:10.1016/j.ajhg.2010.08.001.

Cotter K, Stransky L, McGuire C and Forgac M. (2015). "Recent Insights into the Structure, Regulation, and Function of the V-ATPases". *Trends Biochem Sci*. 40;10,611-622. doi:10.1016/j.tibs.2015.08.005.

Couoh-Cardel S, Milgrom E and Wilkens S. (2015). "Affinity Purification and Structural Features of the Yeast Vacuolar ATPase Vo Membrane Sector". *J Biol Chem*. 290;46,27959-27971. doi:10.1074/jbc.M115.662494.

D'Souza-Schorey C and Chavrier P. (2006). "ARF proteins: roles in membrane traffic and beyond". *Nat Rev Mol Cell Biol*. 7;5,347-358. doi:10.1038/nrm1910.

Di Giovanni J, Boudkkazi S, Mochida S, Bialowas A, Samari N, et al. (2010). "V-ATPase membrane sector associates with synaptobrevin to modulate neurotransmitter release". *Neuron*. 67;2,268-279. doi:10.1016/j.neuron.2010.06.024.

Dubos A, Castells-Nobau A, Meziane H, Oortveld MA, Houbaert X, et al. (2015). "Conditional depletion of intellectual disability and Parkinsonism candidate gene ATP6AP2 in fly and mouse induces cognitive impairment and neurodegeneration". *Hum Mol Genet*. 24;23,6736-6755. doi:10.1093/hmg/ddv380.

Eaton AF, Brown D and Merkulova M. (2021). "The evolutionary conserved TLDc domain defines a new class of (H(+))V-ATPase interacting proteins". *Sci Rep*. 11;1,22654. doi:10.1038/s41598-021-01809-y.

Ebrahimi-Fakhari D, Saffari A, Wahlster L, Lu J, Byrne S, et al. (2016). "Congenital disorders of autophagy: an emerging novel class of inborn errors of neuro-metabolism". *Brain*. 139;Pt 2,317-337. doi:10.1093/brain/awv371.

Egashira Y, Takase M and Takamori S. (2015). "Monitoring of vacuolar-type H+ ATPase-mediated proton influx into synaptic vesicles". *J Neurosci*. 35;8,3701-3710. doi:10.1523/JNEUROSCI.4160-14.2015.

Egashira Y, Takase M, Watanabe S, Ishida J, Fukamizu A, et al. (2016). "Unique pH dynamics in GABAergic synaptic vesicles illuminates the mechanism and kinetics of GABA loading". *Proc Natl Acad Sci U S A*. 113;38,10702-10707. doi:10.1073/pnas.1604527113.

Einhorn Z, Trapani JG, Liu Q and Nicolson T. (2012). "Rabconnectin3alpha promotes stable activity of the H+ pump on synaptic vesicles in hair cells". *J Neurosci*. 32;32,11144-11156. doi:10.1523/JNEUROSCI.1705-12.2012.

Esposito A, Falace A, Wagner M, Gal M, Mei D, et al. (2019). "Biallelic DMXL2 mutations impair autophagy and cause Ohtahara syndrome with progressive course". *Brain*. 142;12,3876-3891. doi:10.1093/brain/awz326.

Falace A, Buhler E, Fadda M, Watrin F, Lippiello P, et al. (2014). "TBC1D24 regulates neuronal migration and maturation through modulation of the ARF6-dependent pathway". *Proc Natl Acad Sci U S A*. 111;6,2337-2342. doi:10.1073/pnas.1316294111.

Falace A, Filipello F, La Padula V, Vanni N, Madia F, et al. (2010). "TBC1D24, an ARF6-interacting protein, is mutated in familial infantile myoclonic epilepsy". *Am J Hum Genet*. 87;3,365-370. doi:10.1016/j.ajhg.2010.07.020.

Farsi Z, Gowrisankaran S, Krunic M, Rammner B, Woehler A, et al. (2018). "Clathrin coat controls synaptic vesicle acidification by blocking vacuolar ATPase activity". *Elife*. 7;doi:10.7554/eLife.32569.

Fassio A, Esposito A, Kato M, Saitsu H, Mei D, et al. (2018). "De novo mutations of the ATP6V1A gene cause developmental encephalopathy with epilepsy". *Brain*. 141;6,1703-1718. doi:10.1093/brain/awy092.

Fassio A, Falace A, Esposito A, Aprile D, Guerrini R, et al. (2020). "Emerging Role of the Autophagy/Lysosomal Degradative Pathway in Neurodevelopmental Disorders With Epilepsy". *Front Cell Neurosci*. 14;39. doi:10.3389/fncel.2020.00039.

Fernandes AC, Uytterhoeven V, Kuenen S, Wang YC, Slabbaert JR, et al. (2014). "Reduced synaptic vesicle protein degradation at lysosomes curbs TBC1D24/sky-induced neurodegeneration". *J Cell Biol*. 207;4,453-462. doi:10.1083/jcb.201406026.

Finelli MJ, Aprile D, Castroflorio E, Jeans A, Moschetta M, et al. (2019). "The epilepsy-associated protein TBC1D24 is required for normal development, survival and vesicle trafficking in mammalian neurons". *Hum Mol Genet*. 28;4,584-597. doi:10.1093/hmg/ddy370.

Finelli MJ and Oliver PL. (2017). "TLDc proteins: new players in the oxidative stress response and neurological disease". *Mamm Genome*. 28;9-10,395-406. doi:10.1007/s00335-017-9706-7.

Finelli MJ, Sanchez-Pulido L, Liu KX, Davies KE and Oliver PL. (2016). "The Evolutionarily Conserved Tre2/Bub2/Cdc16 (TBC), Lysin Motif (LysM), Domain Catalytic (TLDc) Domain Is Neuroprotective against Oxidative Stress". *J Biol Chem*. 291;6,2751-2763. doi:10.1074/jbc.M115.685222.

Fischer B, Dimopoulou A, Egerer J, Gardeitchik T, Kidd A, et al. (2012). "Further characterization of ATP6V0A2-related autosomal recessive cutis laxa". *Hum Genet*. 131;11,1761-1773. doi:10.1007/s00439-012-1197-8.

Fischer B, Luthy K, Paesmans J, De Koninck C, Maes I, et al. (2016). "Skywalker-TBC1D24 has a lipid-binding pocket mutated in epilepsy and required for synaptic function". *Nat Struct Mol Biol*. 23;11,965-973. doi:10.1038/nsmb.3297.

Forgac M. (2007). "Vacuolar ATPases: rotary proton pumps in physiology and pathophysiology". *Nat Rev Mol Cell Biol*. 8;11,917-929. doi:10.1038/nrm2272.

Frasa MA, Koessmeier KT, Ahmadian MR and Braga VM. (2012). "Illuminating the functional and structural repertoire of human TBC/RABGAPs". *Nat Rev Mol Cell Biol*. 13;2,67-73. doi:10.1038/nrm3267.

Frattini A, Orchard PJ, Sobacchi C, Giliani S, Abinun M, et al. (2000). "Defects in TCIRG1 subunit of the vacuolar proton pump are responsible for a subset of human autosomal recessive osteopetrosis". *Nat Genet*. 25;3,343-346. doi:10.1038/77131.

Frittoli E, Palamidessi A, Pizzigoni A, Lanzetti L, Garre M, et al. (2008). "The primate-specific protein TBC1D3 is required for optimal macropinocytosis in a novel ARF6-dependent pathway". *Mol Biol Cell*. 19;4,1304-1316. doi:10.1091/mbc.e07-06-0594.

Fuldner HH and Stadler H. (1982). "31P-NMR analysis of synaptic vesicles. Status of ATP and internal pH". *Eur J Biochem*. 121;3,519-524. doi:10.1111/j.1432-1033.1982.tb05817.x.

Glatigny M, Moriceau S, Rivagorda M, Ramos-Brossier M, Nascimbeni AC, et al. (2019). "Autophagy Is Required for Memory Formation and Reverses Age-Related Memory Decline". *Curr Biol*. 29;3,435-448 e438. doi:10.1016/j.cub.2018.12.021.

Goldsmith J, Ordureau A, Harper JW and Holzbaur ELF. (2022). "Brain-derived autophagosome profiling reveals the engulfment of nucleoid-enriched mitochondrial fragments by basal autophagy in neurons". *Neuron*. 110;6,967-976 e968. doi:10.1016/j.neuron.2021.12.029.

Goo MS, Sancho L, Slepak N, Boassa D, Deerinck TJ, et al. (2017). "Activity-dependent trafficking of lysosomes in dendrites and dendritic spines". *J Cell Biol*. 216;8,2499-2513. doi:10.1083/jcb.201704068.

Graf R, Harvey WR and Wieczorek H. (1996). "Purification and properties of a cytosolic V1-ATPase". *J Biol Chem*. 271;34,20908-20913. doi:10.1074/jbc.271.34.20908.

Gu Q, Jiao S, Duan K, Wang YX, Petralia RS, et al. (2021). "The BAD-BAX-Caspase-3 Cascade Modulates Synaptic Vesicle Pools via Autophagy". *J Neurosci*. 41;6,1174-1190. doi:10.1523/JNEUROSCI.0969-20.2020.

Guerrini R, Mei D, Kerti-Szigeti K, Pepe S, Koenig MK, et al. (2022). "Phenotypic and genetic spectrum of ATP6V1A encephalopathy: a disorder of lysosomal homeostasis". *Brain*. 145;8,2687-2703. doi:10.1093/brain/awac145.

Hafner AS, Donlin-Asp PG, Leitch B, Herzog E and Schuman EM. (2019). "Local protein synthesis is a ubiquitous feature of neuronal pre- and postsynaptic compartments". *Science*. 364;6441,doi:10.1126/science.aau3644.

Harrison MA and Muench SP. (2018). "The Vacuolar ATPase - A Nano-scale Motor That Drives Cell Biology". *Subcell Biochem*. 87;409-459. doi:10.1007/978-981-10-7757-9_14.

Hegedus K, Takats S, Boda A, Jipa A, Nagy P, et al. (2016). "The Ccz1-Mon1-Rab7 module and Rab5 control distinct steps of autophagy". *Mol Biol Cell*. 27;20,3132-3142. doi:10.1091/mbc.E16-03-0205.

Hernandez D, Torres CA, Setlik W, Cebrian C, Mosharov EV, et al. (2012). "Regulation of presynaptic neurotransmission by macroautophagy". *Neuron*. 74;2,277-284. doi:10.1016/j.neuron.2012.02.020.

Hiesinger PR, Fayyazuddin A, Mehta SQ, Rosenmund T, Schulze KL, et al. (2005). "The v-ATPase V0 subunit a1 is required for a late step in synaptic vesicle exocytosis in Drosophila". *Cell*. 121;4,607-620. doi:10.1016/j.cell.2005.03.012.

Hirosawa M, Nagase T, Ishikawa K, Kikuno R, Nomura N, et al. (1999). "Characterization of cDNA clones selected by the GeneMark analysis from size-fractionated cDNA libraries from human brain". *DNA Res*. 6;5,329-336. doi:10.1093/dnares/6.5.329.

Hirose T, Cabrera-Socorro A, Chitayat D, Lemonnier T, Feraud O, et al. (2019). "ATP6AP2 variant impairs CNS development and neuronal survival to cause fulminant neurodegeneration". *J Clin Invest*. 129;5,2145-2162. doi:10.1172/JCI79990.

Hnasko TS and Edwards RH. (2012). "Neurotransmitter corelease: mechanism and physiological role". *Annu Rev Physiol*. 74;225-243. doi:10.1146/annurev-physiol-020911-153315.

Ho CY, Alghamdi TA and Botelho RJ. (2012). "Phosphatidylinositol-3,5-bisphosphate: no longer the poor PIP2". *Traffic*. 13;1,1-8. doi:10.1111/j.1600-0854.2011.01246.x.

Hoffmann S, Orlando M, Andrzejak E, Bruns C, Trimbuch T, et al. (2019). "Light-Activated ROS Production Induces Synaptic Autophagy". *J Neurosci*. 39;12,2163-2183. doi:10.1523/JNEUROSCI.1317-18.2019.

Homma Y, Hiragi S and Fukuda M. (2021). "Rab family of small GTPases: an updated view on their regulation and functions". *FEBS J*. 288;1,36-55. doi:10.1111/febs.15453.

Honda A, Nogami M, Yokozeki T, Yamazaki M, Nakamura H, et al. (1999). "Phosphatidylinositol 4-phosphate 5-kinase alpha is a downstream effector of the small G protein ARF6 in membrane ruffle formation". *Cell*. 99;5,521-532. doi:10.1016/s0092-8674(00)81540-8.

Hurtado-Lorenzo A, Skinner M, El Annan J, Futai M, Sun-Wada GH, et al. (2006). "V-ATPase interacts with ARNO and Arf6 in early endosomes and regulates the protein degradative pathway". *Nat Cell Biol*. 8;2,124-136. doi:10.1038/ncb1348.

Itakura E, Kishi-Itakura C and Mizushima N. (2012). "The hairpin-type tail-anchored SNARE syntaxin 17 targets to autophagosomes for fusion with endosomes/lysosomes". *Cell*. 151;6,1256-1269. doi:10.1016/j.cell.2012.11.001.

Iwata M, Imamura H, Stambouli E, Ikeda C, Tamakoshi M, et al. (2004). "Crystal structure of a central stalk subunit C and reversible association/dissociation of vacuole-type ATPase". *Proc Natl Acad Sci U S A*. 101;1,59-64. doi:10.1073/pnas.0305165101.

Jaskolka MC, Winkley SR and Kane PM. (2021). "RAVE and Rabconnectin-3 Complexes as Signal Dependent Regulators of Organelle Acidification". *Front Cell Dev Biol*. 9;698190. doi:10.3389/fcell.2021.698190.

Johansen T and Lamark T. (2020). "Selective Autophagy: ATG8 Family Proteins, LIR Motifs and Cargo Receptors". *J Mol Biol*. 432;1,80-103. doi:10.1016/j.jmb.2019.07.016.

John A, Ng-Cordell E, Hanna N, Brkic D and Baker K. (2021). "The neurodevelopmental spectrum of synaptic vesicle cycling disorders". *J Neurochem*. 157;2,208-228. doi:10.1111/jnc.15135.

Kallergi E, Daskalaki AD, Kolaxi A, Camus C, Ioannou E, et al. (2022). "Dendritic autophagy degrades postsynaptic proteins and is required for long-term synaptic depression in mice". *Nat Commun*. 13;1,680. doi:10.1038/s41467-022-28301-z.

Kammenga JE. (2017). "The background puzzle: how identical mutations in the same gene lead to different disease symptoms". *FEBS J*. 284;20,3362-3373. doi:10.1111/febs.14080.

Kane PM. (1995). "Disassembly and reassembly of the yeast vacuolar H(+)-ATPase in vivo". *J Biol Chem*. 270;28,17025-17032.
Kane PM. (2006). "The where, when, and how of organelle acidification by the yeast vacuolar H+-ATPase". *Microbiol Mol Biol Rev*. 70;1,177-191. doi:10.1128/MMBR.70.1.177-191.2006.

Kellokumpu S. (2019). "Golgi pH, Ion and Redox Homeostasis: How Much Do They Really Matter?". *Front Cell Dev Biol*. 7;93. doi:10.3389/fcell.2019.00093.

Khan MM, Lee S, Couoh-Cardel S, Oot RA, Kim H, et al. (2022). "Oxidative stress protein Oxr1 promotes V-ATPase holoenzyme disassembly in catalytic activity-independent manner". *EMBO J*. 41;3,e109360. doi:10.15252/embj.2021109360.

Khosrowabadi E and Kellokumpu S. (2020). "Golgi pH and Ion Homeostasis in Health and Disease". *Rev Physiol Biochem Pharmacol*. doi:10.1007/112_2020_49.

Klinkert K and Echard A. (2016). "Rab35 GTPase: A Central Regulator of Phosphoinositides and F-actin in Endocytic Recycling and Beyond". *Traffic*. 17;10,1063-1077. doi:10.1111/tra.12422.

Klionsky DJ, Abdalla FC, Abeliovich H, Abraham RT, Acevedo-Arozena A, et al. (2012). "Guidelines for the use and interpretation of assays for monitoring autophagy". *Autophagy*. 8;4,445-544. doi:10.4161/auto.19496.

Koh JY, Kim HN, Hwang JJ, Kim YH and Park SE. (2019). "Lysosomal dysfunction in proteinopathic neurodegenerative disorders: possible therapeutic roles of cAMP and zinc". *Mol Brain*. 12;1,18. doi:10.1186/s13041-019-0439-2.

Kornak U, Schulz A, Friedrich W, Uhlhaas S, Kremens B, et al. (2000). "Mutations in the a3 subunit of the vacuolar H(+)-ATPase cause infantile malignant osteopetrosis". *Hum Mol Genet*. 9;13,2059-2063. doi:10.1093/hmg/9.13.2059.

Kortum F, Caputo V, Bauer CK, Stella L, Ciolfi A, et al. (2015). "Mutations in KCNH1 and ATP6V1B2 cause Zimmermann-Laband syndrome". *Nat Genet*. 47;6,661-667. doi:10.1038/ng.3282.

Kuijpers M, Kochlamazashvili G, Stumpf A, Puchkov D, Swaminathan A, et al. (2021). "Neuronal Autophagy Regulates Presynaptic Neurotransmission by Controlling the Axonal Endoplasmic Reticulum". *Neuron*. 109;2,299-313 e299. doi:10.1016/j.neuron.2020.10.005.

Laemmli UK. (1970). "Cleavage of Structural Proteins during the Assembly of the Head of Bacteriophage T4". *Nature*. 227;5259,680-685. doi:10.1038/227680a0.

Lafourcade C, Sobo K, Kieffer-Jaquinod S, Garin J and van der Goot FG. (2008). "Regulation of the V-ATPase along the endocytic pathway occurs through reversible subunit association and membrane localization". *PLoS One*. 3;7,e2758. doi:10.1371/journal.pone.0002758.

Lee JH, McBrayer MK, Wolfe DM, Haslett LJ, Kumar A, et al. (2015). "Presenilin 1 Maintains Lysosomal Ca(2+) Homeostasis via TRPML1 by Regulating vATPase-Mediated Lysosome Acidification". *Cell Rep*. 12;9,1430-1444. doi:10.1016/j.celrep.2015.07.050.

Lee JH, Yu WH, Kumar A, Lee S, Mohan PS, et al. (2010). "Lysosomal proteolysis and autophagy require presenilin 1 and are disrupted by Alzheimer-related PS1 mutations". *Cell*. 141;7,1146-1158. doi:10.1016/j.cell.2010.05.008.

Liberman R, Bond S, Shainheit MG, Stadecker MJ and Forgac M. (2014). "Regulated assembly of vacuolar ATPase is increased during cluster disruption-induced maturation of dendritic cells through a phosphatidylinositol 3-kinase/mTOR-dependent pathway". *J Biol Chem*. 289;3,1355-1363. doi:10.1074/jbc.M113.524561.

Lin L, Lyu Q, Kwan PY, Zhao J, Fan R, et al. (2020). "The epilepsy and intellectual disability-associated protein TBC1D24 regulates the maintenance of excitatory synapses and animal behaviors". *PLoS Genet*. 16;1,e1008587. doi:10.1371/journal.pgen.1008587.

Liu GY and Sabatini DM. (2020). "mTOR at the nexus of nutrition, growth, ageing and disease". *Nat Rev Mol Cell Biol*. 21;4,183-203. doi:10.1038/s41580-019-0199-y.

Liu KX, Edwards B, Lee S, Finelli MJ, Davies B, et al. (2015). "Neuron-specific antioxidant OXR1 extends survival of a mouse model of amyotrophic lateral sclerosis". *Brain*. 138;Pt 5,1167-1181. doi:10.1093/brain/awv039.

Lozano R, Herman K, Rothfuss M, Rieger H, Bayrak-Toydemir P, et al. (2016). "Clinical intrafamilial variability in lethal familial neonatal seizure disorder caused by TBC1D24 mutations". *Am J Med Genet A*. 170;12,3207-3214. doi:10.1002/ajmg.a.37933.

Lu M, Ammar D, Ives H, Albrecht F and Gluck SL. (2007). "Physical interaction between aldolase and vacuolar H+-ATPase is essential for the assembly and activity of the proton pump". *J Biol Chem*. 282;34,24495-24503. doi:10.1074/jbc.M702598200.

Martinu L, Masuda-Robens JM, Robertson SE, Santy LC, Casanova JE, et al. (2004). "The TBC (Tre-2/Bub2/Cdc16) domain protein TRE17 regulates plasma membrane-endosomal trafficking through activation of Arf6". *Mol Cell Biol*. 24;22,9752-9762. doi:10.1128/MCB.24.22.9752-9762.2004.

Maxfield FR and McGraw TE. (2004). "Endocytic recycling". *Nat Rev Mol Cell Biol*. 5;2,121-132. doi:10.1038/nrm1315.

Mazhab-Jafari MT, Rohou A, Schmidt C, Bueler SA, Benlekbir S, et al. (2016). "Atomic model for the membrane-embedded V(O) motor of a eukaryotic V-ATPase". *Nature*. 539;7627,118-122. doi:10.1038/nature19828.

McGuire C, Cotter K, Stransky L and Forgac M. (2016). "Regulation of V-ATPase assembly and function of V-ATPases in tumor cell invasiveness". *Biochim Biophys Acta*. 1857;8,1213-1218. doi:10.1016/j.bbabio.2016.02.010.

McGuire CM and Forgac M. (2018). "Glucose starvation increases V-ATPase assembly and activity in mammalian cells through AMP kinase and phosphatidylinositide 3-kinase/Akt signaling". *J Biol Chem*. 293;23,9113-9123. doi:10.1074/jbc.RA117.001327.

Merkulova M, Paunescu TG, Azroyan A, Marshansky V, Breton S, et al. (2015). "Mapping the H(+) (V)-ATPase interactome: identification of proteins involved in trafficking, folding, assembly and phosphorylation". *Sci Rep*. 5;14827. doi:10.1038/srep14827.

Merkulova M, Paunescu TG, Nair AV, Wang CY, Capen DE, et al. (2018). "Targeted deletion of the Ncoa7 gene results in incomplete distal renal tubular acidosis in mice". *Am J Physiol Renal Physiol*. 315;1,F173-F185. doi:10.1152/ajprenal.00407.2017.

Michaelson DM and Angel I. (1980). "Determination of delta pH in cholinergic synaptic vesicles: its effect on storage and release of acetylcholine". *Life Sci*. 27;1,39-44. doi:10.1016/0024-3205(80)90017-x.

Milh M, Falace A, Villeneuve N, Vanni N, Cacciagli P, et al. (2013). "Novel compound heterozygous mutations in TBC1D24 cause familial malignant migrating partial seizures of infancy". *Hum Mutat*. 34;6,869-872. doi:10.1002/humu.22318.

Mindell JA. (2012). "Lysosomal acidification mechanisms". *Annu Rev Physiol*. 74;69-86. doi:10.1146/annurev-physiol-012110-142317.

Miyazaki H, Yamazaki M, Watanabe H, Maehama T, Yokozeki T, et al. (2005). "The small GTPase ADP-ribosylation factor 6 negatively regulates dendritic spine formation". *FEBS Lett*. 579;30,6834-6838. doi:10.1016/j.febslet.2005.11.022.

Morel N, Dedieu JC and Philippe JM. (2003). "Specific sorting of the a1 isoform of the V-H+ATPase a subunit to nerve terminals where it associates with both synaptic vesicles and the presynaptic plasma membrane". *J Cell Sci*. 116;Pt 23,4751-4762. doi:10.1242/jcs.00791.

Morel N, Dunant Y and Israel M. (2001). "Neurotransmitter release through the V0 sector of V-ATPase". *J Neurochem*. 79;3,485-488. doi:10.1046/j.1471-4159.2001.00611.x.

Morel N and Poea-Guyon S. (2015). "The membrane domain of vacuolar H(+)ATPase: a crucial player in neurotransmitter exocytotic release". *Cell Mol Life Sci*. 72;13,2561-2573. doi:10.1007/s00018-015-1886-2.

Nah J, Yuan J and Jung YK. (2015). "Autophagy in neurodegenerative diseases: from mechanism to therapeutic approach". *Mol Cells*. 38;5,381-389. doi:10.14348/molcells.2015.0034.

Nakamura S. (2004). "Glucose activates H(+)-ATPase in kidney epithelial cells". *Am J Physiol Cell Physiol*. 287;1,C97-105. doi:10.1152/ajpcell.00469.2003.

Nikoletopoulou V, Sidiropoulou K, Kallergi E, Dalezios Y and Tavernarakis N. (2017). "Modulation of Autophagy by BDNF Underlies Synaptic Plasticity". *Cell Metab*. 26;1,230-242 e235. doi:10.1016/j.cmet.2017.06.005.

Nishi T and Forgac M. (2002). "The vacuolar (H+)-ATPases--nature's most versatile proton pumps". *Nat Rev Mol Cell Biol*. 3;2,94-103. doi:10.1038/nrm729.

Nishi T, Kawasaki-Nishi S and Forgac M. (2001). "Expression and localization of the mouse homologue of the yeast V-ATPase 21-kDa Subunit c" (Vma16p)". *J Biol Chem*. 276;36,34122-34130. doi:10.1074/jbc.M104682200.

Oliver PL, Finelli MJ, Edwards B, Bitoun E, Butts DL, et al. (2011). "Oxr1 is essential for protection against oxidative stress-induced neurodegeneration". *PLoS Genet*. 7;10,e1002338. doi:10.1371/journal.pgen.1002338.

Oot RA, Couoh-Cardel S, Sharma S, Stam NJ and Wilkens S. (2017). "Breaking up and making up: The secret life of the vacuolar H(+) -ATPase". *Protein Sci*. 26;5,896-909. doi:10.1002/pro.3147.

Oot RA, Kane PM, Berry EA and Wilkens S. (2016). "Crystal structure of yeast V1-ATPase in the autoinhibited state". *EMBO J*. 35;15,1694-1706. doi:10.15252/embj.201593447.

Oot RA, Yao Y, Manolson MF and Wilkens S. (2021). "Purification of active human vacuolar H(+)-ATPase in native lipid-containing nanodiscs". *J Biol Chem*. 297;2,100964. doi:10.1016/j.jbc.2021.100964.

Pan X, Eathiraj S, Munson M and Lambright DG. (2006). "TBC-domain GAPs for Rab GTPases accelerate GTP hydrolysis by a dual-finger mechanism". *Nature*. 442;7100,303-306. doi:10.1038/nature04847.

Parra KJ, Chan CY and Chen J. (2014). "Saccharomyces cerevisiae vacuolar H+-ATPase regulation by disassembly and reassembly: one structure and multiple signals". *Eukaryot Cell*. 13;6,706-714. doi:10.1128/EC.00050-14.

Parra KJ and Kane PM. (1998). "Reversible association between the V1 and V0 domains of yeast vacuolar H+-ATPase is an unconventional glucose-induced effect". *Mol Cell Biol*. 18;12,7064-7074. doi:10.1128/MCB.18.12.7064.

Poea-Guyon S, Ammar MR, Erard M, Amar M, Moreau AW, et al. (2013). "The V-ATPase membrane domain is a sensor of granular pH that controls the exocytotic machinery". *J Cell Biol*. 203;2,283-298. doi:10.1083/jcb.201303104.

Rehman AU, Santos-Cortez RL, Morell RJ, Drummond MC, Ito T, et al. (2014). "Mutations in TBC1D24, a gene associated with epilepsy, also cause nonsyndromic deafness DFNB86". *Am J Hum Genet*. 94;1,144-152. doi:10.1016/j.ajhg.2013.12.004.

Rogov V, Dotsch V, Johansen T and Kirkin V. (2014). "Interactions between autophagy receptors and ubiquitin-like proteins form the molecular basis for selective autophagy". *Mol Cell*. 53;2,167-178. doi:10.1016/j.molcel.2013.12.014.

Roh SH, Stam NJ, Hryc CF, Couoh-Cardel S, Pintilie G, et al. (2018). "The 3.5-A CryoEM Structure of Nanodisc-Reconstituted Yeast Vacuolar ATPase V(o) Proton Channel". *Mol Cell*. 69;6,993-1004 e1003. doi:10.1016/j.molcel.2018.02.006.

Santy LC and Casanova JE. (2001). "Activation of ARF6 by ARNO stimulates epithelial cell migration through downstream activation of both Rac1 and phospholipase D". *J Cell Biol*. 154;3,599-610. doi:10.1083/jcb.200104019.

Sarkar S. (2013). "Regulation of autophagy by mTOR-dependent and mTOR-independent pathways: autophagy dysfunction in neurodegenerative diseases and therapeutic application of autophagy enhancers". *Biochem Soc Trans*. 41;5,1103-1130. doi:10.1042/BST20130134.

Sautin YY, Lu M, Gaugler A, Zhang L and Gluck SL. (2005). "Phosphatidylinositol 3-kinase-mediated effects of glucose on vacuolar H+-ATPase assembly, translocation, and acidification of intracellular compartments in renal epithelial cells". *Mol Cell Biol*. 25;2,575-589. doi:10.1128/MCB.25.2.575-589.2005.

Seol JH, Shevchenko A, Shevchenko A and Deshaies RJ. (2001). "Skp1 forms multiple protein complexes, including RAVE, a regulator of V-ATPase assembly". *Nat Cell Biol*. 3;4,384-391. doi:10.1038/35070067.

Shehata M, Matsumura H, Okubo-Suzuki R, Ohkawa N and Inokuchi K. (2012). "Neuronal stimulation induces autophagy in hippocampal neurons that is involved in AMPA receptor degradation after chemical long-term depression". *J Neurosci*. 32;30,10413-10422. doi:10.1523/JNEUROSCI.4533-11.2012.

Sidibe DK, Vogel MC and Maday S. (2022). "Organization of the autophagy pathway in neurons". *Curr Opin Neurobiol*. 75;102554. doi:10.1016/j.conb.2022.102554.

Smardon AM and Kane PM. (2007). "RAVE is essential for the efficient assembly of the C subunit with the vacuolar H(+)-ATPase". *J Biol Chem*. 282;36,26185-26194. doi:10.1074/jbc.M703627200.

Smardon AM, Nasab ND, Tarsio M, Diakov TT and Kane PM. (2015). "Molecular Interactions and Cellular Itinerary of the Yeast RAVE (Regulator of the H+-ATPase of Vacuolar and Endosomal Membranes) Complex". *J Biol Chem*. 290;46,27511-27523. doi:10.1074/jbc.M115.667634.

Smardon AM, Tarsio M and Kane PM. (2002). "The RAVE complex is essential for stable assembly of the yeast V-ATPase". *J Biol Chem*. 277;16,13831-13839. doi:10.1074/jbc.M200682200.

Stenmark H. (2009). "Rab GTPases as coordinators of vesicle traffic". *Nat Rev Mol Cell Biol*. 10;8,513-525. doi:10.1038/nrm2728.

Stransky LA and Forgac M. (2015). "Amino Acid Availability Modulates Vacuolar H+-ATPase Assembly". *J Biol Chem*. 290;45,27360-27369. doi:10.1074/jbc.M115.659128.

Sudhof TC. (2013). "Neurotransmitter release: the last millisecond in the life of a synaptic vesicle". *Neuron*. 80;3,675-690. doi:10.1016/j.neuron.2013.10.022.

Sudhof TC and Rothman JE. (2009). "Membrane fusion: grappling with SNARE and SM proteins". *Science*. 323;5913,474-477. doi:10.1126/science.1161748.

Sumner JP, Dow JA, Earley FG, Klein U, Jager D, et al. (1995). "Regulation of plasma membrane V-ATPase activity by dissociation of peripheral subunits". *J Biol Chem*. 270;10,5649-5653. doi:10.1074/jbc.270.10.5649.

Tagliatti E, Fadda M, Falace A, Benfenati F and Fassio A. (2016). "Arf6 regulates the cycling and the readily releasable pool of synaptic vesicles at hippocampal synapse". *Elife*. 5;doi:10.7554/eLife.10116.

Takamori S, Holt M, Stenius K, Lemke EA, Gronborg M, et al. (2006). "Molecular anatomy of a trafficking organelle". *Cell*. 127;4,831-846. doi:10.1016/j.cell.2006.10.030.

Tan YZ, Abbas YM, Wu JZ, Wu D, Keon KA, et al. (2022). "CryoEM of endogenous mammalian V-ATPase interacting with the TLDc protein mEAK-7". *Life Science Alliance*. 5;11,e202201527. doi:10.26508/lsa.202201527.

Taoufiq Z, Ninov M, Villar-Briones A, Wang HY, Sasaki T, et al. (2020). "Hidden proteome of synaptic vesicles in the mammalian brain". *Proc Natl Acad Sci U S A*. 117;52,33586-33596. doi:10.1073/pnas.2011870117.

Tata B, Huijbregts L, Jacquier S, Csaba Z, Genin E, et al. (2014). "Haploinsufficiency of Dmxl2, encoding a synaptic protein, causes infertility associated with a loss of GnRH neurons in mouse". *PLoS Biol*. 12;9,e1001952. doi:10.1371/journal.pbio.1001952.

Thorpe GW, Fong CS, Alic N, Higgins VJ and Dawes IW. (2004). "Cells have distinct mechanisms to maintain protection against different reactive oxygen species: oxidative-stress-response genes". *Proc Natl Acad Sci U S A*. 101;17,6564-6569. doi:10.1073/pnas.0305888101.

Tona R, Chen W, Nakano Y, Reyes LD, Petralia RS, et al. (2019). "The phenotypic landscape of a Tbc1d24 mutant mouse includes convulsive seizures resembling human early infantile epileptic encephalopathy". *Hum Mol Genet*. 28;9,1530-1547. doi:10.1093/hmg/ddy445.

Trombetta ES, Ebersold M, Garrett W, Pypaert M and Mellman I. (2003). "Activation of lysosomal function during dendritic cell maturation". *Science*. 299;5611,1400-1403. doi:10.1126/science.1080106.

Uytterhoeven V, Kuenen S, Kasprowicz J, Miskiewicz K and Verstreken P. (2011). "Loss of skywalker reveals synaptic endosomes as sorting stations for synaptic vesicle proteins". *Cell*. 145;1,117-132. doi:10.1016/j.cell.2011.02.039.

Van Damme T, Gardeitchik T, Mohamed M, Guerrero-Castillo S, Freisinger P, et al. (2017). "Mutations in ATP6V1E1 or ATP6V1A Cause Autosomal-Recessive Cutis Laxa". *Am J Hum Genet*. 100;2,216-227. doi:10.1016/j.ajhg.2016.12.010.

Vasanthakumar T and Rubinstein JL. (2020). "Structure and Roles of V-type ATPases". *Trends Biochem Sci*. 45;4,295-307. doi:10.1016/j.tibs.2019.12.007.

Vavassori S and Mayer A. (2014). "A new life for an old pump: V-ATPase and neurotransmitter release". *J Cell Biol*. 205;1,7-9. doi:10.1083/jcb.201403040.

Wang D, Epstein D, Khalaf O, Srinivasan S, Williamson WR, et al. (2014). "Ca2+-Calmodulin regulates SNARE assembly and spontaneous neurotransmitter release via v-ATPase subunit V0a1". *J Cell Biol*. 205;1,21-31. doi:10.1083/jcb.201312109.

Wang J, Rousseau J, Kim E, Ehresmann S, Cheng YT, et al. (2019). "Loss of Oxidation Resistance 1, OXR1, Is Associated with an Autosomal-Recessive Neurological Disease with Cerebellar Atrophy and Lysosomal Dysfunction". *Am J Hum Genet*. 105;6,1237-1253. doi:10.1016/j.ajhg.2019.11.002.

Wang L, Wu D, Robinson CV and Fu TM. (2022). "Identification of mEAK-7 as a human V-ATPase regulator via cryo-EM data mining". *Proc Natl Acad Sci U S A*. 119;35,e2203742119. doi:10.1073/pnas.2203742119.

Wang L, Wu D, Robinson CV, Wu H and Fu TM. (2020a). "Structures of a Complete Human V-ATPase Reveal Mechanisms of Its Assembly". *Mol Cell*. 80;3,501-511 e503. doi:10.1016/j.molcel.2020.09.029.

Wang R, Long T, Hassan A, Wang J, Sun Y, et al. (2020b). "Cryo-EM structures of intact V-ATPase from bovine brain". *Nat Commun*. 11;1,3921. doi:10.1038/s41467-020-17762-9.

Wilkens S, Inoue T and Forgac M. (2004). "Three-dimensional structure of the vacuolar ATPase. Localization of subunit H by difference imaging and chemical cross-linking". *J Biol Chem*. 279;40,41942-41949. doi:10.1074/jbc.M407821200.

Wu JJ, Cai A, Greenslade JE, Higgins NR, Fan C, et al. (2020). "ALS/FTD mutations in UBQLN2 impede autophagy by reducing autophagosome acidification through loss of function". *Proc Natl Acad Sci U S A*. 117;26,15230-15241. doi:10.1073/pnas.1917371117.

Xu T and Forgac M. (2001). "Microtubules are involved in glucose-dependent dissociation of the yeast vacuolar [H+]-ATPase in vivo". *J Biol Chem*. 276;27,24855-24861. doi:10.1074/jbc.M100637200.

Xu Y, Parmar A, Roux E, Balbis A, Dumas V, et al. (2012). "Epidermal growth factor-induced vacuolar (H+)-atpase assembly: a role in signaling via mTORC1 activation". *J Biol Chem*. 287;31,26409-26422. doi:10.1074/jbc.M112.352229.

Yan Y, Denef N and Schupbach T. (2009). "The vacuolar proton pump, V-ATPase, is required for notch signaling and endosomal trafficking in Drosophila". *Dev Cell*. 17;3,387-402. doi:10.1016/j.devcel.2009.07.001.

Yang Z and Klionsky DJ. (2010). "Eaten alive: a history of macroautophagy". *Nat Cell Biol*. 12;9,814-822. doi:10.1038/ncb0910-814.

Yim WW and Mizushima N. (2020). "Lysosome biology in autophagy". *Cell Discov*. 6;6. doi:10.1038/s41421-020-0141-7.

Yoon J, Hwang YS, Lee M, Sun J, Cho HJ, et al. (2018). "TBC1d24-ephrinB2 interaction regulates contact inhibition of locomotion in neural crest cell migration". *Nat Commun*. 9;1,3491. doi:10.1038/s41467-018-05924-9.

Yuan Y, Zhang J, Chang Q, Zeng J, Xin F, et al. (2014). "De novo mutation in ATP6V1B2 impairs lysosome acidification and causes dominant deafness-onychodystrophy syndrome". *Cell Res*. 24;11,1370-1373. doi:10.1038/cr.2014.77.

Zara F, Gennaro E, Stabile M, Carbone I, Malacarne M, et al. (2000). "Mapping of a locus for a familial autosomal recessive idiopathic myoclonic epilepsy of infancy to chromosome 16p13". *Am J Hum Genet*. 66;5,1552-1557. doi:10.1086/302876.

Zhang W, Wang D, Volk E, Bellen HJ, Hiesinger PR, et al. (2008). "V-ATPase V0 sector subunit a1 in neurons is a target of calmodulin". *J Biol Chem*. 283;1,294-300. doi:10.1074/jbc.M708058200.

Zhen Y and Stenmark H. (2015). "Cellular functions of Rab GTPases at a glance". *J Cell Sci*. 128;17,3171-3176. doi:10.1242/jcs.166074.

Zoncu R, Bar-Peled L, Efeyan A, Wang S, Sancak Y, et al. (2011). "mTORC1 senses lysosomal amino acids through an inside-out mechanism that requires the vacuolar H(+)-ATPase". *Science*. 334;6056,678-683. doi:10.1126/science.1207056.

APPENDIX

Scientific Publications

1. Muzzi L, Di Lisa D, Falappa M, **Pepe S**, Maccione A, et al. (2023) “Human Excitatory Cortical Neurospheroids Coupled to High-Density MEAs: A Valid Platform for Functional Tests.” *bioRxiv*, doi: https://doi.org/10.1101/2022.02.04.478858

2. Andolfi A, Arnaldi P, Di Lisa D, **Pepe S**, Frega M, et al. (2022). "A micropatterned thermoplasmonic substrate for neuromodulation of in vitro neuronal networks". *Acta Biomater*. doi:10.1016/j.actbio.2022.12.036.

3. Di Lisa D, Muzzi L, **Pepe S**, Dellacasa E, Frega M, et al. (2022). "On the way back from 3D to 2D: Chitosan promotes adhesion and development of neuronal networks onto culture supports". *Carbohydr Polym*. 297;120049. doi:10.1016/j.carbpol.2022.120049.

4. Guerrini R, Mei D, Kerti-Szigeti K, **Pepe S**, Koenig MK, et al. (2022). "Phenotypic and genetic spectrum of ATP6V1A encephalopathy: a disorder of lysosomal homeostasis". *Brain*. 145;8,2687-2703. doi:10.1093/brain/awac145.

Congresses and Conferences

- **“TBC1D24 interacts with V-ATPase and regulates pH homeostasis and autophagy in neurons”** ORAL PRESENTATION at SIF YRP 2022. 13-15 June 2022. Bertinoro, Italy
- **Pepe S.**, Aprile D., Castroflorio E., Parsons A., Soares T., Benfenati F., Oliver P. and Fassio A. “TBC1D24 interacts with V-ATPase and regulates pH homeostasis and autophagy in neurons”. POSTER at FENS FORUM 2022. 9-13 July 2022. Paris, France
- **Pepe S.**, Aprile D., Castroflorio E., Parsons A., Soares T., Benfenati F., Oliver P. and Fassio A. “TBC1D24 interacts with V-ATPase and regulates pH homeostasis and autophagy in neurons”. POSTER at EMBO Workshop “Autophagy in brain health and disease”. 11-14 May 2022. Sant Feliu de Guixols, Spain;

- Eposito A., **Pepe S.**, Cerullo M.S., Cortese K., Maragliano L., Guerrini R., Benfenati F. and Fassio A. POSTER at IRCCS Ospedale Policlinico San Martino Scientific Retreat. 4-5 November 2021. Genoa, Italy;
- **Pepe S.**, Maragliano L., Conti V., Mei D., Benfenati F., Guerrini R. and Fassio A. "Structure/function study on *de novo* mutations in *ATP6V1A* causing developmental encephalopathy with epilepsy." POSTER presentation at BraYn Conference. 25-26 November 2020 (web conference);
- Esposito A., Falace A., Mei D., Conti V., **Pepe S.**, Giovedì S., Benfenati F., Guerrini R. and Fassio A. "ATP6V1A and DMXL2 loss of function impacts on lysosomal homeostasis and autophagy causing developmental and synaptic defects in neurons." POSTER at FENS 2020. 11-15 July 2020. Glasgow, Scotland (web conference).